THE UNIVERSITY
of EDINBURGH

The role of the P2X7 receptor in the renal vasculature in a mouse model of chronic kidney disease

Amelia Rose Howarth

Thesis for the Degree of Doctor of Philosophy (PhD)

The University of Edinburgh, 2019

Declaration

I hereby declare that all work carried out during this PhD was performed by myself, unless otherwise stated, under the supervision of Prof. Matthew Bailey and Dr. Bryan Conway. This thesis has not previously been submitted for any other degree or qualification.

Amelia Rose Howarth

Acknowledgements

I have a lot of people to thank, but I'll try and keep it brief. First and foremost, thank you to my supervisor, Prof. Matthew Bailey. He has been consistently supportive throughout my research – always providing sound advice, strong resources and clear direction. He has also been kind enough to extend these qualities beyond the realm of science, into the chaos of life, and I doubt I would have made it this far in my research or my career without him. Thanks also to Dr. Bryan Conway, who has given flawless advice and provided invaluable resources, as well as vital humour, throughout my PhD.

Thank you to everyone in the Bailey, Conway and Mullins lab teams, special thanks to Jess, Charlotte, Adrienne, Morag, Carolynn and Audrey. Within this circle, I want to give a special nod to Natalie Jones a.k.a the golden child, who has been unendingly supportive and inspirational in her approach to science and to life. Thank you to all of our collaborators, from Prof. Robert Unwin and Dr. Fred Tam, to Dr. Patrick Hadoke, Dr. James Dear and Dr. Nheeraj Dhaun, to all of the CVS network, including the FACS and Histology teams, who seem ready to lend a hand at all times. Extra thanks to LF2, particularly Duncan and Larraine, who have provided many a comedic phone calls as well as much appreciated animal support.

Thank you to all my CVS pals: Callam, Emma, Rob, Amber, and the wider group: Clare, Matt, Kate. You helped to keep me sane, especially Clare, who I don't think realises how important she has been to me! Extra thanks to Raphaël and Marlène, colleagues, friends and briefly flatmates, for annoying me no end and always being there when I was in a pickle. Thanks to my friends outside of Edinburgh, who remain unnamed here for the sake of keeping it brief, but who have existed so powerfully as satellites of my PhD sphere, just their presence has been a comfort. Thanks to all my new friends as I've moved forward from Edinburgh into Bristol, but who have inspired me so much and given me the motivation to eventually finish my PhD, I am very grateful to have them in this new chapter (yes that's a thesis pun) of my life.

Thank you, most of all, to my family. Kim, John, Janice, Tom, Molly, Noah, Alfie – there aren't words that can express my gratitude for you all in my life, I'm not even going to attempt it.

Finally, thank you to all the scientists and artists of Earth, past, present and future, who keep the planet spinning, and who are trying relentlessly to understand the world we live in. I'm constantly amazed by the resilience, diversity, curiosity and bravery we exhibit.

Abstract

Chronic kidney disease (CKD) is a global disease affecting 10% of the world population and is largely treated by dialysis and organ transplant at late stages of disease. As rates of CKD rise, it is increasingly evident that novel drug targets are required for intervention before these late stages are reached. The purinergic receptor sub-type 7 (P2X7) may represent such a drug target. P2X7, an ATP-gated ion channel, is part of the purinergic signalling pathway and antagonists are safe and well-tolerated in clinical trials as a treatment for inflammatory disease. These trials did not show therapeutic benefit, but recent findings suggest that vascular, rather than immune, functions of P2X7 may be important for renal disease. This project aimed to investigate the expression and role of P2X7 in the renal vasculature in both normal and hypertensive mice. A mouse model of multi-hit renal vascular injury was established and characterised through the administration of angiotensin II (ANGII), deoxycorticosterone (DOCA) and a high salt diet (ANGII DOCA salt model). ANGII DOCA salt mice exhibited mild hypertension, moderate albuminuria, vascular dysfunction, perivascular fibrosis, and a marked increase in renal injury markers in both whole kidney and urine, compared to sham-operated (Sham) littermates. A systematic immunofluorescence study localised P2X7 to the endothelium of renal vessels and glomerular capillaries in both Sham and ANGII DOCA salt mice, as well as localising to areas of injury in ANGII DOCA salt mouse kidneys. The P2X7 antagonist A438079 was able to inhibit ATP-stimulated release of IL-1B in LPS-primed mouse macrophages and was therefore used to assess vascular function in isolated aorta by wire myography. These studies found that activation of P2X7 via agonist BzATP led to vasoconstriction in both mouse groups, an effect that was amplified upon P2X7 inhibitions. Following these findings, it is possible that this is due to a shift in the expression of different P2X7 isoforms with potentially opposing vasoactivity in ANGII DOCA salt mice, compared to Sham mice. This is supported by the observation of differential expression of P2X7 according to the tissue used, the method of detection used, and the disease model investigated. This thesis highlights the importance of considering splice variation under normo- and pathophysiological conditions, both their expressional and functional differences.

Lay Summary

Chronic kidney disease (CKD) is a global disease affecting more than 10% of the world population. It is an illness that establishes itself over the course of many years, eventually leading to kidney failure, which requires treatment through dialysis and organ transplant. These treatments are difficult and costly, and so current research focuses on identifying drugs that can be used to combat CKD early on in its progression. One potential drug is a blocker of P2X7. P2X7 is a protein found on cells in renal blood vessels that binds energy molecules called ATP, that circulate in our blood. It has been observed that, in both humans and rodents with kidney disease, levels of P2X7 are increased and that blocking P2X7 may improve the symptoms of kidney disease, through lowering blood pressure and restoring blood flow to the kidney. However, little is known about the function of P2X7 in this area. To investigate this, we observed P2X7 in both healthy mice and mice with kidney disease. We saw that, although P2X7 was seen in similar places in the kidneys of both groups of mice, it appeared to be present at areas of injury in the kidneys of mice with renal disease at much higher levels. When we investigated the activity of P2X7 in these mice, we saw that activating P2X7 caused blood vessels to tighten i.e. vasoconstrict. We therefore hypothesised that blocking P2X7 would cause vessels to widen i.e. vasodilation. However, this was not the case. It is possible that this is because there are many different types of P2X7 in our bodies, called isoforms. These isoforms are encoded into our genes and are a natural part of human evolution. However, different P2X7 isoforms may have different functions in different parts of our bodies. We have seen some differences in P2X7 isoform expression and location in healthy mouse and diseased mouse kidneys. The work presented here highlights the importance of P2X7 isoforms when researching P2X7 in kidney disease and investigating new treatments for CKD.

Abbreviations

%	Percentage
Ach	Acetylcholine
ADP	Adenosine diphosphate
AMP	Adenosine monophosphate
ANG II	Angiotensin II
ANOVA	Analysis of variance
ARG	Arginase
ATP	Adenosine 5'-triphosphate
AU	Arbitrary
BHT	Butylated hydroxytoluene
BMDM	Bone marrow derived macrophages
BMP	Bone morphogenic protein
BP	Blood pressure
BV	Blue-Violet
BW	Body weight
BzATP	3'-0-(4-Benzoyl)benzoyl ATPATP triethylammonium salt
°C	Degrees Celsius
Ca	Calcium
$CaCl_2$	Calcium chloride
CCD	Cortical collecting duct
CD31	Cluster of differentiation 31
CD68	Cluster of differentiation 68
cDNA	Complimentary DNA
CI	Confidence intervals
CKD	Chronic Kidney Disease
CO_2	Carbon dioxide
COL	Collagen
CY7	Cyanine 7
Da	Dalton
DAPI	4′,6-diamidino-2-phenylindole
ddH_2O	Double distilled water
DMSO	Dimethyl sulphoxide
DNA	Deoxyribonucleic acid
DOCA	Deoxycorticosterone
EC50	Half maximal effective concentration
ECM	Extracellular matrix
EDTA	Ethylenediaminetetraacetic acid
eGFR	Estimated GFR
ELISA	Enzyme-linked immunosorbent assay
EMT	Epithelial-mesenchymal transition

eRPF	Estimated RPF
F4/80	EGF-like module-containing mucin-like hormone receptor-like 1
FACS	Fluorescence-activated cell sorting
FDA	Food and drug administration
FE	Fractional excretion
FITC	Fluorescein isothiocyanate
g	grams
GFR	Glomerular filtration rate
H	Hours
H_2O	Water
HAVCR	Hepatitis A virus cellular receptor
HIER	Heat-induced epitope retrieval
HIF	Hypoxia inducible factor
HPRT	Hypoxanthine-guanine phosphoribosyltransferase
HRP	Horseradish peroxidase
HTN	Hypertension
ICAM	Intercellular adhesion molecule
IF	Immunofluorescence
IHF	Immunohistofluorescence
IL	Interleukin
IP	Intraperitoneal
IRI	Ischaemic reperfusion injury
K	Potassium
KCl	Potassium chloride
kg	kilograms
$K2HPO_4$	Dipotassium phosphate
KIM	Kidney injury molecule
KO	Knock out
KPSS	High potassium physiological salt
L	Litres
LPS	Lipopolysaccharide
LTL	Lotus tetragonolobus lectin
M	Molarity
MABP	Mean arterial blood pressure
Mac	Macrophage
mg	Milligrams
$MgSO_4$	Magnesium sulphate
ml	Millilitres
mmHg	Millimetres mercury
mmol	Millimoles
mN	Millinewtons
mol	Moles

mRNA	Messenger RNA
N	Newtons
Na	Sodium
NaCl	Sodium chloride
$NaHCO_3$	Sodium bicarbonate
ng	Nanograms
NICE	National institute for health and care excellence
NLPR3	Cryopyrin
nmol	Nanomoles
NO	Nitric oxide
NOS	Nitric oxide synthase
NTN	Nephrotoxic nephritis
p	Probability value
P1R	Purinergic 1 receptors
P2R	Purinergic 2 receptors
P2X	Purinergic 2 X receptor
P2X7	Purinergic 2 X receptor 7
P2X7(e)	Purinergic 2 X receptor 7 intracellular targeting antibody
P2X7(i)	Purinergic 2 X receptor 7 extracellular targeting antibody
P2X713B	Purinergic 2 X receptor 7 variant 13B
P2X713C	Purinergic 2 X receptor 7 variant 13C
P2X7k	Purinergic 2 X receptor 7 variant k
p2xr7	Gene encoding P2X7
p2xr7-/-	P2X7 knock out
P2Xx	Purinergic 2 X receptor *x*
P2Y	Purinergic 2 Y Receptor
PAH	para-aminohippuric acid
PCR	Polymerase chain reaction
PDGFR	Platelet derived growth factor receptor
PE	Phenylephrine
PECAM	Platelet-endothelial cell adhesion molecule
PFA	Paraformaldehyde
PN	Pressure natriuresis
PSS	Physiological salt solution
qPCR	quantitative PCR
RAAS	Renin angiotensin aldosterone system
RBF	Renal blood flow
RNA	Ribonucleic acid
RPF	Renal plasma flow
RVR	Renal vascular resistance
S.D	Standard deviation
S.E.M	Standard error of the mean
SBP	Systolic blood pressure

SMA	Smooth muscle actin
SNP	Sodium nitroprusside
TGF	Transforming growth factor
TIM	T-cell immunoglobulin and mucin domain
TNF	Tumour necrosis factor
TRITC	Tetramethylrhodamine
U	Urinary volume
UDP	Uridine diphosphate
µg	Microgram
µmol	Micromoles
UTP	Uridine triphosphate
UUO	Unilateral ureteral obstruction
V	Volts
V	Flow rate
VEGF	Vascular endothelial growth factor
WB	Western blot
WT	Wild type

Table of Contents

Chapter 1: General Introduction

1.1 Chronic Kidney Disease

1.1.1 Overview of Chronic Kidney Disease

Chronic kidney disease (CKD) is a global disease affecting 10% of the world's population and its patients are one of the most 'at-risk' groups for the progression of cardiovascular conditions (Eckardt et al. 2013; Gansevoort et al. 2013). CKD represents a complex condition, with many contributors to its progression, including hypoxia, inflammation, vascular dysfunction and hypertension (Nakayama et al. 2011). Despite high socio-economic burden and widespread prevalence, treatment options for CKD are limited and hypertension remains a major modifiable risk factor for the disease. There is therefore an unmet need to identify new druggable targets to expand CKD treatment options (Remuzzi et al. 2013).

1.1.2 CKD: a cycle of injury and fibrosis

An extensive literature places sustained tubulointerstitial inflammation at the heart of CKD. Such inflammation primes the kidney for a cycle of injury and fibrosis and can impair the acute pressure natriuresis response (PN), the physiological processes through which the kidney regulates long-term blood pressure (Franco et al. 2013). Under normal circumstances, an increase in blood pressure (BP) leads to increased renal arterial perfusion, which stimulates the kidney to excrete sodium, reducing extracellular fluid volume and intravascular vascular volume and hence normalizing BP. If the PN response becomes impaired, long term BP control is lost and barotrauma of the renal microvasculature can provoke a further cycle of injury and inflammation, ultimately leading to fibrosis and a decline in renal function (Ivy & Bailey 2014).

This cycle can be broken down into stages of pathophysiology, which overlap and influence each other as disease progresses. Microvasculature damage and thus, hypoxia and endothelial dysfunction can lead to vasoconstriction and reduced blood flow in the kidney, leading to release of HIFs (hypoxia-induced factors) and loss of VEGFs (vascular endothelial growth factors), both of which play roles in inflammation.

Upon induction of interstitial inflammation and recruitment of macrophages, neutrophils, T-cells and B-cells, ILs (interleukins) and damage-associated molecular patterns (DAMPs) are activated and released, further amplifying the immune response.

As the damage continues, reparatory cells such as inflammatory cells and newly activated myofibroblasts contribute to a build-up of collagen in order to alleviate cellular injury. Matrix deposition increases and fibrosis occurs, first at interstitial, glomerular and perivascular areas, and later at tubular epithelial cells, resulting in further dysregulation, damage and injury. (For comprehensive reviews of these processes, please see Romagnani *et al.* 2017 & Guzzi *et al.* 2019)

As is evident, there are many layers and potential points of entry into the cycle of CKD. Historically, pharmacological treatment of CKD has focussed on targeting fibrosis. This, and other treatment potentials, are discussed below.

1.2 Treatment of CKD

1.2.1 Targeting fibrosis as a CKD treatment option

Fibrosis is an essential part of tissue repair, acting as a short term 'wound healing' response to injury. However, in chronic injury, when fibrosis is maintained over a long period of time, it can prevent the organ affected from functioning properly. This is true of the kidneys, where extensive fibrosis is a common end point of CKD (Rockey et al. 2015). Fibrosis is often the focus of CKD therapeutics, as it isn't until fibrosis is established and resultant changes in renal function translate to symptoms and thus patient presentation, that CKD is treated. However, the process of cross linking of extracellular matrix that occurs during fibrosis, makes it difficult to reverse. In the kidney, reversal of fibrosis and resulting damage to tubules is a difficult and lengthy process. Studies have found that reversal of renal fibrosis in rodents is possible, for example through administration of bone morphogenic protein (BMP-7) following transforming growth factor (TGF)-β1-induced epithelial-to-mesenchymal transition (EMT). EMT is a biological process that occurs in which epithelial cells transition into the mesenchymal cells that participate in tissue repair and the pathological process of fibrosis) (Zeisberg et al. 2003). In this paper, reversal of fibrosis was observed after treatment – however, the rodent model used captured only one aspect of fibrosis (EMT) and the treatment was given from 1 week after injury induction, a full 3 weeks

before end stages of CKD were reached. The observation that many studies often give treatment at these time scales, or even prophylactic treatment, is difficult to align with human pathology, where treatment occurs at end stages of disease. As such, no clinical studies have yet provided evidence for fibrosis reversal in humans (Zeisberg & Zeisberg 2015). The complex signalling pathways involved in fibrosis across many different cell types makes fibrosis difficult to treat and many studies aiming to target such pathways in the treatment of CKD have been unsuccessful (Boor et al. 2007). At present, early stage biomarkers of renal disease are sparse; currently, kidney injury molecule-1 (KIM-1) is the only FDA approved renal injury biomarker. Emerging research into biomarkers could make identification of early kidney injury more and more plausible, as treatment at preclinical stages of CKD is becoming more and more appealing (Tampe & Zeisberg 2014).

Under these circumstances, injury can be halted early on, before fibrosis even sets in, entirely avoiding any associated decline in renal function. The exact origins and starting point of CKD is often debated, making its diagnosis difficult. Current NICE guidelines advise creatinine-based estimation of glomerular filtration rate (eGFR) as the first point of call for diagnosis of CKD, along with albuminuria tests (https://www.nice.org.uk/guidance/cg182). However, this method carries limitations, such as variability in results and low sensitivity in certain subjects. Research efforts are therefore currently focussing on identifying biomarkers at early stages of CKD. Characterising and understanding early stages of CKD at the molecular and physiological level is vital in identifying novel drug targets and markers at this phase.

1.2.2 Targeting the vasculature as a CKD treatment option

In 1998, it was proposed that vascular dysfunction was a common early hallmark of CKD and more than this, sustained vascular abnormalities played a causal role in the progression to renal disease (Fine et al. 1998). This hypothesis, proposed by Fine and colleagues, suggested that primary glomerular diseases, such as hypertension, leads to changes in the microvasculature which compromise renal blood supply, generating a local hypoxic environment at the tubule-interstitium. Hypoxia encourages production of hypoxia inducible factor (HIF)-1α, which acts as a transcription factor for a multitude of pro-fibrotic factors that act to build the extracellular matrix (ECM),

induce fibrosis and promote further loss of vasculature and decline of renal blood flow (Norman & Fine 2006). Thus, the 'chronic hypoxia hypothesis' posits that renal microvascular dysfunction and/or rarefaction creates a hostile, pro-inflammatory environment in the renal medulla and locks the kidney in a cycle of declining renal function (Fine et al. 1998).

Whether or not this cycle of progressive renal disease has a single point of entry is not established but it is likely that interstitial inflammation is also an important early event underlying vascular dysfunction (Rodríguez-Iturbe et al. 2014; Johnson et al. 2005). Anti-inflammatory strategies can restore the acute PN response and improve blood pressure control in hypertensive rodents (Franco et al. 2013; Ji et al. 2012a; Ji et al. 2012b). Treatment of early vascular dysfunction and inflammation may therefore be much more effective than an attempt to treat end stage symptoms of CKD, such as fibrosis. Pharmaceutical companies are currently turning to these time points; identification of drug targets active within this time period may be crucial in the treatment of early stage CKD, and prevent later stages, of CKD.

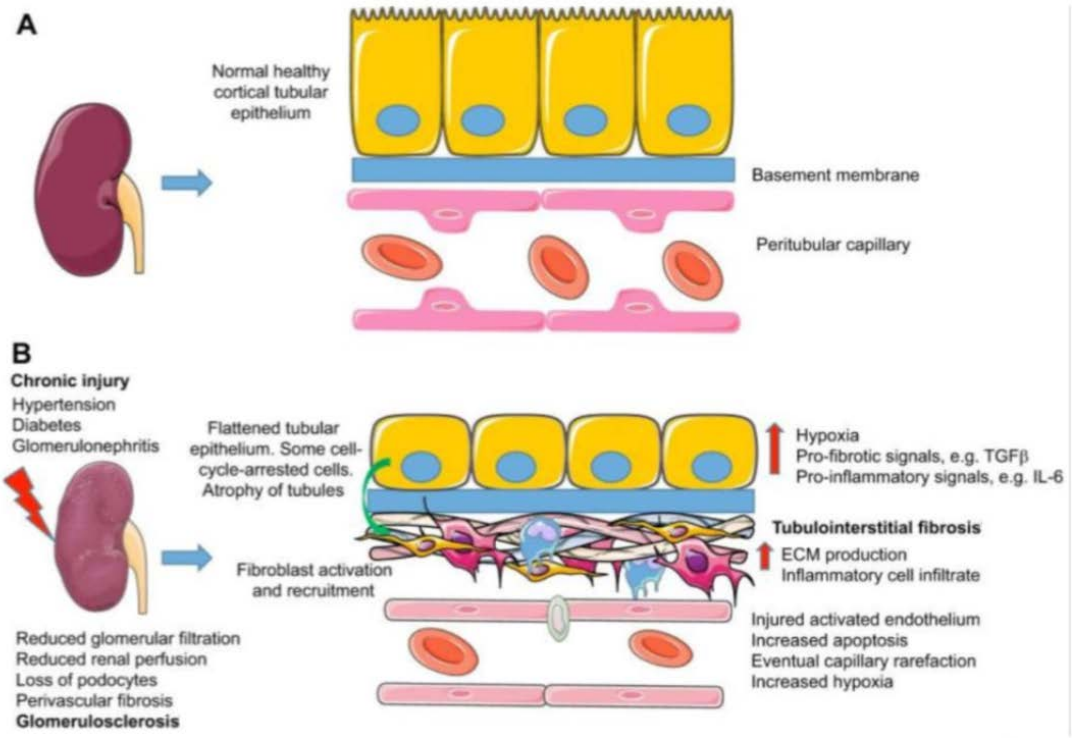

Figure 1.1 - The pathophysiological processes linked to kidney disease. Schematics of (A) a normal, healthy kidney and (B) a kidney with chronic injury, exhibiting hypoxia, capillary rarefaction and activated endothelium. Source: (Mullins et al. 2016)

1.3 Models of CKD

To explore treatment options for CKD, a range of rodent models are characterised, primarily in the rat and the mouse. Many of these models apply focus on fibrosis, and some have a vascular focus; these are discussed below.

One model that uses genetic intervention is the *mRen2* rat. This model exhibits hypertension and characteristics of a dysfunctional renin aldosterone angiotensin system (RAAS) and abnormal renal vascular tone, such as increased angiotensin II (ANGII) production, vasoconstriction and upregulated sodium reabsorption. Fibrosis in this model is rapid and intense, reaching end organ damage by 8 weeks (Mullins et al. 2016). This captures many of fibrotic and vascular elements common at late stages of CKD, however does not realistically capture the timeline of human CKD, which takes years to progress.

A surgical model of rapid fibrosis, commonly used in both rats and mice is the unilateral ureteral obstruction (UUO) model, which demonstrates phenotypes of interstitial inflammation, tubular dilation and atrophy, alongside fibrosis and a drop in renal blood flow (RBF) and glomerular filtration rate (GFR)(Yang et al. 2010; Mullins et al. 2016). This model also progresses rapidly, again missing the slow progression of human CKD.

Renal injury can also be induced through renal mass reduction, such as through the 5/6 nephrectomy model, with added ischaemic reperfusion injury (IRI) (Mullins et al. 2016). Vascular phenotypes are also observed in this model alongside progressive fibrosis, such as capillary rarefaction and downregulation of vascular endothelial growth factor (VEGF), which is required for growth of new blood vessels. Because of the progressive nature of this model, as well as the establishment of vascular and fibrotic phenotypes, it's an interesting model to study in the context of CKD, however the surgery is complex and carries a high mortality rate, making it difficult to access (Mullins et al. 2016).

Components of CKD can also be induced through pharmacological intervention; nephrotoxic nephritis (NTN) can be achieved through administration of anti-

glomerular immunoglobulins (IgG). This results in glomerular nephritis, which is to be expected, alongside proteinuria and histological changes in the kidney that mimic human disease (Mullins et al., 2016). This model does, however, only capture some elements of CKD, and exhibits high rate of disease variation between animal cohorts, making it difficult to obtain reproducible data with reliable conclusions.

Deoxycortisone acetate and a high salt diet (DOCA-salt) can also be used in conjunction with a unilateral nephrectomy to induce hypertension and renal injury in rodents, particularly in C57BL/6 mice which are quite resistant to renal injury. Interestingly, the vascular elements of CKD are well captured in this model, with impaired endothelial-dependant relaxation observed as well as increased extracellular matrix deposition (Yang et al. 2010). However, this is again a rapidly progressing model, with severe hypertension observed within a few weeks.

These are just a few examples of models currently used to explore CKD. They capture different elements of the disease; vascular, inflammatory, fibrotic, and each has its uses and limitation. Reviewing these models shows there is a wide range of potential mediators for the establishment of CKD. In many of the models described above, function and/or expression of purinergic signalling is disrupted, representing one mediator of CKD; this is the focus of my PhD thesis.

1.4 Purinergic Signalling

1.4.1 Overview of Purinergic Signalling

Two categories of purinergic receptor are defined; P1, which bind adenosine and P2, which can be activated by purine or pyrimidine nucleotides. This binding leads to an array of cellular responses, often in the form of an increase in cellular calcium ions (Booth et al. 2012).

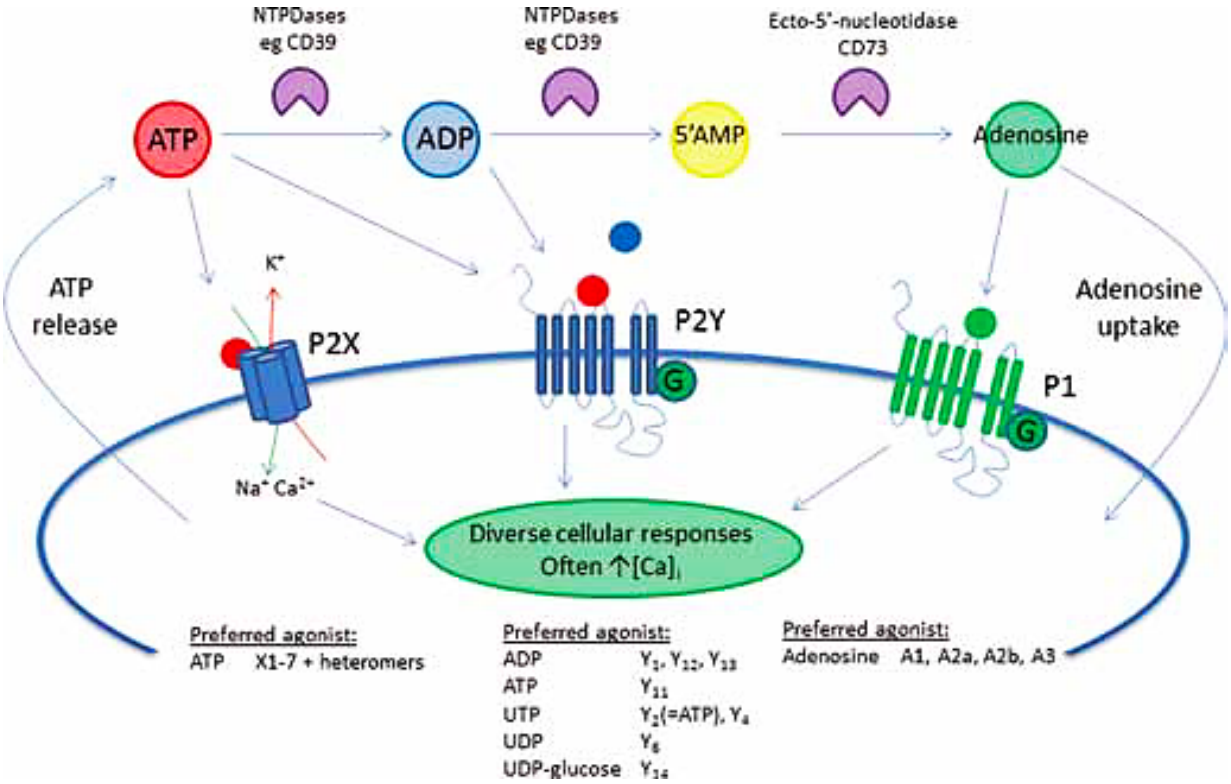

Figure 1.2 – An overview of purinergic signalling. In extracellular spaces, ATP can be broken down into a sequence of products, ADP, 5'AMP and Adenosine. Each of these products then binds to a different type of purinergic receptor to mediate a range of downstream cellular responses. Source: (Booth et al. 2012).

P2R are further subdivided: P2Y are G-protein coupled receptors and the 7 subtypes have differential selectivity for ATP, ADP, UTP and UDP; P2XR are ligand-gated ion channels (IUPHAR database: http://www.iuphar-db.org/) activated by ATP. Most P2R subtypes are expressed in the kidney and purinergic signalling exerts marked physiological effects on renal blood flow and epithelial transport properties, as reviewed in detail (Shirley et al. 2013; Burnstock et al. 2014).

1.4.2 The role of purinergic receptors in renal disease

Targeting the purinergic receptor family is one current avenue for the treatment of renal disease.

It is increasingly recognised that ATP signalling via P2R contributes to a variety of pathophysiological conditions, ranging from hypertension (Menzies et al. 2015), transplant rejection and polycystic kidney disease (Solini et al. 2013).

Purinergic receptors can be found throughout the nephron, and they have been identified as playing physiological roles in tubuloglomerular feedback, the autoregulatory response of renal vasculature, electrolyte transport and control of renin release. Given these widespread locations and roles within the kidney, it's not surprising that purinergic signalling is also associated with the renal pathophysiological conditions listed above, as well as nephritis, diabetes and nephrotoxicant injury (Burnstock & Ralevic 2014).

Purinergic receptors are present in both renal vascular tissue and immune cells and the role of P2X receptors in both locations has been explored (Lewis & Evans 2001; Menzies et al. 2013; North 2002). Increased P2X7 activation in particular is strongly associated with kidney disease and elevated expression of these receptors in the "normal" state increases the susceptibility to hypertensive renal vascular injury (Menzies et al. 2013; Menzies et al. 2017). P2X7 expression is also upregulated in rodent models of type 1 diabetes and hypertension, as well as in human and experimental glomerulonephritis (Vonend et al. 2004a; Turner et al. 2007; Taylor et al. 2009; Menzies et al. 2017). Human studies are more limited but genetic association studies in human populations have uncovered significant association between a singular P2X7 single nuclear polymorphism and increased blood pressure (Palomino-Doza et al. 2008). These studies strongly link the dysregulation of P2X7 expression with hypertension and renal injury and pose P2X7 as a promising target therapeutic for renal injury and CKD.

1.5 The P2X7 receptor: structure and function

1.5.1 Overview of P2X7 structure and function

There is additional complexity in studying P2X receptors, as a number of splice variants of P2X7 receptors have also been reported, both in rodents and humans (Masin et al. 2012; Cheewatrakoolpong et al. 2005; Nicke et al. 2009). Such splice variants have been deemed responsible for a range of altered phenotypes, including varied pain responses, differential response to agonists and even mistargeted gene knockout (Hansen et al. 2011; Xu et al. 2012; Nicke et al. 2009; Bartlett et al. 2014). P2X7 splice variants have also been shown to vary in their interaction with pannexin-1, which, as mentioned, plays an important role in the inflammatory action of P2X7 (Xu et al. 2012; Pelegrin & Surprenant 2006; Hung et al. 2013).

Table 1.1 - An overview of the P2X7 splice isoforms in mice, including GlaxoSmithKline knock out (GSK KO) and Pfizer knock out (Pfizer KO)

Isoform	NCBI RefSeq	Alt. name	Reference	Properties	GKS KO	Pfizer KO
E	NM_001284402.1	P2X7k	Nicke *et al* 2009	- fully functional variant	Present	Absent
				- 8-fold higher sensitivity to P2X7 agonists		
				- slower deactivation		
				- increased propensity to form P2X7 pores		
				- preferentially expressed by T cells		
A	NM_011027.3	P2X7	Surprenant et al, 1996	- canonical	Absent	Absent
				- preferentially expressed by macrophages		
B	NM_001038845.2	P2X713C	Masin et al 2012	- strongest expressin in brain, salivary glands, lung	Absent	Present
				- low cell surface expression, low channel function, no pore formation		
C	NM_001038839.2	P2X713B	Masin et al 2012	- strongest expressin in brain, salivary glands, spleen	Absent	Present
				- low cell surface expression, low channel function, no pore formation		
				- apparently hetero-oligomerizess with P2X7 to inhibit it		
D	NM_001038887.1	-	Predicted	-	-	-

The number of splice variants observed across different species and the functional significance they may have in disease is still unclear and must be further investigated in order to effectively target any unfavourable action of P2X7.

1.5.2 P2X7 in inflammation and renal fibrosis

Enhanced P2X signalling has long been thought to be contributory in chronic inflammatory disease. P2X7 is expressed on many immune cells, including macrophages and other antigen-presenting cells (Surprenant et al. 1996; Lister et al. 2007), as well as blood mononucleic cells in models of CKD (Lajdova et al. 2012; Lajdova et al. 2017). Expression of P2X7 on such cells via ATP leads to release of interleukin-1B (IL-1B) and interleukin-18 (IL-18) which generate a pro-inflammatory environment conducive to kidney tissue degeneration, injury and cell death (Gentile et al. 2015; Pelegrin & Surprenant 2006; Fadok et al. 1998; Le Feuvre et al. 2002). This effect is mediated through activation of the NLPR3 inflammasome, potentially by a P2X7/P2X4/pannexin-1 complex that initiates pore formation, priming the cell for apoptosis (Pelegrin & Surprenant 2006; Solini et al. 2013; Hung et al. 2013). P2X7 blockade actually protects against renal nephrotoxic injury by reducing inflammatory response, reducing apoptosis and the NLRP3 inflammasome (Yan et al. 2015; Zhang et al. 2014; Danquah et al. 2016).

By regulating cell death in this way, P2X7 can regulate the turnover of the cells upon which it is expressed, including granulocytes (Le Feuvre et al. 2002; Wang et al. 2004). Leucocytes, such as granulocytes, are vital in the normal regulation of a sustained inflammation, and dysregulation can promote disease (Walker et al. 2005). Indeed, *scid* mice lacking lymphocytes show an attenuated hypertensive phenotype upon ANGII administration (Crowley et al. 2010). Furthermore, P2X7 deficient mice lack leukocyte responses to ATP seen in wild type mice and exhibit attenuated inflammatory responses, renal injury and hypertension (Labasi et al. 2002; Ji, Naito, Weng, et al. 2012). Add to this the finding that administration of the immunosuppressant, mycophenolate mofetil, in hypertensive mice leads to an attenuated PN response, the alteration of which is the driving force of salt-sensitive hypertension (Franco et al. 2013; Sathanoori et al. 2015; Stachon et al. 2017).

P2X7 is functionally, if not structurally linked to P2X4 – a purinergic receptor with which it shares almost 50% homology in both the human and the rat (Craigie et al. 2013). There is continued debate about whether or not P2X7 and P2X4 form heterotrimers (Guo et al. 2007; Antonio et al. 2011), however their functional relationship to each other within a renal environment is much clearer. A recent study

found increased expression of P2X4 in renal tubule cells from patients with diabetic nephropathy (Chen et al. 2013). P2X4-mediated activation of the NLRP3 inflammasome in *ex vivo* cell studies and receptor expression had a strong positive correlation with renal excretion of IL-1B in diabetic patients. P2X4 also promotes apoptosis in human mesangial cells (Solini et al. 2013), a process that contributes to glomerular injury in chronic renal disease. P2X4 deficient mice are also protected against inflammation in models of arthritis (Li et al. 2014): its role in kidney disease is not clear as a recent study found that that P2X4 deficient mice displayed an exaggerated injury response to unilateral ureteric obstruction (UUO), a model of chronic renal inflammatory disease (Kim et al. 2014).

P2X7 has also been linked to fibrosis, with activation of P2X7 leading to release of TGF-β and a resultant increase in extracellular matrix production in glucose treated rat mesangial cells (Solini et al. 2005; Gentile et al. 2015). Knock out of P2X7 in UUO mice also has a protective effect with reduction in TGF-β, fibrosis positive staining and inflammatory cell infiltration in $P2X7^{-/-}$ UUO mouse kidneys, compared to WT UUO.

Despite substantial existing evidence supporting the inflammatory role of P2X7 in renal injury and disease, exploiting P2X7 antagonists in clinical trials for basic inflammatory diseases, such as rheumatoid arthritis, have failed, with no significant benefit of using the drug seen compared to the placebo (Arulkumaran et al. 2011; Keystone et al. 2012; Stock et al. 2012). This indicates that there are other pathways acting in such diseases that may act independently of inflammation to drive the pathological phenotype.

1.5.3 P2X7 in the renal vasculature

One promising complementary contributor of P2X receptors to renal disease is their vascular role. The vasoactive effects of nucleotides have been well-documented and whether constriction or dilation of vessels is stimulated depends on a number of factors. The source of ATP, location or type of P2 receptor and the basal vascular tone all influence the overall effect.

In terms of renal disease, P2 receptors are involved in key regulatory processes in the kidney which, if disrupted, can have significant effects on renal function. P2X1, for example, is a key mediator of autoregulation in the kidney (Inscho et al. 2003). Upon increased systemic blood pressure, increase in renal blood flow is buffered by P2X1-mediated vasoconstriction in the afferent arteriole, protecting the glomerulus from pressure induced injury. Vessels from P2X1 null mice exhibit blunted vasoconstriction during the pressure-mediated autoregulatory response; this leads to failure of autoregulation and resultant barotrauma (Inscho et al. 2003).

Autoregulation is a vital process in the kidney, but has been shown to be more effective in the cortex than the medulla, meaning a loss of haemodynamic control in this area (Cowley et al. 1992). An increase in BP in the medullary vasa recta leads to release of nitric oxide (NO) via a sheer stress response, which promotes sodium retention, leading to an impaired PN and thus hypertension and injury (O'Conner & Cowley Jr. 2010). Indeed, inhibition of NO release under these circumstances reduces medullary blood flow (Mattson et al. 1992). However, NO inhibition does not alter the PN response, suggesting that NO is not the sole mediator of a renal injury observed following a medullary blood pressure increase. Under these circumstances, ATP and purinergic receptors may also contribute to a disease phenotype and evidence for this is building, including findings of P2X receptor expression in the microvasculature.

P2X1, P2X4 and P2X7 have all been identified in rat renal vessels (Lewis & Evans 2001) with P2X4 and P2X7 expression observed in the pre-glomerular microvasculature as well as in the smooth muscle of larger vessels (Menzies et al. 2013). In human endothelial cells, P2X4 is identified as the most abundant P2X receptor, followed by P2X7 (Yamamoto et al. 2000). The observation of these receptors in both the smooth muscle and endothelial layers of vasculature imply direct roles in both signalling and vascular tone. These findings therefore strongly suggest a major role for P2X receptors in the renal vasculature, both physiologically and pathophysiologically.

In terms of vasoactivity, P2X4 has a vasodilatory effect, consistent with its role in NO release (Yamamoto et al. 2006), but has also been shown to act in conjunction with P2X1 to cause sustained constriction in cerebral arteries and regulate vascular tone in

renal smooth muscle cells (Harhun et al. 2014; Harhun et al. 2010). P2X7 has been shown to cause vasoconstriction in rat retinal vessels via pericytes, with similar vasoactive roles suggested in the kidney, although experiments supporting this hypothesis are lacking (Kawamura et al. 2003; Menzies et al. 2013). Blockade of P2X receptors leads to altered control of pericyte-mediated vascular tone in the kidney (Crawford et al. 2013) and picking apart the role of each P2X subtype could give great insight into the contribution of these receptors to modulated vasoactivity and thus, BP and renal injury.

Evidence of P2X vascular involvement in renal pathophysiology is also building. Both P2X4 and P2X7 have been identified via microarray analysis as key molecules in renal injury susceptibility in rodents, presenting a pathophysiological function (Menzies et al. 2013). P2X4 deficiency has been shown to induce loss of blood pressure control in response to altered blood flow, presenting a primary candidate for the correlation between renal ATP levels and vascular resistance (Nishiyama et al. 2000; Yamamoto et al. 2006). P2X1 and P2X7 have more recently been shown to contribute to the control of glomerular haemodyamics in models and ANGII-induced hypertension (Franco et al. 2017). P2X4 has also been identified as a receptor that mediates NO release under shear stress, meaning that its dysregulation could have severe effects of sodium and hence blood pressure control (Yamamoto et al. 2000).

These studies provide evidence for the role of P2X receptors in renal vasculature control, with strong support that impaired control through these receptors may have consequences for PN, hypertension and resultant renal injury. This is shown by Ji and colleagues whereby P2X7 deficiency in DOCA-salt treated mice and P2X7 inhibition in Dahl salt-sensitive rats both lead to attenuated hypertension (Ji et al. 2012a; Ji et al. 2012b). Furthermore, treatment of ANGII-induced hypertension in F344 rats with a highly selective P2X7 antagonist restores the PN response, normalises BP and improves renal oxygenation (Menzies et al. 2015). Finally, endothelial expression of P2X7 has been shown to be vital in the recruitment of Mac-1/ICAM-1 dependent leukocytes in a murine model of septic encephalopathy (Wang et al. 2015). Such studies are adding the growing evidence that the vascular role of P2X7 is of extreme significance.

P2X7 deficiency in mice has been implicated in lipopolysaccharide-induced vascular dysfunction, reducing downstream production of inflammatory agents (Chiao et al. 2008; Chiao et al. 2013), further supporting the theory that P2X-mediated vascular dysfunction is the priming step in the setup of CKD. However, the vasoactivity of these receptors on different vessels and vascular surfaces needs to be further clarified before any solid mechanisms can be revealed: inflammatory or vascular.

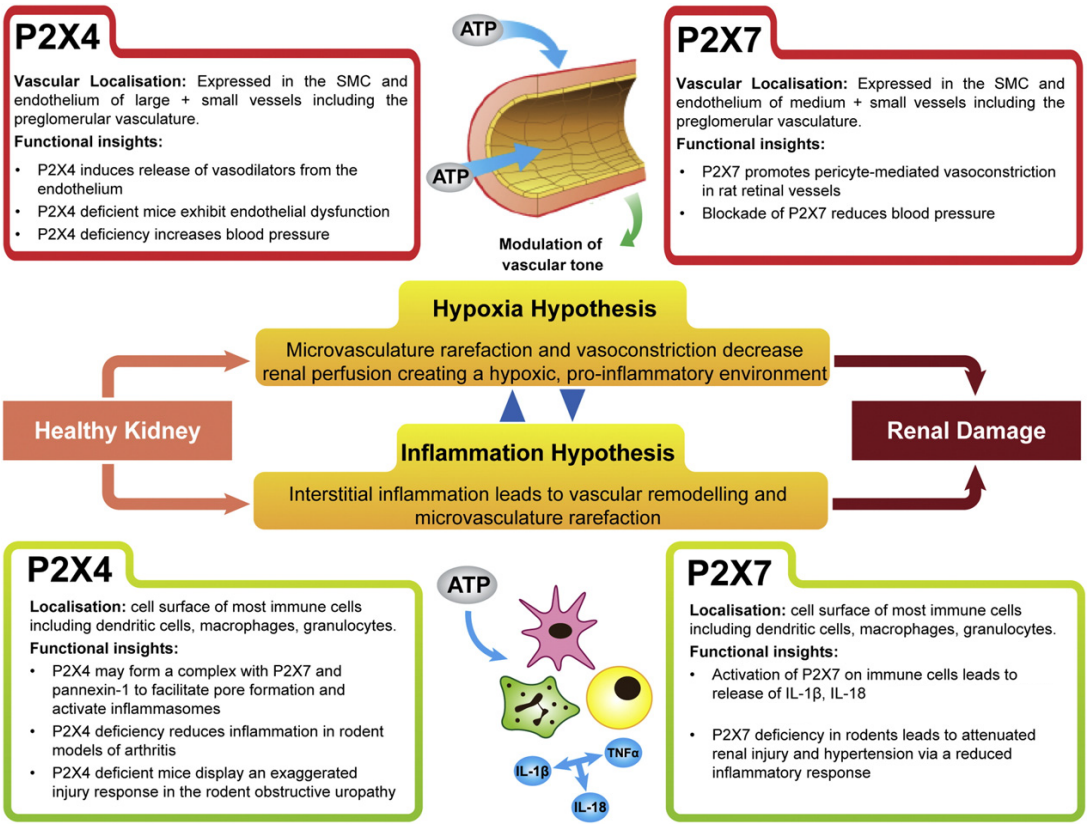

Figure 1.3 - Vascular and inflammatory pathways of establishing renal injury and the role that P2X4 receptors (R) andP2X7R may play in each. Expression of P2X4R and P2X7R on renal vascular may mediate vascular tone and hence renal blood flow and pressure. Increased expression of P2XR may lead to abnormal regulation of these functions and thus loss of microvasculature, hypoxia and renal injury. Expression of P2X4R and P2X7R on immune cells contributes to release and modulation of cytokines, such as interleukin (IL)-1β, IL-18. Upregulation of these P2XR may lead to increased inflammation, which results in renal injury. SMC, smooth muscle cell. Source: (Howarth et al. 2015)

1.5.4 P2X7 in clinical trials

The arguments for the inflammatory roles of P2X receptors versus their vascular role in CKD have been proposed, yet the likelihood is that they work in conjunction, especially since clinical trials for the P2X7 antagonists, AZD9056 and CE-224,535 in inflammatory treatment have thus far failed to show any benefit over the placebo (Keystone et al. 2012; Stock et al. 2012). Although P2X7 antagonists have been shown to be well-tolerated in humans, inefficacy of the drug have prevented progression of these clinical trials beyond Phase 3 (Arulkumaran et al. 2011). There are further complications surrounding P2X7 which may account for this, such as its functional link to P2X4, or its splice variant profile. However, the problem may also be the intervention point of treatment in these trials. If P2X7 is indeed playing a role in very early time points of CKD, at the vascular level, then treatment with antagonists must be aligned with this phase of P2X7 activity. Elucidating the role of P2X7 in the vasculature of preclinical CKD will further understanding of this.

General Hypotheses

My hypotheses are:

1. ANGII DOCA salt model (Figure 2.1) will capture phenotypes relevant to early CKD, specifically: hypertension, vascular dysfunction, limited inflammation, limited fibrosis. As this model represents early CKD, rather than late CKD, I do not expect to see adverse changes in renal function, such as glomerular filtration rate and renal blood flow

2. P2X7 will be present in the renal vasculature of mice, particularly in cell types that play a role in modulation of vascular tone; endothelial cells, vascular smooth muscle cells and pericytes. From review of the literature, I hypothesise that P2X7 will be present at higher levels in the ANGII DOCA salt mouse model of vascular renal injury.

3. Activation of P2X7 will induce a vasoconstriction of the isolated mouse aorta, exaggerated in ANGII DOCA salt animals. I hypothesise that antagonism of P2X7 will reduce this constrictive effect which will lead to a reduction in blood pressure and restoration of renal blood flow in ANGII DOCA salt mice.

Each one is explored and discussed in Results Chapters 3 – 5.

Chapter 2: Materials and Methods

Animals

All experiments were performed on C57BL6/J male mice between the ages of 10 – 16 weeks (Charles River, UK). Mice were housed in the animal unit at Little France under controlled conditions of temperature (21±1°C), humidity (50±10%) and light/dark (light 7am–7pm). Mice had *ad libitum* access to water and a standard rodent chow (0.25% Na) unless otherwise specified. Procedures were performed in accordance with the UK Home Office Animals (Scientific Procedures) Act of 1986 after ethical review by The University of Edinburgh.

ANGII, DOCA and salt diet administration

Male C57BL6/J mice were split into two groups: sham; consisting of sham operated animals implanted with an osmotic minipump (Alzet, 2002 model) containing 0.9% saline, a blank pellet, receiving standard chow, and experimental; consisting of animals receiving ANGII (100ng/kg/min) via osmotic mini-pump, a deoxycorticosterone (DOCA, Sigma-Aldrich) pellet and receiving a 3% sodium chow (DBM Ltd). As per the timeline below, mice were implanted with minipumps and pellets on day 0, the experimental group received sodium chow on day 3 and all mice were culled or underwent experimental procedure on day 28.

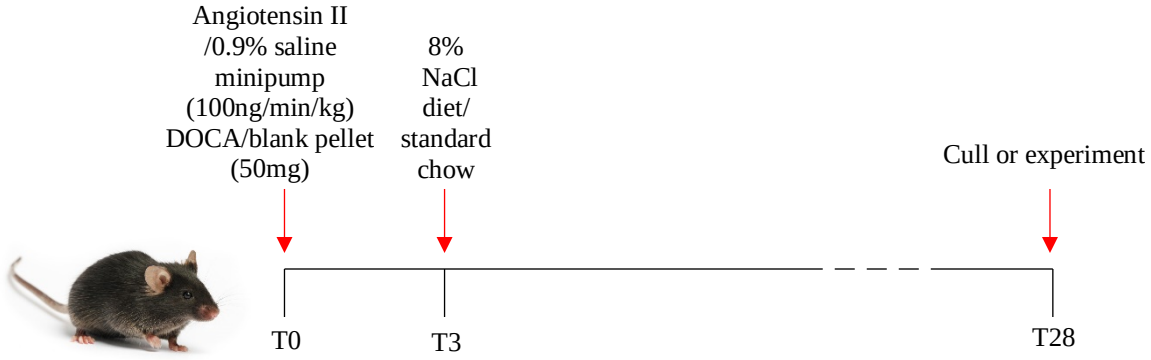

Figure 2.1 - Timeline of Sham and ANGII DOCA salt mice from surgery at day 0 (T0) to cull at day 28 (T28)

Four cohorts of mice have been carried out to date as detailed below (See Table 1). More details on experimental protocol can be found under the relevant methods and materials heading. Mortality rate across these cohorts currently stands at 5.3%.

Table 2.1 - Details of ANGII DOCA salt mouse cohorts

Cohort	Group size	Experimental protocol
1	6	Mice were culled via cervical dislocation and the kidneys and heart removed, weighed and either transferred to 4% PFA in preparation for IHC, or snap frozen in preparation for WB.
2	12	Systolic blood pressure (SBP) measurements were made at baseline (before surgery, after training), 2 weeks (mid-point) and 4 weeks (pre-terminal) via tail cuff pleismography. At day 28, mice underwent renal clearance surgery, after which they were culled by cervical dislocation. Kidneys and hearts were removed and weighed before disposal.
3	10	Urine collections were taken from mice at baseline (before surgery), 2 weeks (mid-point) and 4 weeks (pre-terminal) through the use of 24-hour metabolic cages. Mice were culled by exposure to CO_2 and aortas and mesenteric arteries removed for myography. Kidneys, heart, spleen and liver were removed, weighed and halved – half was transferred to 4% PFA in preparation for IHC, and half frozen in preparation for WB and PCR. Aorta not needed for myography was also snap frozen for RNA extraction.
4	16	Mice were culled by exposure to CO_2 and aortas removed for myography. Kidneys were removed, weighed and homogenised for separation of cells via FACS. Aorta not needed for myography was also snap frozen for RNA extraction.

Immunofluorescence

C57BL6/J mouse kidneys in Sham or ANGII-DOCA salt mice, or from a WT C57BL6/J colony, were perfusion fixed with 4% paraformaldehyde (PFA) and incubated at 4°C in 4% PFA for 24 hours before replacing with 70% ethanol. Kidneys were paraffin embedded, dried and sectioned at 4µm. Following dewaxing, dehydrating and heat-induced epitope recovery (HIER) at 90°C with citrate buffer, sections were incubated with 0.1% Sudan black B solution (Sigma Aldrich), 0.1% Triton-X-100 (Sigma Aldrich) and 3% hydrogen peroxidase, each for 10 minutes. Sections were then blocked overnight at 4°C in 10% normal donkey serum. Sections were incubated in primary antibody for 2 hours at room temperature. Primary rabbit polyclonal antibodies against the P2X1 (1:500, APR-001, Alomone Labs), P2X4 (1: 500, APR-002, Alomone Labs), and P2X7 ((i) intracellular targeting APR-004 at 1:500 and (e) extracellular targeting APR-008 at 1:500, Alomone Labs) were used. After washing, sections were subjected to incubation with a peroxidase linked donkey anti-rabbit secondary antibody (1:750, Jackson Immuno Research) for 1 hour at room temperature and then incubation with a green tyramide amplification reagent (1:50, Perkin Elmer) for 10 minutes. Sections underwent a mild retrieval protocol via microwaving in citrate buffer before incubation with one of three second primary antibodies, overnight at 4°C, which are as follows: rabbit anti-CD31 (1:50, Abcam), rabbit anti-αSMA (1:250, Abcam) or rabbit anti-PDGFRβ (1:250, Abcam). The following day, sections were again subjected to incubation with a peroxidase linked donkey anti-rabbit secondary antibody (1:750, Jackson Immuno Research) for 1 hour at room temperature. Slides were finally incubated with a red tyramide signal amplification reagent (1:50, Perkin Elmer) before mounting with Vectashield DAPI medium (Vector labs). Images were taken using a Leica SP5 confocal microscope under the following channels and excitations/emissions: DAPI (blue); 405nm/482nm, FITC (green); 488nm/530nm and TRITC (red); 543nm/650nm. Images were analysed using Fiji (is just Image J) software (Schindelin et al. 2012).

Measurement of fibrotic injury

C57BL6/J mouse kidneys in sham (n=6) or ANGII DOCA salt (n=5) mice were perfusion fixed with 4% paraformaldehyde (PFA) and incubated at 4°C in 4% PFA for 24 hours before replacing with 70% ethanol. Kidneys were paraffin embedded, dried and sectioned at 4µm. Following dewaxing and dehydration, slides were stained with Picrosirius red. Three sections were taken per kidney, at least 50 µm apart. Ten non-overlapping images were taken per kidney across the cortex and medulla using an Olympus BX51 light microscope at a 20x objective. Images were analysed using Image J software by converting to an RGB stack and setting thresholds to detect red collagen staining. This was done for overall interstitial fibrosis and perivascular fibrosis. For the latter, area fibrosis (pixels) was normalised to the mean of each vessel thickness (pixels). Data are presented as mean ± s.d area collagen staining *(AU)* per 20x image. Statistical analysis was performed by unpaired t-test.

ELISAs

Urine from both Sham (n=10) and ANGII DOCA salt (n=9) mice at baseline and pre-terminal time points were analysed via commercial ELISA kits for albumin (Mouse Albumin ELISA Kit; Abcam), KIM-1 (Mouse TIM-1/KIM-1/HAVCR Quantikine ELISA Kit; R&D Bioteche) and 8-isoprostane (8-Isoprostane ELISA Kit; Cayman Chemical). For 8-isoprostane analysis, samples were treated with butylated hydroxyl-toluene (BHT, 0.005%) upon collection and immediately frozen at -80°C. For KIM-1 and albumin ELISA analysis, samples were immediately frozen after collection at -20°C. Data are presented as mean ± s.e.m. Statistical analysis was performed by unpaired t-test.

qPCR

RNA extraction from frozen kidney and aorta samples was carried out using the RNAeasy Micro Kit (Quiagen). RNA integrity was checked by running RNA samples on a 1.2% agarose gel containing 0.6% ethidium bromide for 2 hours at 100V and visualising bands under UV light. RNA quantity was measured using the Nanodrop-1000 spectrophotometer (Labtech International). 1µg of RNA was used to generate cDNA using Applied Biosystem High Capacity cDNA Reverse Transcription Kits (Thermo Fischer Scientific). Taqman gene assays (Thermo Fisher Scientific) were used in conjunction with the Lightcycler 480 (Roche) to measure mRNA levels of various genes between Sham (n=10) and ANGII DOCA salt (n=8) mouse kidneys;

probes detailed in the table below (See Table 2.2). Data are presented as mean ± s.e.m. Statistical analysis was performed by unpaired t-test.

Table 2.2 - Taqman probes used in qPCR

Gene	NCBI Reference Target Sequence	Cat #
hprt	NM_013556.2	Mm_03034075_m1
kim-1	NM_001166631.1	Mm_00506686_m1
col1a1	NM_007742.3	Mm_00801666_g1
col3a1	NM_009930.2	Mm_01234476_m1
cd68	NM_001291058.1	Mm_00839636_m1
arg1	NM_007482.3	Mm_00475988_m1
nos2	NM_010927.3	Mm_00440502_m1
il1β	NM_008361.3	Mm_01336186_m1
cd31	NM_001305158.1	Mm_01242584_m1
acta2	NM_007392.3	Mm_00725412_m1
pdgfrβ	NM_008809.2	Mm_00735546_m1
p2x7r	NM_011027.3	Mm00440578_m1

End Point PCR

RNA extraction from frozen kidney samples was carried out using the RNAeasy Micro Kit (Quiagen). RNA integrity was checked by running RNA samples on a 1.2% agarose gel containing 0.6% ethidium bromide for 2 hours at 100V and visualising bands under UV light. RNA quantity was measured using the Nanodrop-1000 spectrophotometer (Labtech International). 1µg of RNA was used to generate cDNA using Applied Biosystem High Capacity cDNA Reverse Transcription Kits (Thermo Fischer Scientific).

A KOD Hotstart PCR Kit (INFO) was used to amplify *p2x7* gene variants as detailed in the table below (**Table 2.2**). Resultant cDNA was then ran on a 1.2% agarose gel containing 0.6% ethidium bromide for 1.5 hours at 80V, with bands visualised under UV light. Primers were used to observe the presence or absence of *p2xr7* variants in Sham kidneys (n=7), ANGII DOCA salt kidneys (n=7), Sham aorta (n=8) and ANGII DOCA salt aorta (n=8).

Table 2.2 - *p2xr7* primers used for end-point PCR

Gene	NCBI Reference Target Sequence	Primer sequence	Annealing temp.	Amplicon length
p2x7a variant	NM_011027.3	FWD: 5' - CTGTGTGCATTGAC TTGCTC - 3' REV: 5' - CAGTAGGGATACT TGAAGCC - 3'	61°C	745bp
p2x7c variant	NM_001038845.2	FWD: 5' - CTGTGTGCATTGAC TTGCTC - 3' REV: 5'- TCAGGTGCGCATAC ATACATG - 3'	62°C	286bp

FACS analysis of kidneys

Kidneys from Sham (n=6) and ANGII DOCA salt mice (n=6) were halved, diced and added to a digestion buffer comprised of collagenase V (Sigma), collagenase D (Roche), dispase (Gibco) and DNase (Roche). This mixture was then incubated at 37°C for 45 minutes. Samples were then immediately removed to ice and 2ml ice-cold FACS buffer (2% FBS in PBS) was added. This solution was then filtered at 70µm and 40µm before spinning at 500xg at 4°C for 5 minutes. The resultant cell pellet was incubated for 1 minute with red blood cell lysis buffer before adding 15ml ice-cold FACS buffer. This solution was again spun at 500xg at 4°C for 5 minutes. Cell pellets were resuspended in 1ml FACS buffer. Fc receptors were blocked at 4ºC for 20 minutes with anti-mouse or anti-human CD16/CD32 antibody (BD Biosciences). Primary conjugated antibodies (PE-PDGFRβ - Biolegend, BV-CD31 - Biolegend, CY7-F4/80 - eBioscience and FITC-LTL - Vector) were added to the samples at 1:100, before vortexing and incubating at 4°C for 30 minutes. Cells were then washed in FACS buffer before cell sorting using an Aria FACS sorter (BD Biosciences). Analysis

was carried out using FlowJo analysis software. FMO controls were included for each fluorescent antibody used.

Western blot

Whole kidneys were homogenized in 250mmol/L sucrose, 10mmol/L triethanolamine isolation buffer with added protease inhibitors (Cocktail set III, Thermoscientific). Following quantification of total protein content of each kidney sample by BCA Protein Assay Kit (Pierce), samples were added to Laemli buffer containing 2-mercaptoethanol and 48µg of each sample separated by SDS-PAGE on Precise Protein 12% gels (Thermoscientific). A segment of gels was taken for Coomassie staining and the remainder subject to semi-dry transfer after which the membranes were blocked in skimmed milk and incubated overnight at 4°C with primary antibody. Primary rabbit polyclonal antibodies against the P2X1 (1:100, APR-001, Alomone Labs), P2X4 (1: 1000, APR-002, Alomone Labs), and P2X7 ((i) intracellular targeting APR-004 at 1:500 and (e) extracellular targeting APR-008 at 1:500, Alomone Labs) were used. A goat-antirabbit HRP secondary antibody (1:10,000, Santa Cruz Biotechnology) was then added and the bands visualized by ECL. Band intensity was quantified by densitometry using ImageJ software(Schindelin et al. 2012). Values were normalized to the total protein intensity (as visualised by Coomassie staining) at the appropriate molecular weight. Data are presented as mean ± s.e.m. Statistical analysis was performed by unpaired t-test, normal distribution assumed.

Renal Functional Studies

Mice were anaesthetized with an IP injection of thiabutabarbital sodium salt hydrate (110mg per kg BW). Supplemental doses of anaesthesia were administered as required by monitoring toe reflex. Once a stable level of anaesthesia was obtained, mice were placed on a surgical table with servocontrol of temperature to maintain body temperature at 37°C. Renal clearance studies were performed as previously described (Zhao & Navar 2008). After shaving the incision site, a tracheotomy was performed with polyethylene (PE)-90 tubing. The right jugular vein was cannulated with PE-10 tubing and a bolus injection of isotonic saline given. The right carotid artery was cannulated with PE-10 tubing for continuous measurement of BP and blood sampling. BP was recorded continuously at 1 kHz via a brass transducer (MLT844; Capto) connected to a Powerlab (AD Instruments). After surgery, an isotonic saline solution

containing 0.25% FITC Inulin and 0.5% PAH was infused at 0.2mL/10 g BW/hour. After a 60-minute equilibration period, urine was collected for 40 minutes. Either AZ11657312 (6.2mg/kg) (Sham; n=6, ANGII-DOCA salt; n=4) or 0.1% DMSO vehicle (Sham; n=5, ANGII-DOCA salt; n=4) was then injected intravenously. A subsequent urine collection of 40 minutes was then performed. Plasma samples were taken before and after each urine collection period with a terminal plasma sample being taken at the end of the experiment. Inulin-FITC and PAH assays were carried out as previously described to determine concentration (Lorenz & Gruenstein 1999; Bratton & Marshall 1939; Smith et al. 1945).

The following calculations were then used to determine renal functional values:

$C_x = (U_x \times V) / P_x$

$C_{inulin} = GFR$

$C_{PAH} = eRPF = RPF \times 0.9$

$RBF = (eRPF/0.9) \times (1/[1\text{-haematocrit}])$

$FE_x = (U_x \times P_{inulin}) / (P_x \times U_{inulin})$

$U_V = V \times U_x$

$RVR = MABP/RBF$

Where:

C = clearance
x = cleared substance
U = urinary concentration
V = flow
U_V = urine flow
P = plasma concentration
eRPF = effective renal plasma flow
RPF = renal plasma flow
RBF = renal blood flow
Inulin = FITC-inulin
PAH = para-aminohippuric acid
FE_x = fractional excretion of *x*
RVR = renal vascular resistance
MABP = mean arterial blood pressure, measured under anaesthesia

Data are presented as mean ± s.e.m. Statistical analysis was performed by unpaired t-test.

Vascular Tone Studies

Vascular contractile force was measure by wire myography of C57BL6/J mouse vessels. Mice were asphyxiated with CO_2 and the aorta was isolated and placed in ice cold physiological salt solution (PSS; 119.0mM NaCl, 3.7mM KCl, 2,5mM $CaCl_2$, 1,2mM $MgSO_4$, 25.0mM $NaHCO_3$, 1.2mM KH_2PO_4, 27.0μM EDTA, 5.5mM D-glucose). Vessels were cleaned of fat, cut into 1mm rings and mounted onto a wire myograph (Danish MyoTech). The wells each contained 6ml PSS perfused with 95% O_2 and 5% CO_2 at a temperature of 37°C. The vessels were stretched to a basal tone (aortas: 7.34mN) and left to equilibrate for at least 30 minutes before setting the baseline measurement to 0mN. Initial contractility was measured by adding 125mM KCl (KPSS) to each well in place of PSS. For measurements of changes in vessel function in ANGII DOCA salt mice, compared to Sham (ANGII DOCA salt mice; n=9, Sham mice; n=10), vessels were subject to phenylephrine (PE, Sigma; $1x10^{-9}$ – $1x10^{-6}$M), acetylcholine (Ach, Sigma; $1x10^{-9}$ – $1x10^{-5}$M) and sodium nitroprusside (SNP, Sigma; $1x10^{-9}$ – $1x10^{-5}$M). These mouse vessels were then split into groups treated with either P2X7 antagonist A438079 (Tocris) at 10μM (ANGII DOCA salt; n=5, Sham; n=5) or vehicle (ddH_2O) of the same volume (ANGII DOCA salt mice; n=4, Sham; n=5). Vessels were then subject to a single dose of P2X7 specific agonist BzATP (Tocris) at 50μM and the resultant vascular constriction monitored. This study was repeated with the same protocol, using larger group sizes - P2X7 antagonist A438079 (Tocris) at 10μM (ANGII DOCA salt; n=8, Sham; n=8) or vehicle (ddH_2O) of the same volume (ANGII DOCA salt mice; n=8, Sham; n=8).

A separate vascular tone study to monitor the effects of BzATP on endothelial cell mediated constriction was also carried out. The same protocol for this study was used, with the exclusion of the use of P2X7 antagonist A438079 and the exclusion of SNP. In this study, all aortas were from male C57BL6/J mice aged 10 weeks. Before mounting vessels onto the myography half of the vessels were denuded (n=8) and the endothelium mechanically removed via rubbing a metal insect pin across the inside of

the vessel. The other half of the vessels, i.e. intact vessels (n=8) were undisturbed before mounting.

Data is presented as mean percentage ± s.d of KPSS response for contractile responses, or as mean percentage of max preconstriction ± s.d for dilatory responses, plotted against –log concentration. Statistical analysis was performed by two-way ANOVA with Bonferroni post-hoc test where appropriate.

Statistical Analysis

Analysis was carried out on GraphPad Prism 5.0. Outliers, as determined as outside the range of two standard deviations from the mean, were excluded from data analysis. Data presentation and statistical analysis are detailed under each subheading.

Chapter 3: Establishment and characterisation of an ANGII DOCA salt mouse model of early vascular renal disease

3.1 Introduction

In order to study the role of P2X7 in early CKD, it was necessary to establish and characterise a mouse model representative of this stage of disease. The model chosen was a variation of the angiotensin deoxycorticosterone salt (ANGII DOCA salt) model first described by Kirchhoff and colleagues in 2008 (Kirchhoff et al. 2008). This model involved a 3-week study of uninephrectomised mice on a high salt diet and implanted with an ANGII minipump and DOCA pellet. This group saw heavy fibrosis with high blood pressure, inflammation and albuminuria, which far surpassed the level of injury required for our criteria. We therefore modified this model, forgoing the uninephrectomy and reducing the ANGII dose 10-fold, from 1000ng/kg/min to 100 ng/kg/min. The study was also limited to 4 weeks, in order to maintain the chronic nature of the disease. Control mice were sham operated, implanted with a saline minipump and blank pellet in place of DOCA, and were kept on standard chow.

A full characterisation of the model was then undertaken, with the eventual intention of investigating the role of P2X7 in the renal vasculature.

3.2 Hypothesis and Aims

From pilot studies and review of the relevant literature, I hypothesise that the ANGII DOCA salt model (Figure 3.1) will capture phenotypes relevant to early CKD, specifically:

- Hypertension
- Vascular dysfunction
- Limited inflammation
- Limited fibrosis

As this model represents early CKD, rather than late CKD, I do not expect to see adverse changes in renal function, such as glomerular filtration rate and renal blood flow.

The aim of this study is to measure the above criteria through a combination of *ex vivo*, *in vivo* and histological techniques.

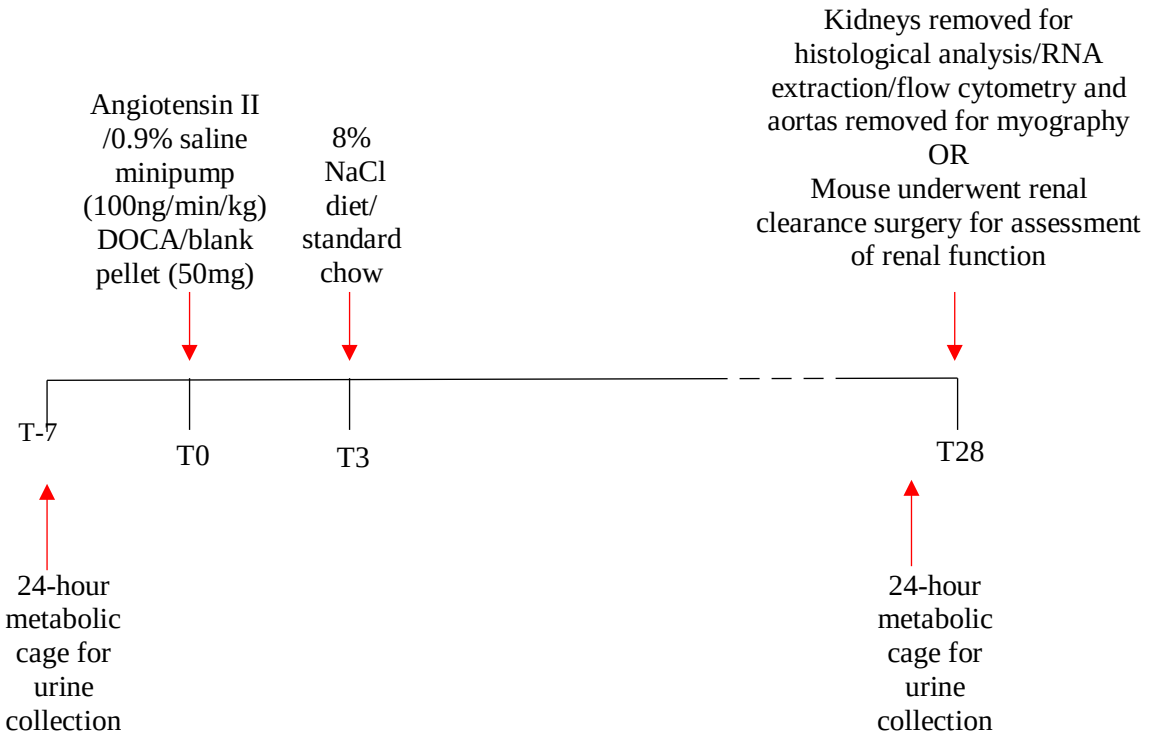

Figure 3.1 - Timeline of Sham and ANGII DOCA salt mice from surgery at day 0 (T0) to cull at day 28 (T28)

3.3 Results

3.3.1 ANGII DOCA salt mice exhibit mild hypertension and changes in sodium and potassium handling, without altering renal function

Over the 4-week experiment, sham mice gained weight, whereas ANGII DOCA salt mice did not and were significantly lighter by week 4 than controls (ANGII DOCA salt: 28.8±0.47g, Sham: 31.5±0.34g at Week 4). ANGII DOCA salt mice also exhibited increased kidney weight compared to Sham (ANGII DOCA salt: 0.072±0.009g/10gBW, Sham: 0.054±0.007g/10gBW at cull) – an effect that was not observed in heart, liver or spleen (Figure 3.2; Figure 3.4).

ANGII DOCA salt mice were also mildly hypertensive with an increased systolic blood pressure (ANGII DOCA salt: 136.5±3.2mmHg, Sham: 113.3±1.9mmHg) but no other significant renal haemodynamic changes were observed (Figure 3.2), when using blood pressure measured under anaesthetic for calculations (Table 3.1).

There was no change in sodium excretion between groups although fractional sodium excretion showed a trend for a small increase in ANGII DOCA salt mice compared to Sham (Figure 3.4). Haematocrit was increased, but not to a significant level (Figure 3.4). A small trend for a decrease in potassium excretion was observed in ANGII DOCA salt mice compared to Sham. However, plasma potassium concentrations were significantly lower in ANGII DOCA salt mice compared to Sham (Table 3.1) and GFR showed a trend to decrease in ANGII DOCA salt mice compared to Sham (Figure 3.2). Therefore, using these parameters to calculate the resultant fractional potassium excretion led to an observed 2-fold increase in the ANGII DOCA salt group compared to Sham (ANGII DOCA salt: 4.1±31.7%, Sham: 1.7±0.7%; Figure 3.3).

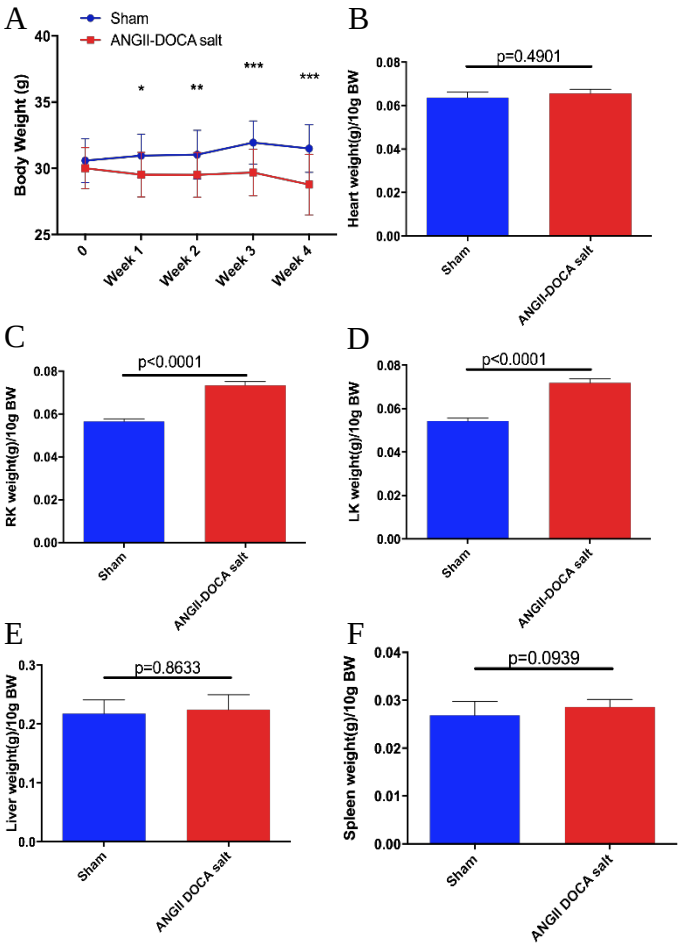

Figure 3.2 - Entire body weight and organ weights in Sham and ANGII DOCA salt mice. (A) Entire body weight of Sham (blue, n=28) and ANGII DOCA salt (red, n=24) mice at weekly time points over 28-day study. Data are mean ± SD, analysed by two-way ANOVA, *p<0.05, **p<0.01, ***p<0.001. (B) Heart weights, (C) right kidney weights, (D) left kidney weights, (E) liver weights and (F) spleen weights at day 28 in grams (g), normalised to 10g body weight (BW) in Sham (blue, n=26) and ANGII DOCA salt (red, n=22) mice. Data are mean ± 95% CI, analysed by t-test.

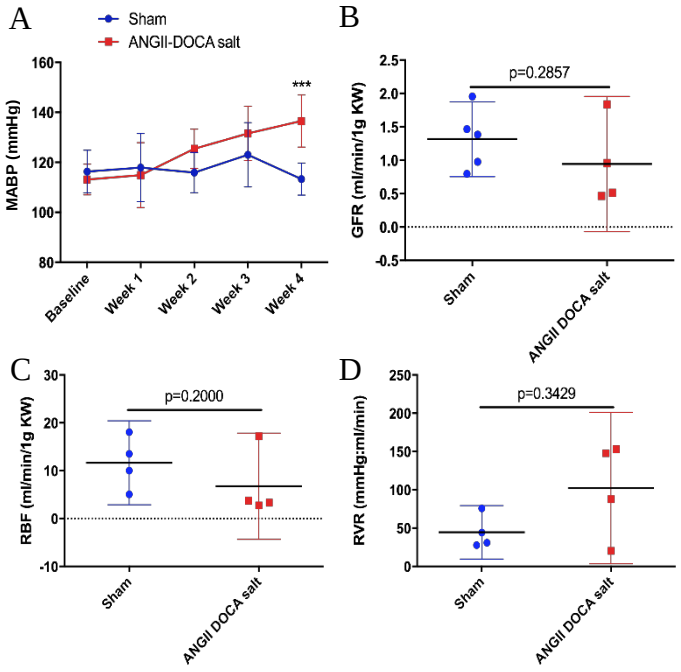

Figure 3.3 - Blood pressure, glomerular filtration rate, renal blood flow and renal vascular resistance in Sham and ANGII DOCA salt mice. (A) Systolic blood pressure (SBP) in ANGII DOCA salt (red, n=11) and Sham (blue, n=12) mice. Data are mean ± SD, analysed by two-wayANOVA, ***p<0.001. (B) Glomerular filtration rate (GFR) normalised to kidney weight, (C) renal blood flow (RBF) normalised to kidney weight and (D) renal vascular resistance (RVR) in ANGII DOCA salt (red ■, n=4) and Sham (blue •, n=4-5) mice. Data are mean ± 95% CI, analysed by t-test.

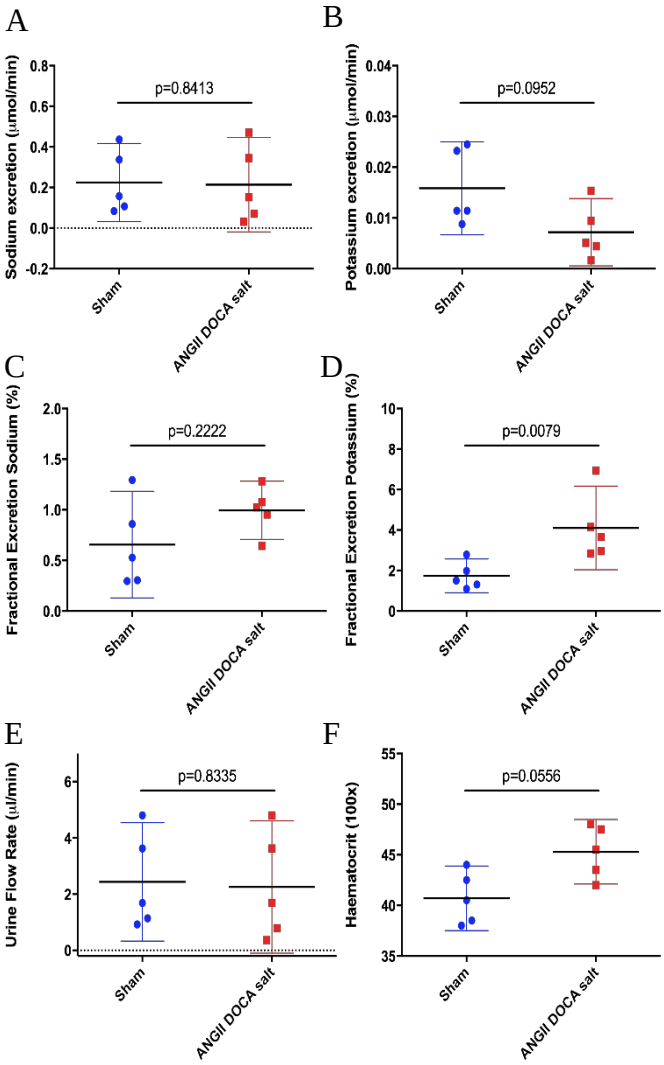

Figure 3.4 – Sodium and potassium handling in Sham and ANGII DOCA salt mice. (A) Sodium excretion, (B) potassium excretion, (C) fractional sodium excretion, (D) fractional potassium excretion, (E) urine flow rate and (F) haematocrit in ANGII DOCA salt mice under anaesthesia (red ■, n=5) and sham (blue •, n=5). Data are mean ± 95% CI, analysed by t-test.

Table 3.1 – Blood pressure and plasma concentrations of sodium and potassium in Sham and ANGII DOCA salt mice

Data are mean ± S.E.M. Data analysis by standard t-test.

Measurement	**Sham mice**	**ANGII DOCA salt mice**	**P value**
Blood Pressure (under anaesthesia; mmHg)	74.2±1.9	75.4±1.7	0.5232
Sodium plasma concentration (mmol)	145.2±1.0	151.4±2.1	0.0794
Potassium plasma concentration (mmol)	3.9±0.1	1.5*	0.0079

* All plasma potassium measurements made in ANGII DOCA salt mice were below the lower limit of detection of equipment used. For the purpose of further calculations, the values for this group were set at the lower limit of detection of 1.5mmol/L.

3.3.2 ANGII DOCA salt mice exhibit increased urinary biomarkers of injury and whole kidney macrophage marker as well as increased levels of PDGFRβ positive cells and renal perivascular fibrosis

Injury marker kidney injury molecule 1 (KIM-1) is increased at the mRNA level in whole kidney (ANGII DOCA salt: 1.17±0.5, Sham: 0.28±0.1) as well as at the protein level in urine (ANGII DOCA salt: 18.5±3.2ng/24H, Sham: 6.7±1.0ng/24H) at pre-terminal time points in ANGII DOCA salt mice compared to Sham mice (Figure 3.5). ANGII DOCA salt mice also have increased levels of albuminuria (ANGII DOCA salt: 357.3±23.2μg/24H, Sham: 22.0±2.1μg/24H) at pre-terminal time points, whereas levels of 8-isoprostane, a marker of oxidative stress, remained constant between groups (Baseline - ANGII DOCA salt: 43.54±4.9pg/24H, Sham: 55.75±4.5pg/24H, Pre-terminal - ANGII DOCA salt: 68.85±6.4pg/24H, Sham: 51.65±8.7pg/24H). In mRNA from whole kidney homogenates, collagen 1 (*col1a1*) marker was increased in ANGII DOCA salt mice compared to sham, but collagen 3 (*col3a1*) (Figure 3.6) was not. Upon investigation at the protein level through immunohistochemistry, collagen deposition was observed at significantly increased levels in perivascular, but not interstitial areas in ANGII DOCA salt mouse kidneys (ANGII DOCA salt: 54.9±3.7pixels, Sham: 40.2±3.2pixels normalised to vessel thickness; Figure 3.6). Collagen deposition was not observed in glomeruli (data not shown). Pan-macrophage marker, *cd68*, was also upregulated in ANGII DOCA salt mice at the mRNA level compared to sham, although there was no change in M1 or M2 specific markers (*nos 2*and *arg1* respectively). There was also no change in markers for vessel density (endothelial marker *pecam-1* and smooth muscle marker *acta2*) or pericytes *(pdgfr*β) between the two groups (Figure 3.5).

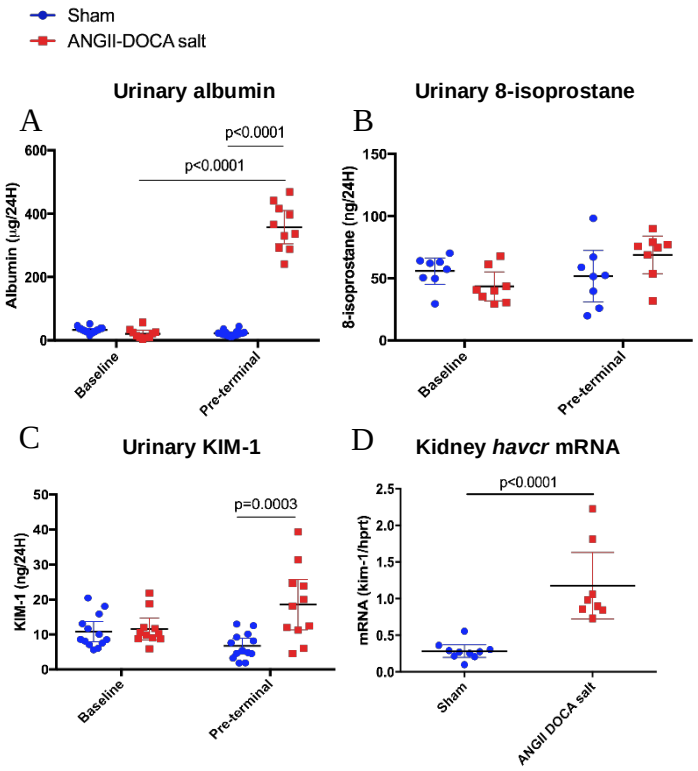

Figure 3.5 – Urinary and whole kidney injury markers in Sham and ANGII DOCA salt mice. (A) Urinary protein levels of albumin, (B) urinary protein levels of 8-isoprostane and (C) urinary protein levels of KIM-1 at baseline and pre-terminal time points of ANGII DOCA salt mice (red, ■, n=8) and sham (blue •, n=10). (D) Whole kidney mRNA levels of *hepatitis a virus cellular receptor 1 (havcr1;* gene for KIM-1 protein*)* at cull. Data are mean ± 95% CI. mRNA *kim-1* data analysed by t-test, all other data analysed by two-way ANOVA.

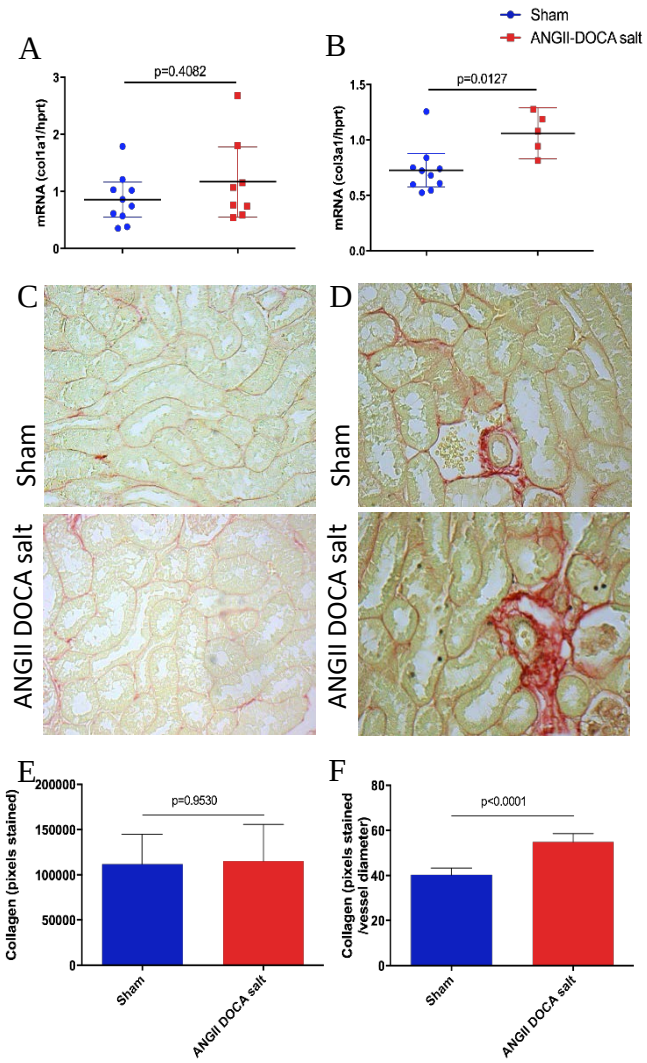

Figure 3.6 – Collagen marker levels in Sham and ANGII DOCA salt mice. (A) Whole kidney mRNA levels of *collagen type 1 (col1a1)* and (B) *collagen type 3 (col3a1)* in ANGII DOCA salt mice (red, ■, n=6-8) and sham mice (blue •, n=10). Data are mean ± 95% CI. Kidney sections were stained immunohistologically for collagen by picrosirius red (PSR). Images are (C) interstitium and (D) perivascular areas of Sham (blue, n=5, 3 sections per animal, 10 images per section) and ANGII DOCA salt (red, n=4, 3 sections per animal, 10 images per section) mice. Quantification of pixels positive for collagen in (E) the interstitium and (F) perivascular areas (normalised to vessel diameter) of ANGII DOCA salt and Sham mice. Data are mean ± SD. All data are analysed by t-test.

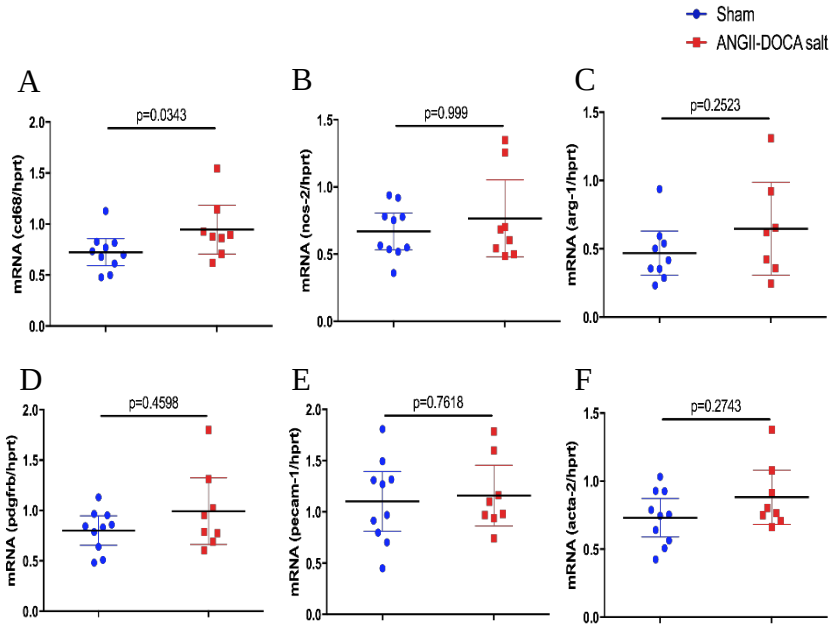

Figure 3.7 – mRNA levels of macrophage markers and vascular density markers in Sham and ANGII DOCA salt mice. mRNA levels of (A) pan-macrophage marker *cd68*, (B) M1 macrophage marker *nitric oxide synthase2 (nos-2)*, (C) M2 macrophage marker *arginase 1 (arg-1)*, (D) pericyte marker *platelet derived growth factor receptor b (pdgfrb)*, (E) endothelial marker *platelet endothelial cell adhesion molecule 1 (pecam-1)* and (F) vascular smooth muscle marker *alpha actin 2 (acta-2)* all normalized to *hprt* housekeeper gene in ANGII DOCA salt mice (red, ■, n=8) and sham (blue •, n=10). Data are mean ± 95% CI, analysed by t-test.

Flow cytometry was also performed on kidney homogenate from Sham and ANGII DOCA salt mice, with separation of tubular cells (LTL +ve), endothelial cells (CD31 +ve), macrophages (F4/80 +ve) and pericytes (PDGFRβ +ve) (Figure 3.8). Counts for tubular cells, endothelial cells and macrophages did not change, however, PDGFRβ +ve counts were significantly higher in ANGII DOCA salt mouse kidneys (Figure 3.).

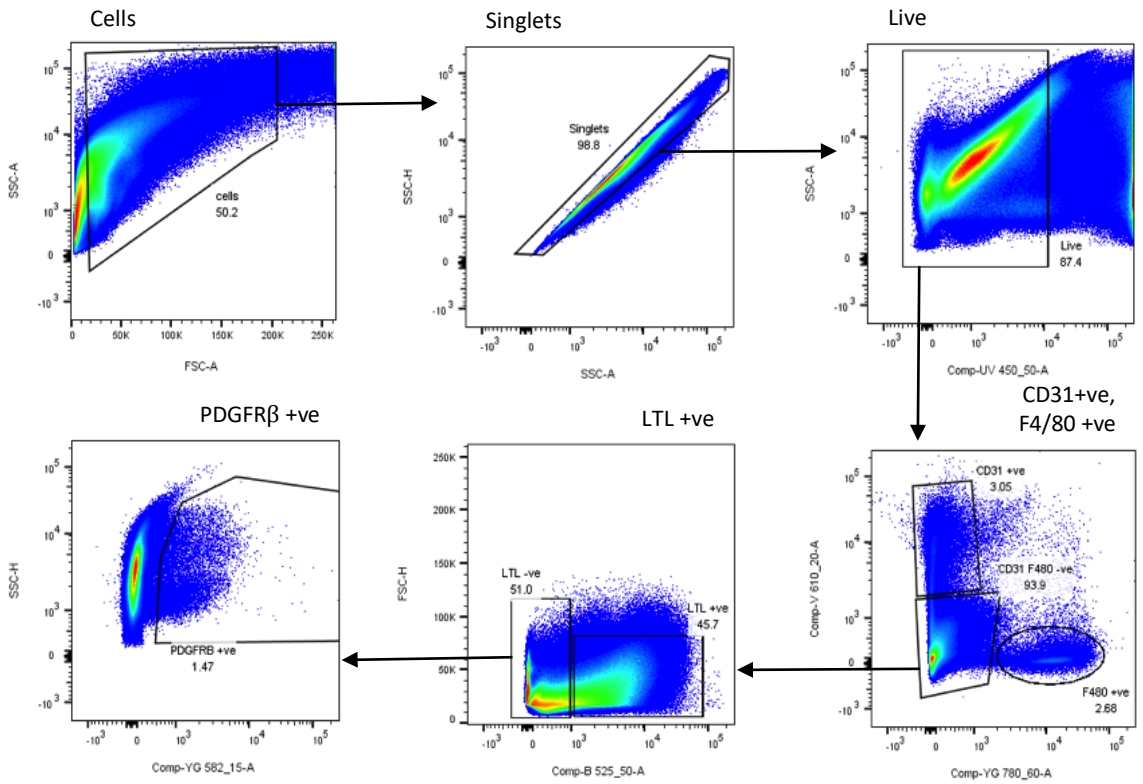

Figure 3.8 – Gating strategy for the separation of endothelial cells (CD31 +ve), macrophages (F4/80 +ve), tubular cells (LTL +ve) and pericytes (PDGFRβ +ve) Demonstration of the gating strategy used to separate cells, with boxes denoting the events identified within the appropriate parameters and arrows following the step by step gating process.

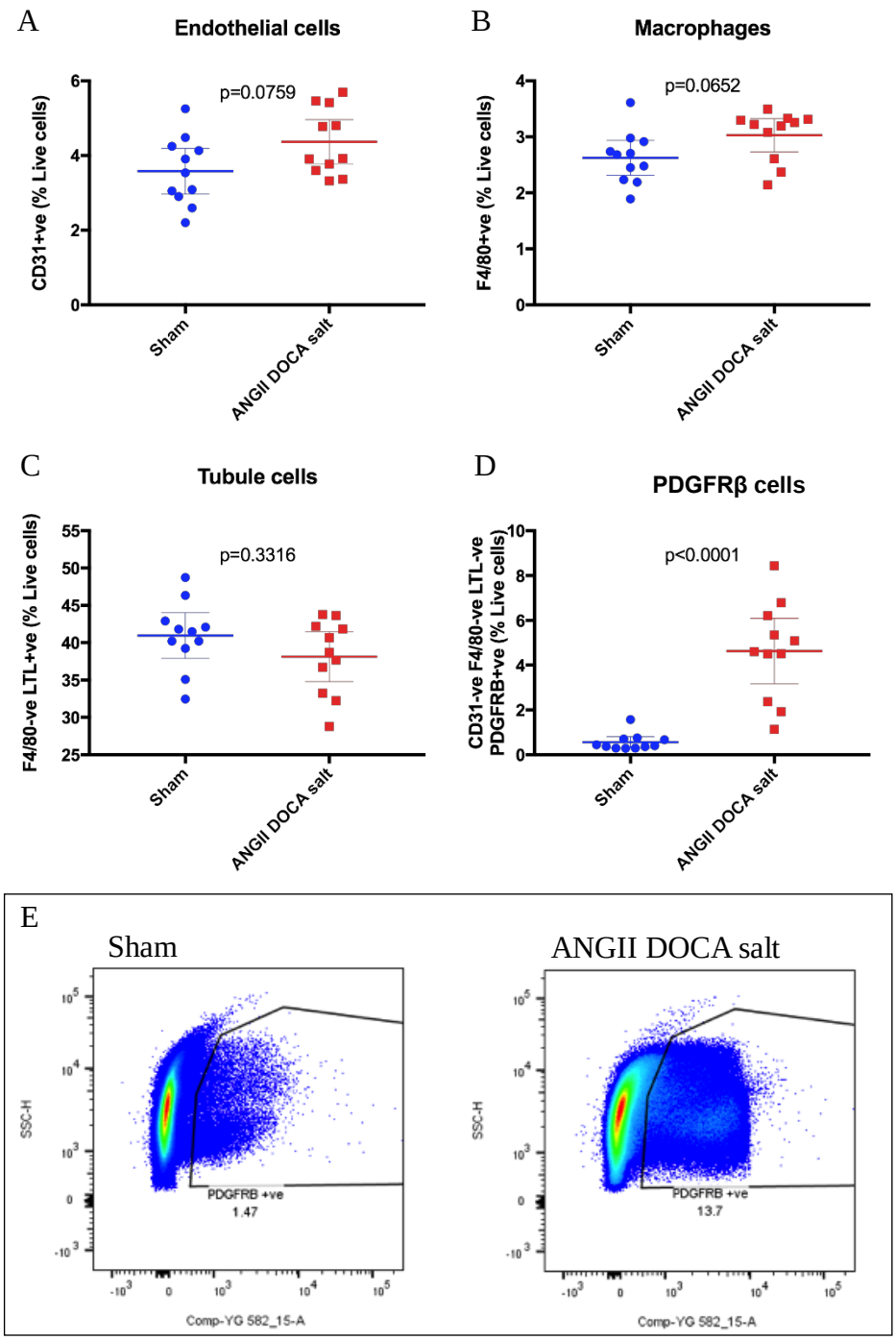

Figure 3.9 – Cell counts of endothelial cell, macrophages, tubule cell and PDGFRβ +ve cell in Sham and ANGII DOCA salt mice. Cell counts of (A) CD31 +ve endothelial cells, (B) F4/80 +ve macrophages, (C) CD31 –ve, F4/80 –ve, LTL +ve tubule cells and (D) CD31 –ve, F4/80 –ve, LTL –ve, PDGFRβ +ve pericytes expressed as percentage live cells in ANGII DOCA salt mice (red, ■, n=11) and sham (blue •, n=12). Data are mean ± 95% CI, analysed by t-test. (E) A visual example of raw data showing increased CD31 –ve, F4/80 –ve, LTL –ve, PDGFRβ +ve cell count events in an ANGII DOCA salt mouse kidney (right) compared to Sham (left).

3.3.3 Aortas from ANGII DOCA salt mice are hyper-responsive to both phenylephrine and acetylcholine, but not sodium nitroprusside

In aortas from ANGII DOCA salt mice, contractile response to phenylephrine (PE) was increased compared to those from Sham mice, as was endothelium-dependant dilatory response to acetylcholine (Table 3.3;Figure 3.10). However, smooth muscle-mediated vasodilator sodium nitroprusside (SNP) was the same in both groups (Table 3.3; Figure 3.10).

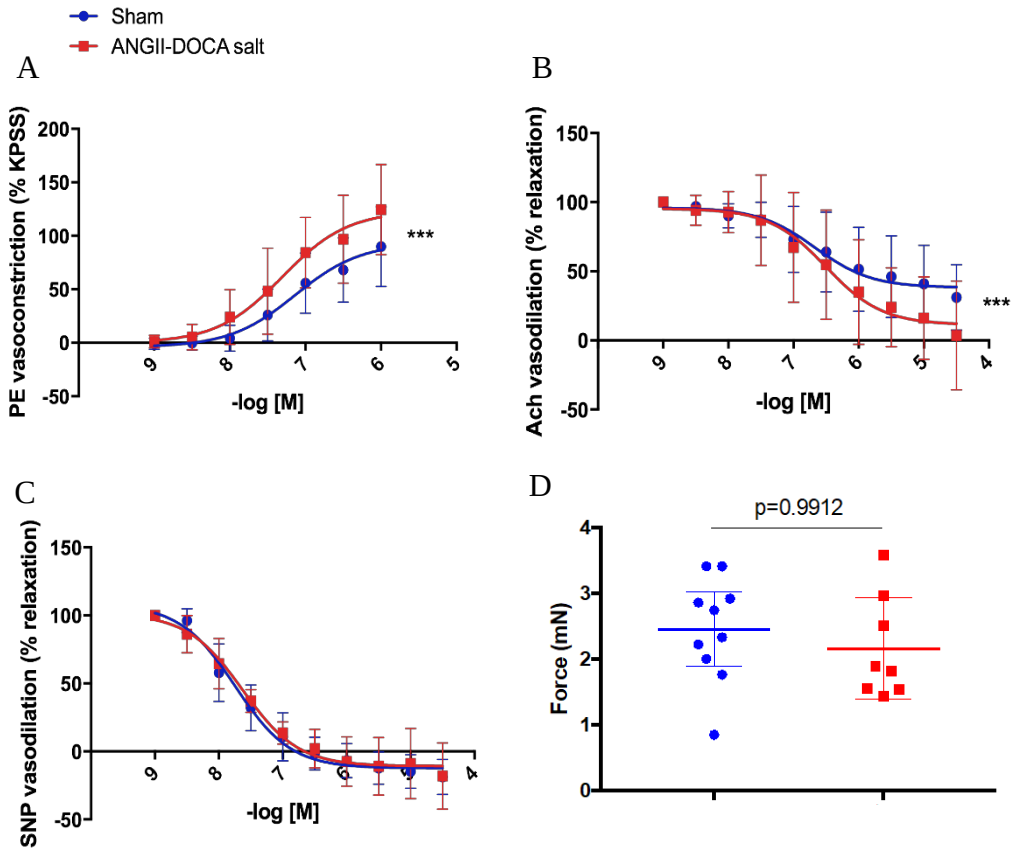

Figure 3.10 – Dose response curves of aortas from Sham and ANGII DOCA salt mice to phenylephrine, acetylcholine and sodium nitroprusside. Response of aortas from ANGII DOCA salt mice (red, ■, n=8) and Sham mice (blue •, n=10) to (A) vasoconstrictor phenylephrine (PE), displayed as percentage force (mN) of maximum force (mN) as determined by (125mM) KCl response, and vasodilators (B) acetylcholine (Ach) and (C) sodium nitroprusside (SNP), displayed as percentage force (mN) of force (mN) at EC50 PE. Data points are mean ± SD with non-linear regression. All data are analysed by two-way ANOVA. (D) Response of same vessels to 125mM KPSS displayed as force in millinewtons (mN). Data points are mean ± 95%C.I. Data are analysed by t-test.

Table 3.3 - EC_{50} and maximal responses of vessels to vasoactive pharmacological agents. EC_{50} expressed as – log [concentration in M] and maximal response of aorta from Sham and ANGII DOCA salt mice to phenylephrine (PE; $1.0E^{-6}$M), acetylcholine (Ach; $1.0E^{-5}$M), sodium nitroprusside (SNP; $1.0E^{-5}$M) and 125mM KCl. PE responses are expressed as %KCl response, Ach and SNP responses are expressed as 100 – % relaxation, KCl responses are expressed in millinewtons (mN). Data are mean±S.E.M.

Group	- log EC_{50} PE [M]	Maximal response to $1.0E^{-6}$M PE (%KPSS)	Maximal response to $1.0E^{-5}$M Ach (%relaxation)	Maximal response to $1.0E^{-5}$M SNP (%relaxation)	Maximal response to 125mM KCl (mN)
Sham	6.36	89.96±11.9	68.98±7.5	118.83±4.1	2.45±0.25
ANGII DOCA salt	6.93	124.51±14.9	96.46±13.9	118.03±8.63	2.16±0.28

3.4 Discussion

In 2008, Kirchhoff and colleagues established a novel model of renal fibrosis in renal injury-resistant C57BL6 mice. Combining a uninephrectomy, administration of high doses of ANGII and DOCA and a high salt diet, the resultant phenotype included moderate hypertension, significant albuminuria, heavy interstitial fibrosis and increased infiltration of macrophages (Kirchhoff et al. 2008). Kirchhoff's model has been used in the study of endoplasmic reticulum stress inhibition and prostaglandin receptor biology in hypertension in rodents (Mohammed-Ali et al. 2017; Bartlett et al. 2012).

This model differs from other models of renal injury such as uninephrectomy, ANGII or DOCA-salt in that it takes numerous components from all of the above to build a multi-factorial model of fibrosis. Individually, DOCA acts to increase salt appetite and to act as a precursor for aldosterone, promoting sodium reabsorption, all of which is augmented with the addition of a high salt diet. ANGII adds to this, not only by increasing aldosterone release, but by acting as a potent vasoconstrictor and vascular remodelling factor. CKD is, in itself, a multifactorial disease, often without a single underlying causation and so combining these factors in a multi-factorial approach in rodents may be a more accurate reflection of human disease (Gansevoort et al. 2013; Norman & Fine 2006; Long et al. 2012; Bidani et al. 2013).

In this study, we used Kirchhoff's model as a basis from which to establish a model of renal vascular dysfunction in mice, with the ANGII and DOCA salt components well defined as contributors to vascular dysfunction (Monassier et al. 2006). However, our criteria were to promote vascular dysfunction, hypertension and mild injury, without inducing heavy interstitial fibrosis or distinct changes in renal function as defined by significant changes in GFR and RBF. We therefore omitted the uninephrectomy and reduced the ANGII dose 5-fold to 100ng/kg/day, although the DOCA administration was kept the same (50mg pellet).

In this study, hypertension was still established, but to a much smaller degree than that seen in Kirchhoff's study, with ANGII DOCA salt mice exhibiting a mild increase in systolic blood pressure of approx. 25 mmHg opposed to the 50mmHg Kirchhoff and colleagues observed. As would be expected in mice fed a high salt diet, sodium

handling in ANGII DOCA salt mice was mildly altered. The potassium plasma concentrations reported, however, were not realistic representations of actual concentrations, as they were below the limit of lower detection of 1.5mmol. Plasma levels that are this low would cause serious side effects and mortality in mice, which were not observed. I therefore expect that this inaccuracy is due to the equipment used, which was designed for clinical use, rather than animal use. Research into more appropriate and accurate methodology is required. Haematocrit was slightly, but not significantly, increased in ANGII DOCA salt mice compared to Sham, indicating a possible decrease in plasma volume, and a potential effect on calculating renal blood flow and renal plasma flow. However, as the difference in haematocrit did not reach significance between the groups, this was not considered moving forwards with renal clearance calculations.

Kidney weight was increased in ANGII DOCA salt mice compared to Sham, which indicates fibrosis, however, this result is not reliable, as the kidney weights were normalised to body weights, a data set that differed significantly between Sham and ANGII DOCA salt mice, with ANGII DOCA salt mice exhibiting a drop in body weight over the 4 week study and Sham mice maintaining their body weight. I would suggest that in future studies, tibias be taken at Week 4 after cull and used to normalise kidney weight, as this is a measurement that should not differ between groups.

Injury marker, KIM-1 was increased, both at whole kidney mRNA level and protein level in urine in ANGII DOCA salt mice, indicating injury of the renal tubules. The increase, however, was about 2-3 fold, much lower than increases usually seen in kidney injury models, suggesting only mild injury. ANGII DOCA salt mice also exhibited significant albuminuria consistent with an increase in intraglomerular pressure and/disruption of the glomerular filtration barrier. This observation was coupled with an increase in mRNA levels of collagen isoform *col1a1*, although *col3a1* remained unchanged. Upon immunohistochemistry investigation, collagen deposition was limited to perivascular areas, and not evident at high levels in the interstitium, or at all in glomeruli. ANGII DOCA salt mice also exhibited a small trend for decreased GFR and RBF with a resultant increase in RVR, which did not reach significance.

These observations all point to a low level of fibrosis and injury in the kidney. Upregulation of KIM-1 suggests tubulointerstitial injury, yet interstitial fibrosis is not yet established after 4 weeks of treatment in ANGII DOCA salt mice. It does signify, however, that the molecular mechanisms that contribute to fibrosis are in play and it may be that that the perivascular fibrosis seen in this model is the beginning of the fibrotic events that triggers the kidney into a cycle of disease progression. This would concur with Fine's hypoxia hypothesis in which it is thought that the degeneration of the kidney begins with glomerular injury, which leads to loss of microvasculature, hypoxia and fibrosis, with primarily a vascular origin (Fine et al. 1998).

However, levels of endothelial marker, *pecam-1*, were unchanged at the mRNA level, suggesting negligible loss of microvasculature. This data was supported by the observation that, upon FACS sorting of kidney homogenate from ANGII DOCA salt and Sham animals, CD31+ve counts were unchanged between groups. Tubular LTL+ve counts were also maintained, which was expected, given the lack of interstitial fibrosis and maintenance of physiological kidney function as defined by GFR and RBF. F4/80+ve counts for macrophages also remained constant which was unsurprising as infiltrating macrophages are a key marker of tubulointerstitial fibrosis, although mRNA macrophage marker *cd68* was increased, suggesting a shift in molecular signalling of macrophages, if not an increase in actual number.

Perhaps most interestingly, PDGFRβ+ve counts for pericytes are upregulated in ANGII DOCA salt mice. This could be an interpretation of an increase in vascular pericyte number, which may occur as a result of vascular injury. Immunostaining for PDGFRβ in ANGII DOCA salt mouse kidney does show a strong localisation of the pericyte marker at perivascular areas (See Chapter 4).

It has been shown that pericytes can differentiate into myofibroblasts (Abraham et al. 2007), the primary cells that deposit collagen in fibrosis, and that blocking PDGFR related pathways can attenuate fibrosis in a rodent UUO model of fibrosis (Lin et al. 2011). It may be that there is an upregulation of pericytes in the kidney in this model, which leads to an increased transformation into and presence of myofibroblasts, firstly at perivascular areas, which deposit collagen in this area, starting fibrosis progression. However, there was no change seen in mRNA markers *pdgfr*β for pericytes or *acta-2*

for myofibroblasts. This observation, paired with the fact that PDGFRβ is not entirely pericyte specific, warrants further exploration of pericyte markers at the protein level, such as CD146 or NG2, and myofibroblast marker αSMA, in order to confirm this theory. Other cell types, such as vascular smooth muscle cells are also PDGFRβ positive and are also suspects for increase in cell number in models of renal injury. Further distinguishing these cell types through identification of more pericyte or vascular smooth muscle cell specific markers through IHC or more FACs would greatly help in accurately identifying the cell type(s) of interest in this model.

The FACs data shown here incorporates FMO controls to account for background fluorescents and normalises to % live cells. However, sample weights were not taken before processing for FACs analysis. To confirm results in future as absolute results rather than relative one, I would weigh kidneys in order to determine cell number and ensure a more reliable normalisation method.

ANGII DOCA salt mice also exhibited significant vascular dysfunction, through hyper-reactivity of aortas to phenylephrine (PE) and acetylcholine (Ach). PE, a vasoconstrictor, acts on α1 adrenergic receptors on smooth muscle, which have been shown to be upregulated upon ANGII administration (Hu et al. 1995; Abdulla et al. 2011), which may explain the hyper-reactivity of vessels from ANGII DOCA salt mice to PE. ANGII also has a significant effect on vascular remodelling, increasing vascular density through smooth-muscle mediated hypertrophy (Hatakeyama et al. 1994; Montezano et al. 2014), so the PE receptor population could also be increased through increased smooth muscle mass within vessels. Further investigation into these receptor populations would be required to explain this phenomenon. Acetylcholine and SNP are both vasodilators, with Ach acting in an endothelial dependent manner and SNP acting in an endothelium independent manner. Hyper-reactivity was observed in ANGII DOCA salt aortas in response to Ach, but not SNP, suggesting that changes in vasodilatory capacity of vessels is due to changes within the endothelium, possibly through modulation of the endothelial nitric oxide synthase (eNOS) pathway by ANGII, which is linked to Ach receptor activation (Förstermann & Münzel 2006). Again, further investigation into single components of this pathway would be required in order to elucidate the mechanism behind this.

Finally, there was a small increase in pan-macrophage marker, *cd68*, in whole kidney of ANGII DOCA salt mice, which could not be defined as either pro-inflammatory M1 or alternatively activated M2 phenotype through measurements of respective markers *nos2* or *arg1*, suggesting only a small amount of macrophage infiltration in ANGII DOCA salt mice kidneys. This is only a small indicator of inflammatory status and further investigation into macrophage infiltration, through immunohistochemical analysis ideally separating the M1/M2 phenotype, would be key in exploring this further.

This model, in conclusion, produces a phenotype of mild hypertension and renal injury, which manifests primarily as perivascular fibrosis and vascular dysfunction. However, before this model is taken forward, it would be sensible to investigate further parameters, such as vascular dysfunction in resistance vessels, as well as the conduit vessels observed in this study. Other measurements, such as macrophage infiltration into vasculature and glomeruli, would also give valuable insights into the inflammatory status of kidneys of ANGII DOCA salt mice.

Data collected thus far indicates that this is a valuable model of renal vascular pathophysiology, with current vascular dysfunction models not specifically targeting renal vessels. Not only this, but this model takes a multi-factorial approach without single causation, as is the case in early stages of human CKD. This model may be used for the investigation of biological agents in early CKD, particularly of those pathways contributing to vascular dysfunction evident at early stages of disease. Coupled with advances in early diagnosis of CKD through biomarker technology (Lopez-Giacoman & Madero 2015), this may aid in identifying novel drug targets for the treatment of CKD before fibrosis, renal dysfunction and significant renal damage are established. For our purposes, this model is used to represent early, vascular injury stages of CKD, in which the role of P2X7 can be investigated.

Chapter 4: P2X7 expression and localisation in WT C57BL6 mouse renal vascular and ANGII DOCA salt mice

4.1 Introduction

P2X7 has been extensively studied, primarily in cells associated with immunity and inflammation and in cells associated with pain (Lister et al. 2007). P2X7 has also been studied in the kidney and is upregulated upon a variety of renal insults at the whole kidney level (Vonend et al. 2004b; Kim et al. 2014) However, the expression and localisation of P2X7 specifically in the renal vasculature is less well known.

In terms of renal vessels, P2X1 is known for its role in autoregulation (Inscho et al. 2003). However, other P2X receptors aren't so well characterised and with regards to P2X7, most studies have been carried out in the rat. In the rat, expression of P2X7 is present in mesangial cells, within the glomerulus, and within the endothelium of renal vessels (Inscho 2009; Turner et al. 2003; Lewis & Evans 2001). More recently in rats, the presence of P2X7 has been found in the endothelium of preglomerular vasculature and interlobar renal arteries, with upregulation and extension to the smooth muscle upon ANGII administration (Menzies et al. 2013; Menzies et al. 2015). P2X7 has also been identified in human endothelial cells (Yamamoto et al. 2000). However, the localisation of P2X7 in the mouse renal vasculature remains largely unexplored.

In order to better understand the role of P2X7 in the renal vasculature of the mouse, it was necessary to undertake a thorough investigation into the localisation and expression of P2X7 in this location. An immunofluorescent method was optimised and validated via P2X1 staining. Further immunofluorescent experiments, co-localising P2X7 to various renal vascular cell types was undertaken, in both sham-operated control and ANGII DOCA salt mouse kidneys. Whole kidney western blot analysis was also carried out, with qPCR results to follow.

4.2 Hypothesis and Aims

I hypothesise that P2X7 will be present in the renal vasculature of mice, particularly in cell types that play a role in modulation of vascular tone; endothelial cells, vascular smooth muscle cells and pericytes. From review of the literature, I hypothesise that P2X7 will be present at higher levels in the ANGII DOCA salt mouse model of vascular renal injury.

The aim of this research is to perform an in-depth localisation study using antibodies targeted to two different epitopes of P2X7, an intracellular and an extracellular epitope. P2X7 will be co-localised, via immunostaining and western blotting techniques, to specific vascular cell markers in order define the vascular cells in which P2X7 is expressed.

4.3 Results

4.3.1 P2X7 expression and localisation in the C57BL6 mouse renal vasculature

Two antibodies were used to detect P2X7; one which targets an intracellular epitope, P2X7(i) and one which targets an extracellular epitope, P2X7(e). Through comparing the epitope amino acid sequence to the five P2X7 isoforms reported in the mouse, it is evident that P2X7(e) antibody targets isoforms A, B, C and E and P2X7(i) antibody target isoforms A and E (Figure 4.1).

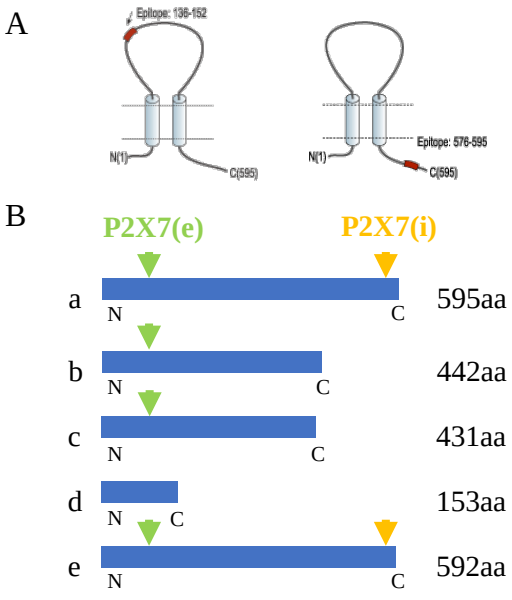

Figure 4.1 - Antibodies used for P2X7 expressions and localisation studies
(A) Two antibodies from Alomone Labs were used for immunofluorescence and western blotting, with each binding to a different set of P2X7 isoforms. (B) P2X7 isoforms represented by blue bars, show amino acid (aa) length, N and C terminals and points at which antibodies bind. P2X7(e) (left) targets an extracellular epitope, present on protein isotopes a, b, c, and e as indicated by green arrows. P2X7(i) (right; yellow) targets an intracellular epitope, present on protein isotopes a and e as indicated by yellow arrows.

These antibodies were used to target P2X7 through western blotting and immunofluorescent techniques. In order to validate these techniques, they were first carried out using a well-documented antibody for P2X1, a member of the P2X family that has been extensively studied in the literature alongside endothelial cell marker CD31. Consistent with the literature, P2X1 was detectable in whole kidney homogenate through western blot (Figure 4.6) and was observed in the smooth muscle of renal vessels (Figure 4.2).

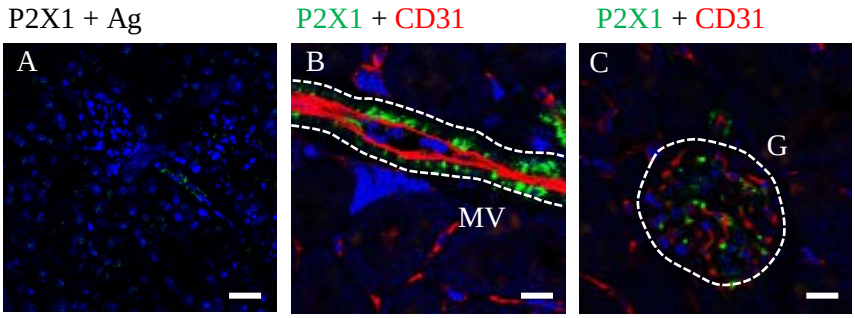

Figure 4.2 - P2X1 expression in the smooth muscle of medium renal vessels and in the interstitium of glomeruli
P2X1 staining (green) (A) pre-incubated with targeted antigen as a negative control, (B) alongside CD31 endothelial (red) staining in a medium renal vessel (V, highlighted with white dashed line) and (C) alongside CD31endothelial (red) staining in the glomerulus (G, highlighted with white dashed line), all with DAPI nuclear staining (blue). Co-localisation (yellow) was not observed. Scale bars = 25µm. All images were taken at 40x objective.

Using the same method with P2X7(e) and P2X7(i) antibodies, kidneys from C57BL6 mice were immunostained for P2X7, alongside vascular markers for endothelium (CD31), vascular smooth muscle (αSMA) and pericytes (PDGFRβ). Depending on the P2X7 antibody used, different expression profiles were observed.

Upon staining using the P2X7(e) antibody, P2X7 was present in renal tubules, glomerular mesangial cells and interstitium. Upon co-staining with vascular markers, P2X7(e) did not localise to the endothelium or smooth muscle of the vasculature. There was co-localisation to pericyte marker PDGFRβ at some focal points throughout the interstitium, but this was not a consistent observation across all PDGFRβ positive cells.

Staining using the P2X7(i) antibody produced different results, with a strong co-localisation of P2X7(i) and CD31 in renal vessel endothelium, both in interstitial vessels and glomerular capillaries. P2X7(i) also localised to PDGFRβ positive cells, particularly at perivascular areas. As with P2X7(e), P2X7(i) did not localise to the vascular smooth muscle. Neither antibody stained positive for P2X7 in *p2xr7*$^{-/-}$ kidney tissue, used as a negative control.

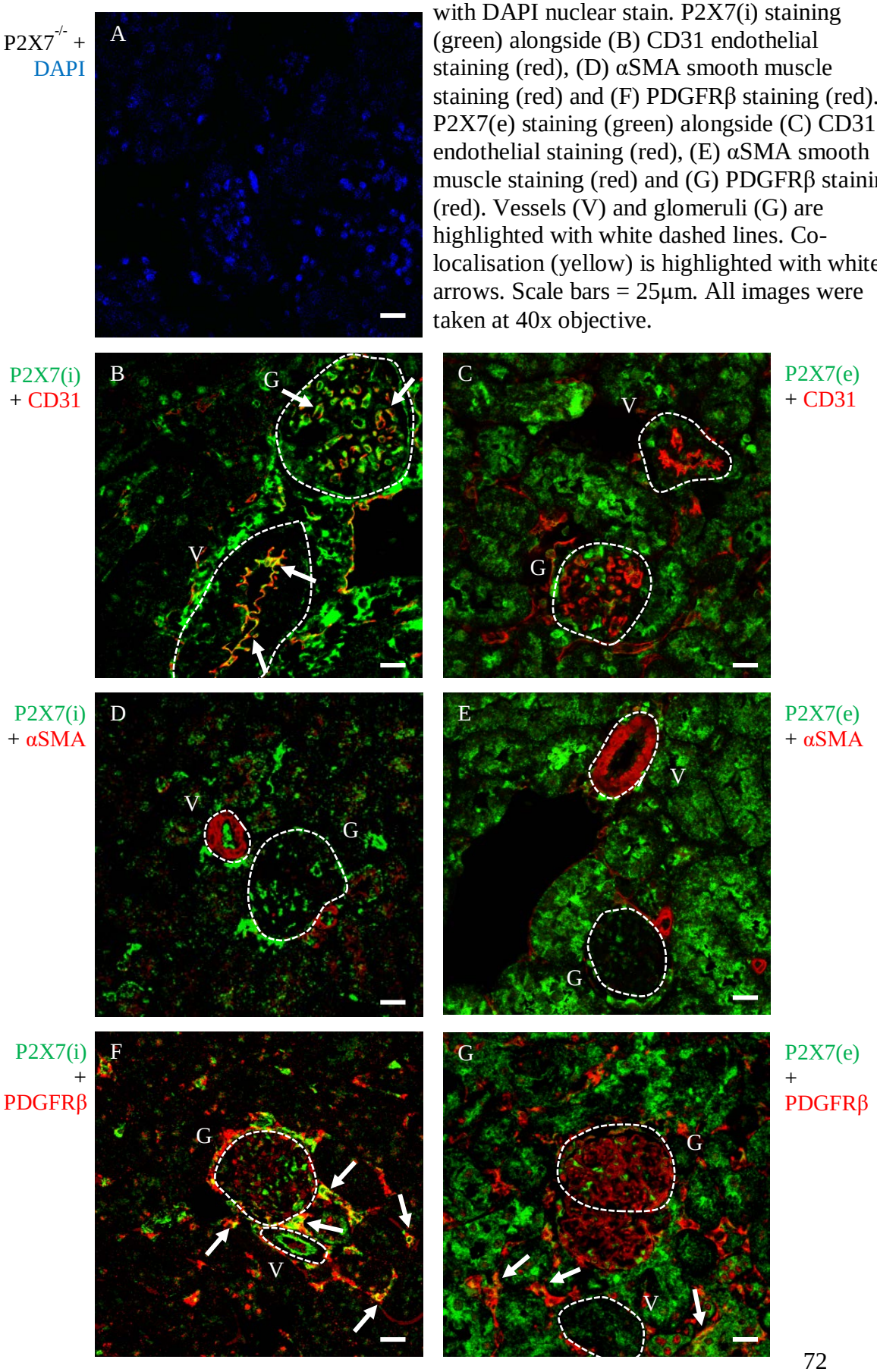

Figure 4.3 - P2X7 expression and vascular markers in the mouse renal vasculature, with two different P2X7 antibodies used. P2X7 staining (green) (A) in *p2x7*$^{-/-}$ kidney with DAPI nuclear stain. P2X7(i) staining (green) alongside (B) CD31 endothelial staining (red), (D) αSMA smooth muscle staining (red) and (F) PDGFRβ staining (red). P2X7(e) staining (green) alongside (C) CD31 endothelial staining (red), (E) αSMA smooth muscle staining (red) and (G) PDGFRβ staining (red). Vessels (V) and glomeruli (G) are highlighted with white dashed lines. Co-localisation (yellow) is highlighted with white arrows. Scale bars = 25µm. All images were taken at 40x objective.

4.3.2 P2X7 expression and localisation in the renal vasculature of the ANGII DOCA salt mouse

The expression pattern observed in C57BL6 mouse kidneys was maintained when kidneys from sham operated and ANGII DOCA salt mice were stained using the same antibodies, co-stained with CD31. P2X7(e) once again localised to renal tubules, interstitium and glomerular mesangium and P2X7(i) to endothelium and perivascular areas (Figure 4.4).

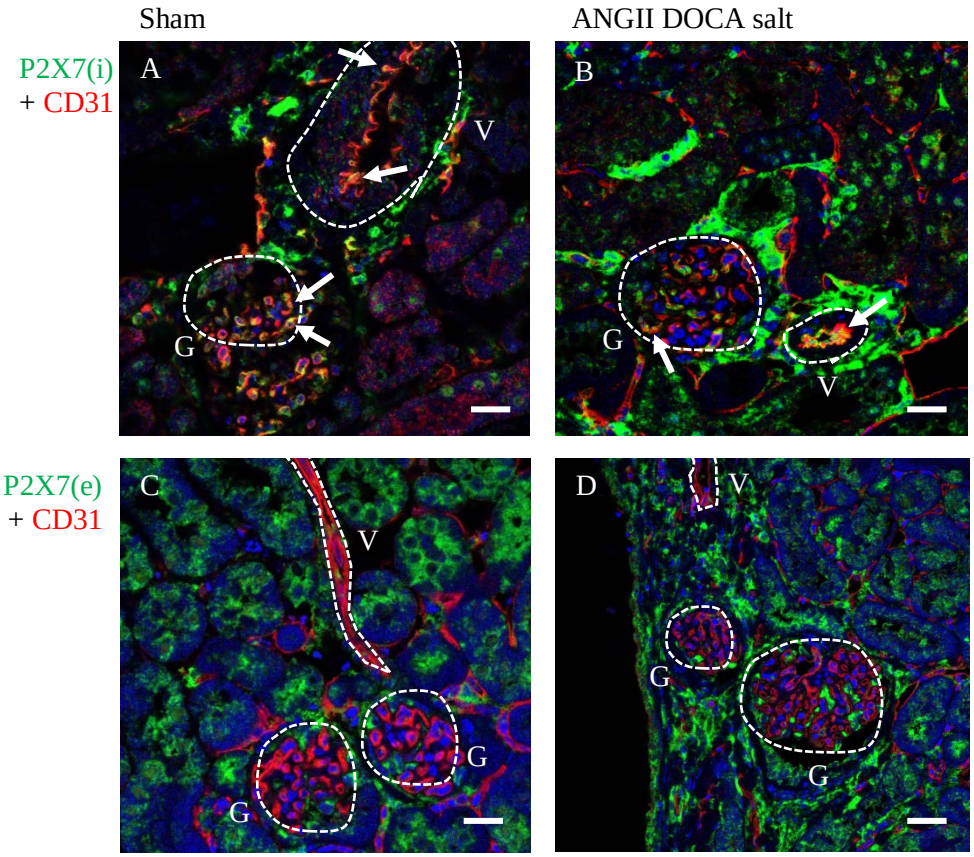

Figure 4.4 - P2X7 expression in the mouse renal vasculature of Sham and ANGII DOCA salt mice, with two different antibodies used.
P2X7(i) staining (green) and CD31 staining (red) in (A) Sham and (B) ANGII DOCA salt mouse kidneys. P2X7(e) staining (green) and CD31 staining (red) in (C) Sham and (D) ANGII DOCA salt mouse kidneys. Vessels (V) and glomeruli (G) are highlighted with white dashed lines. Co-localisation (yellow) is highlighted with white arrows. DAPI nuclear staining is present in all images (blue). Scale bars = 25µm. All images were taken at 40x objective.

Although the localisation of P2X7 did not change between Sham and ANGII DOCA salt mouse kidneys, the P2X7(i) staining at perivascular areas in ANGII DOCA salt mouse kidneys appeared more intense and exhibited a similar pattern to collagen deposition as detected through picrosirius red staining (Figure 4.5).

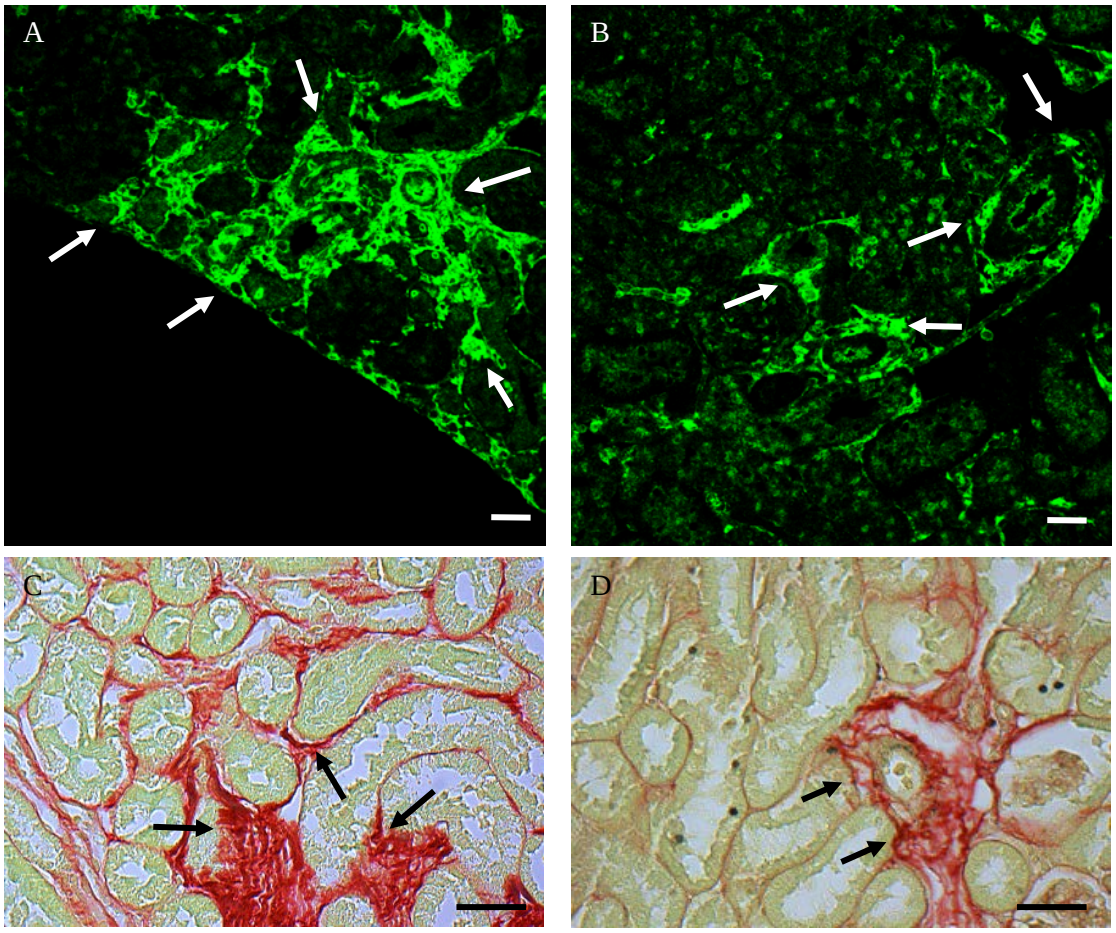

Figure 4.5 - P2X7(i) and collagen staining in the interstitium of the ANGII DOCA salt mouse kidney.
P2X7(i) immunofluorescent staining at (A) cortex and (B) perivascular areas. White arrows highlight positive P2X7 staining. Picrosirius red staining for collagen in fibrosis at (C) cortex and (D) perivascular area. Black arrows highlight positive collagen staining Scale bars = 25µm, images were taken at 40x objective.

This increased intensity of P2X7(i) staining at perivascular areas was not, however, reflected at whole kidney level. When whole kidney homogenate was processed through Western blotting using the same antibodies, total levels of P2X1, P2X7(i) and P2X7(e) were unchanged (Figure 4.6).

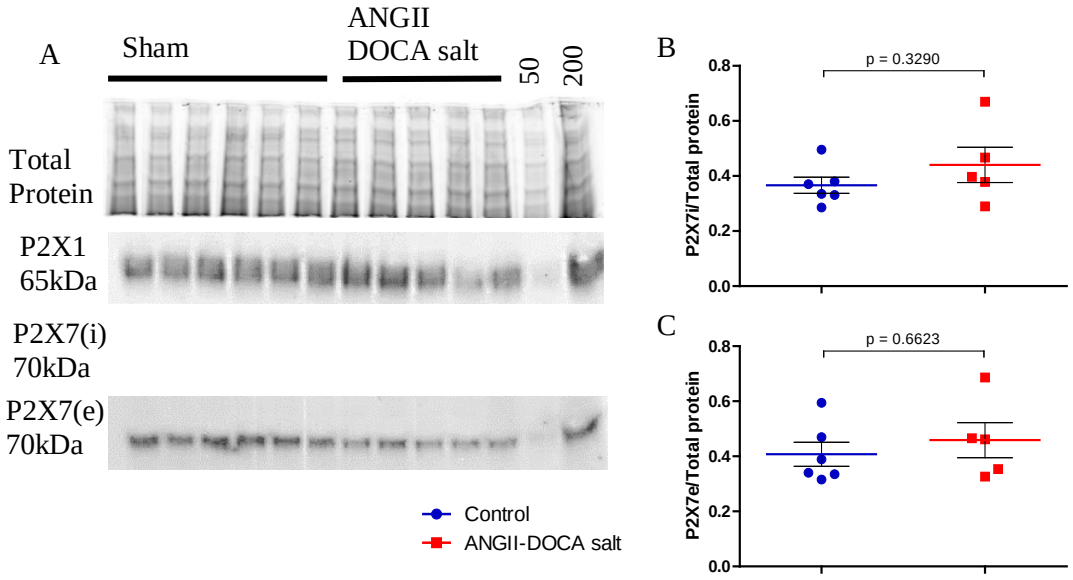

Figure 4.6 - Western blot analysis of whole kidney homogenate to target canonical P2X7 with two different antibodies.
(A) Total protein as measured via Coomassie Blue staining, used for normalisation and P2X1, P2X7(i) and P2X7(e) membranes as visualised by electrochemiluminescence (ECL). 50 = 50% protein control, 200 = 200% protein control. Quantification of membranes showed no significant difference in (B) P2X7(i) or (C)P2X7(e) expression in sham (blue; n=6) compared to ANGII DOCA salt (red; n=5) mice. Statistical analysis by t-test, data presented are mean±95% C.I

Although canonical P2X7(i) and P2X7(e) at 60kDa was unchanged in ANGII DOCA salt mouse kidney homogenate, a smaller band detected on the same blot was upregulated in ANGII DOCA salt mice (Figure 4.7). Interestingly, this band, at 25kDa, was detectable using both P2X7(i) and P2X7(e) antibodies and does not correlate to amino acid length of any known P2X7 isoform.

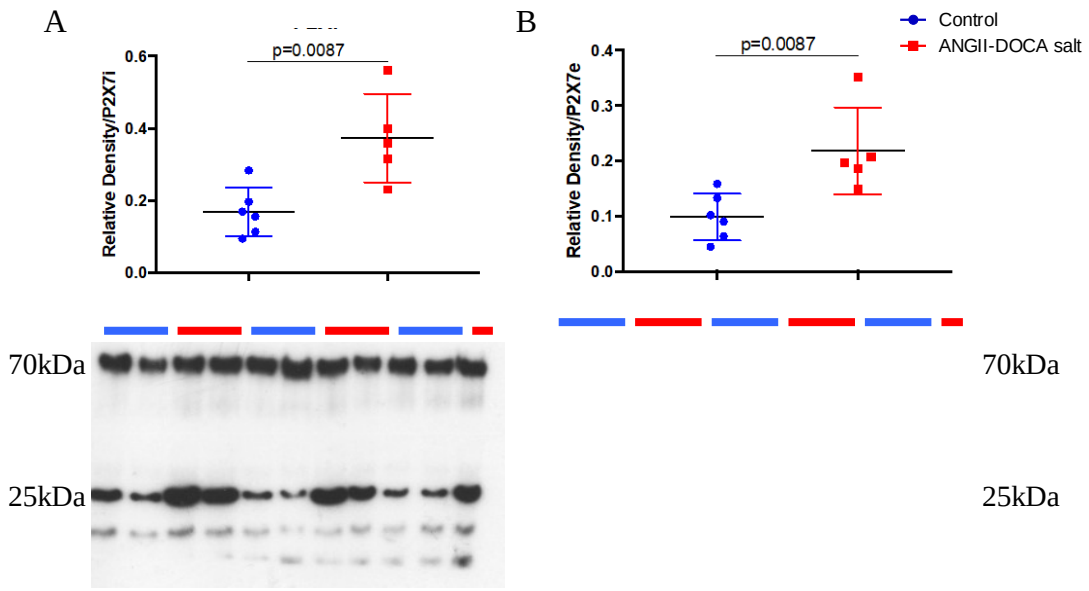

Figure 4.7 - Western blot analysis of whole kidney homogenate to target all P2X7 bands with two different antibodies.
Western blot membrane of (A) P2X7(i) antibody and (B) P2X7(e) antibody in whole kidney homogenate from Sham (blue lanes; n=6) and ANGII DOCA salt mice (red lanes; n=5). 70kDa band represents canonical form of P2X7. 25kDa band (highlighted with black arrow) represents unknown band. Semi-quantitative analysis of the 25kDa band suggest a significant increase in expression of this band in ANGII DOCA salt mice. Data are mean ±95% C.I. Analysis by standard t-test.

P2X7 was also measured at the mRNA level, using primers targeted to *a*, *b* and *c* splice variants, which code for isoforms A, B and C. qPCR was carried out in whole kidney, aorta and spleen of Sham and ANGII DOCA salt mice. No change was seen in *p2x7* expression in whole kidney or in spleen, but a decrease in *p2x7* was evident in the aortas of ANGII DOCA salt mouse aortas compared with those taken from Sham animals (Figure 4.8).

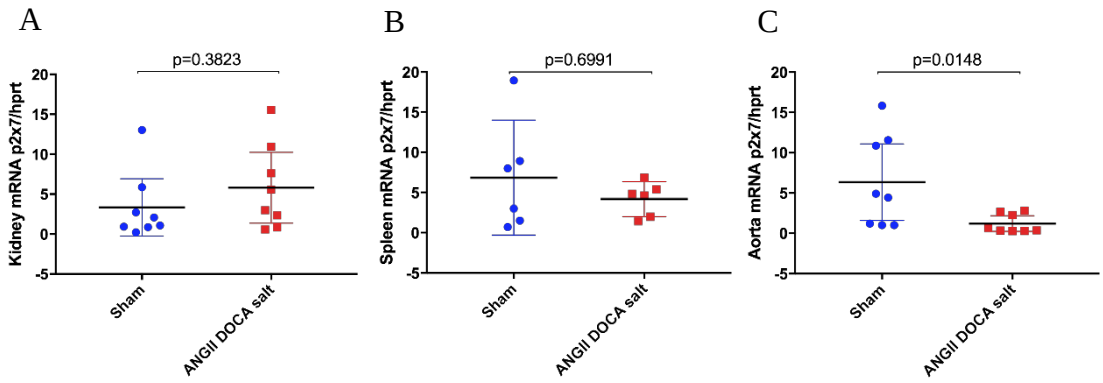

Figure 4.8 - mRNA levels of *p2x7* in Sham and ANGII DOCA salt mice.
mRNA levels of *p2x7* normalised to *hprt* housekeeper gene using primers that target protein coding mRNA for P2X7 isoforms A, B and C in (A) whole kidney, (B) spleen and (C) aorta from ANGII DOCA salt mice (red, ■, n=8) and sham (blue •, n=8). Data are mean ± 95% CI, analysed by t-test.

4.3.3 Evidence for expression of P2X7 splice variants in mouse models of renal injury

Given the observation of differential staining patterns of P2X7 using antibodies targeting different P2X7 isoforms and upregulation of an unknown 25kDa band targeted with P2X7 antibodies in ANGII DOCA salt mice, we decided to investigate *p2xr7* splice variants in the ANGII DOCA salt mouse model and other models available to us. One such model was the reversal unilateral ureteral obstruction (R-UUO) mouse model of renal fibrosis. RNAseq data for this model was available and thus mined for information on *p2xr7* splice variants. Seven splice variants were identified, three of which were upregulated upon instigation of UUO (Figure 4.9). These expression levels did not drop in the week following reversal of this model through removal of the ureteric obstruction. These splice variants correlated to P2X7 isoform A (splice variant 4), P2X7 isoform C (splice variant 5) and a non-coding piece of *p2xr7* exon (splice variant 3).

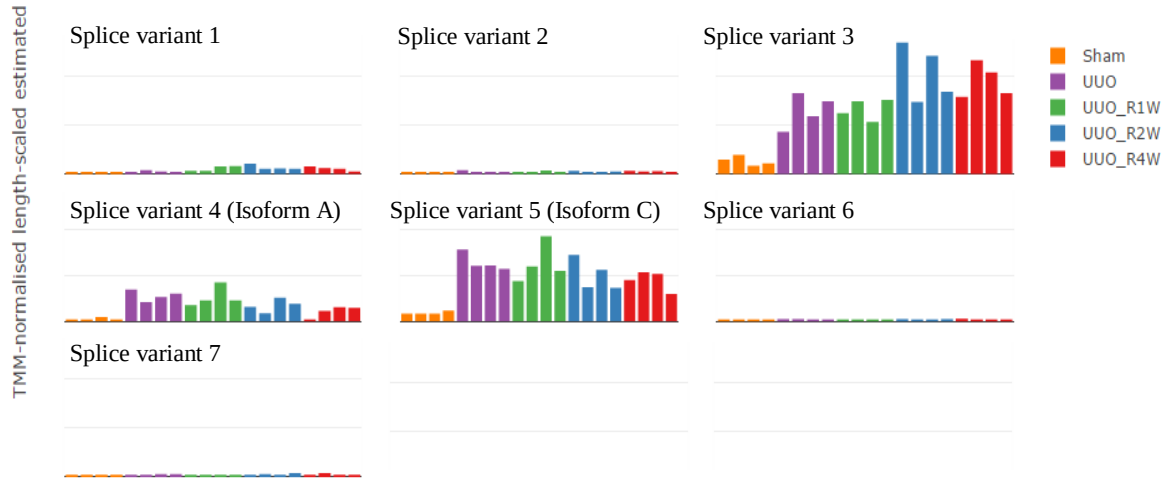

Figure 4.9 - P2X7 splice variant expression in a reversal unilateral ureteric obstruction (R-UUO) mouse model of renal injury

RNA sequencing data for whole kidney RNA from Sham operated mice (Sham; orange) UUO mice (purple: UUO), UUO mice plus 7 days reversal (green; UUO_R1W), UUO mice plus 14 day reversal (blue; UUO_R2W) and UUO mice plus 28 day reversal (red; UUO_R4W), with each bar representing a different animal within the group. Splice variants are labeled 1 – 6 in the order that they were identified through the software. Splice variant 4 corresponds to canonical P2X7 receptor isoform A. Splice variant 5 corresponds to alternative exon P2X7 receptor isoform C. Data collected and analysed by Carolynn Cairns and Dr. Bryan Conway, QMRI, Edinburgh.

Previous primers used for qPCR analysis of tissue targeted a range of *p2xr7* splice variants, so primers were designed against the canonical receptor mRNA *p2xr7a* which appeared to be upregulated in a UUO model of renal injury (Figure 4.9). These primers were used to observe levels of this splice variant in the kidneys and aortas of both Sham and ANGII DOCA salt mice through end-point PCR. The levels of *p2xr7a* did not alter between Sham and ANGII DOCA salt mice in either the kidney or the aorta, but levels were variable between individual animals regardless of experimental grouping (Figure 4.10).

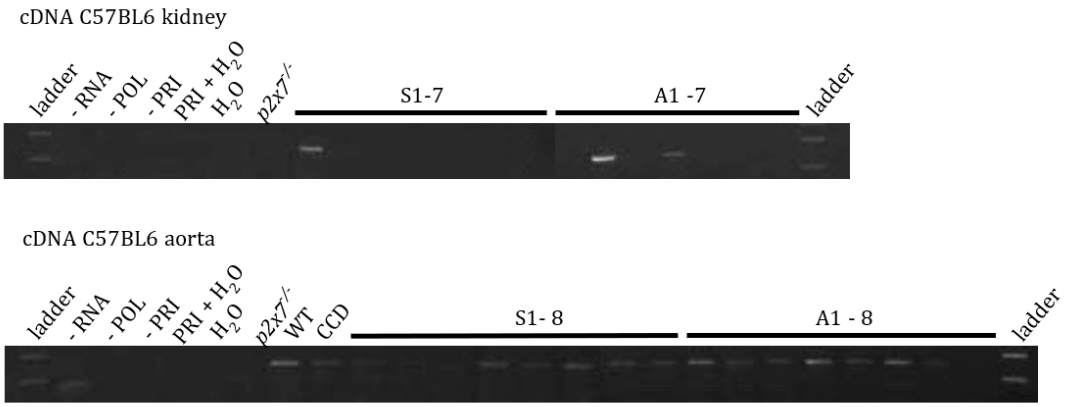

Figure 4.10 – Expression of canonical *p2x7a* splice variant in kidney and aorta mRNA from Sham and ANGII DOCA salt mice
End point PCR showing levels of *p2x7a* in kidney (above) and aorta (below) of either Sham (S1 – *x*) or ANGII DOCA salt (A1 – *x*) mice. Negative controls were without RNA (-RNA), without DNA polymerase (-DNA), without primers (-PRI) and *p2x7*$^{-/-}$ kidney tissue. Primers with nuclease free water (PRI + H_2O) and nuclease free water (H_2O) were ran to check purity and contamination. On the aorta gel (below), WT C57BL6 kidney cDNA (WT) and murine cortical collecting duct cell cDNA (CCD) were ran as positive controls.

4.4 Discussion

The aim of this study was to provide an in-depth localisation profile of P2X7 in the C57BL6 mouse kidney and to observe how this might change upon renal injury. Immunofluorescence and Western Blotting protocols were first performed with the use of P2X1, which localised to the expected areas, validating the method for continuation with P2X7 antibodies. Two antibodies were used, targeting different P2X7 splice variants, of which five are reported as present at the protein level. P2X7(i) targeted isoforms A and E, and P2X7(e) targeted isoforms A, B, C and E. Given the overlap in isoforms targeted by each antibody, it was surprising that the expression profiles were so different, with P2X7(i) localising primarily to the endothelium, glomerular mesangium and perivascular areas and P2X7(e) localising to the renal tubules and interstitium. It is possible that one of the isoforms targeted only by the P2X7(e) antibody (i.e. B or C) is present in the kidney at such high levels that expression of A and E in the CD31 positive endothelium and in PDGFRβ positive cells was undetectable in comparison. The positive staining of P2X7(i) is interesting as it localises to cells that play a role in the modulation of vascular tone, as hypothesised, providing supportive evidence that P2X7 plays a role in vasoactivity.

P2X7(i) co-localised to PDGFRβ, as a marker of pericytes, however, this co-localisation was not consistent throughout the kidney and occurred primarily at perivascular areas. PDGFRβ is not specific to pericytes and also target other cells such as fibroblasts and myofibroblasts, so further markers would be required to confirm the presence of P2X7 in pericytes, as seen in the literature (Am et al. 2013). It is, however, of interest that P2X7 may also be present in perivascular fibroblasts which play a role on collagen deposition (Greenhalgh et al. 2013). Data presented here show a similarity in P2X7(i) staining and collagen staining by picrosirius red, although co-localisation would be required to confirm this. If confirmed, this observation would be consistent with some findings in the literature whereby P2X7 has been linked to fibrosis (Gentile et al. 2015), such as the finding that P2X7 deficiency confers resistance to macrophage infiltration and collagen deposition in the murine UUO model of renal fibrosis (Gonçalves et al. 2006).

The antibodies used for immunostaining were also used for measuring P2X7 levels in Sham and ANGII DOCA salt mouse kidneys, although no change was seen using either antibody for the canonical P2X7 receptor at 60kDa. However, a smaller band detectable at 25kDa was upregulated in ANGII DOCA salt mice, although this does not correlate to the size of any of the known protein isoforms of P2X7. It is possible that this represents an as of yet unidentified isoform, as there are many more reported *p2x7* splice variants in the mouse that have not been identified at the protein level (Bartlett et al. 2014b). However, it may also be a cleavage product released as a result of regulation of the receptor, for example. Amino acid sequencing of this band is required in order to give further insight into its origins.

This finding, along with the contrasting localisation profiles observed using the different P2X7(i) and P2X7(e) antibodies, does suggest that there may be greater complexity of P2X7 and its splice variants than previously thought. In order to investigate this more closely, we also measured levels of P2X7 at the mRNA level.

Firstly, this was carried out on kidney, spleen and aorta tissue from both Sham and ANGII DOCA salt mice using primers that targeted variants *a*, *b* and *c*. P2X7 is present at high levels in haemopoietic cells and so spleen tissue was used as a positive control. Levels of P2X7 were unchanged between groups in both the kidney and spleen, but were downregulated in the aorta. This is particularly interesting as we show that aortas from ANGII DOCA salt mice are dysfunctional when challenged with vasoconstrictor phenylephrine and vasodilator acetylcholine. However, these primers targeted three different splice variants and it was necessary to design primers against these individual splice variants to ascertain what specific renal area they are expressed in.

In order to make a more informed choice of which splice variants to target, we explored data available us from the kidney RNA of mice from a UUO reversal study, which, of the seven identified as present, showed that three variants were upregulated upon injury in mice. These variants also remained highly expressed upon reversal of injury. One of these splice variants mapped to a non-protein coding short single exon, which could not therefore be detected through qPCR, but the remaining two mapped to *p2xr7a* and *p2xr7c*. Primers were therefore designed against these two variants, however; only the primers that targeted *p2xr7a* were successfully optimised, so data

is not available for *p2xr7c* at present. Expression of *p2xr7a* was unchanged between Sham and ANGII DOCA salt mice, both in kidneys and in aortas. What was more striking in this observation was the expression between individual mice, which was highly variable regardless of grouping. It may be that *p2xr7a* is variably expressed and there are shifts or important roles of other splice variants, such as *p2xr7c* in the kidney and aorta of WT mice, as well as those challenged with renal injury. Successful optimisation of primers targeting these variants is required to further investigate their expression levels and potential roles in the murine kidney.

In conclusion, this study provides a comprehensive overview of the expression of P2X7 in the mouse renal vascular and supports the hypothesis that P2X7 plays a role in modulation of vascular tone. It also provides emerging evidence for the role of P2X7 splice variants as a vasoactive component in the physiological function of the mouse kidney, with a noted change in expression in vessels upon renal injury through ANGII DOCA salt administration.

Chapter 5: The role of P2X7 in vasoactivity in ANGII DOCA salt mice

5.1 Introduction

P2X7 overexpression and abnormal activity has been linked to renal disease in both rodents and humans (Vonend et al. 2004b; Ji et al.2012a; Ji et al. 2012b; Gonçalves et al. 2006). Most studies suggested that this is due to an inflammatory role of receptor activation and in a wider context, P2X7 antagonists were developed for deployment in conditions of chronic inflammation. However, clinical trials to use P2X7 antagonists in treatment of inflammatory disease, such as rheumatoid arthritis, have been unsuccessful (Stock et al. 2012; Keystone et al. 2012). More recent studies reflect on the role of P2X7 in the vasculature, suggesting that it may contribute to vasoactivity and influence the interaction between the vascular endothelium and immune cells. For example, in rat retina, P2X7 activation causes constriction of capillaries (Kawamura et al. 2003). In a mouse model of septic encephalopathy, P2X7 is a vital component in the recruitment of leukocytes in to the cerebral endothelium (Wang et al. 2015) and is also implicated in the vascular dysfunction induced by LPS (Chiao et al. 2008; Chiao et al. 2013). In a renal context, acute blockade of P2X7 reduces blood pressure and increases renal blood flow in a rat model of ANGII-induced kidney injury (Menzies et al. 2015) and restores glomerular inulin space, an indicator of GFR, in a rat model of diabetic nephropathy (Kreft et al. 2015).

In sum, these studies suggest that P2X7 activation exerts a tonic vasoconstriction, particularly in renal disease, supporting the hypothesis that its overexpression could result in reduced renal blood flow and contribute to a renal disease phenotype. However, at the start of this work, direct observation of the effect of specific P2X7 agonists and antagonists on vascular tone was lacking. In this chapter, I therefore investigated the effect of the P2X7-selective agonist BzATP and P2X7-specifc antagonist AZ11657312 on vasoconstriction in mouse aorta from both sham and ANGII DOCA salt mice. In vivo, the effect of the P2X7 antagonist on renal blood flow and blood pressure was assessed in sham and ANGII DOCA salt mice.

5.2 Hypothesis

I hypothesise that activation of P2X7 will induce a vasoconstriction of the isolated mouse aorta, exaggerated in ANGII DOCA salt animals. I hypothesise that antagonism of P2X7 will reduce this constrictive effect which will lead to a reduction in blood pressure and restoration of renal blood flow in ANGII DOCA salt mice.

5.3 Results

5.3.1 P2X7 agonism results in an endothelial independent vasoconstriction in mouse aortas

Wire-myography was performed on mouse aorta dissected from untreated C57BL6 mice. Measurements were made in both endothelium-intact and endothelium- denuded states. Removal of the endothelium did not significantly alter the response to phenylephrine (PE) (Figure 5.1A). However, the PE curve for denuded vessels was shifted slightly to the left and exhibited a slightly higher EC50 than was observed for intact aorta. This is to be expected as in intact vessels, PE activates α_1-adrenoceptor present on both smooth muscle cells and endothelial cells. These receptors mediate a strong vasoconstriction via smooth muscle cells through increasing intracellular calcium but mediate a moderate vasodilation via endothelial cells through increasing nitric oxide (NO) production. The overall effect is that endothelial deficient vessels are slightly more responsive to phenylephrine as they lack the opposing vasodilatory effect mediated by endothelial cells.

Denuded aortas were significantly less responsive to the endothelium-dependent vasodilator acetylcholine (Ach; Figure 5.1B). However, the response of intact aortas was still relatively low in intact vessels compared to intact EC50 baseline, retaining approximately 50% of PE-induced constriction at the highest concentration of Ach (Table 5.1).

BzATP, a P2X7-selective agonist, induced a vasoconstriction in both intact and denuded vessels (Figure 5.1C) but there was no significant difference in the constriction between groups (Figure 5.1C).

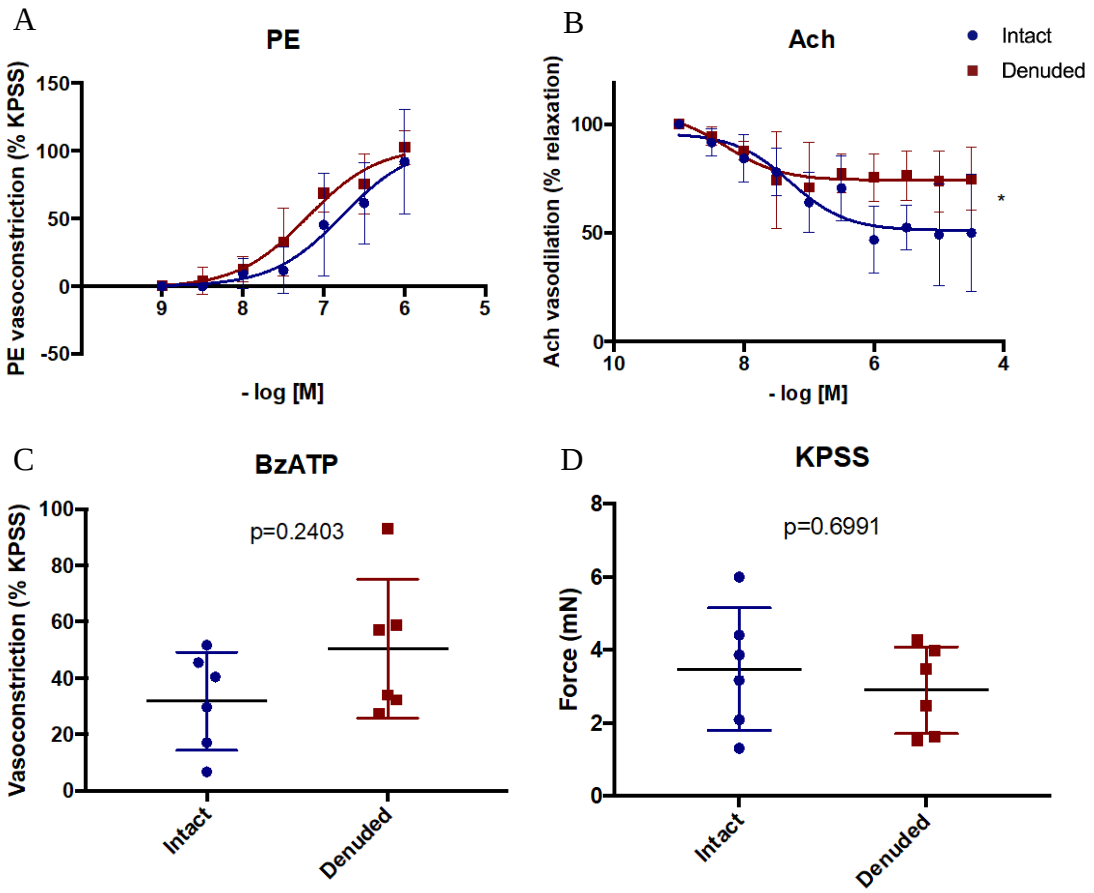

Figure 5.1 - Dose response curves of intact and denuded aortas from C57BL6 male mice to phenylephrine, acetylcholine, BzATP and KPSS. Response of denuded aortas (red, ■, n=6) and intact aortas (blue •, n=6) from C57BL6 mice to (A) vasoconstrictor phenylephrine (PE), displayed as percentage force (mN) of maximum force (mN) as determined by (125mM) KCl response, vasodilator (B) acetylcholine (Ach), displayed as percentage force (mN) of force (mN) at EC50 PE and (C) BzATP displayed as percentage force (mN) of maximum force (mN) as determined by (125mM) KCl response. Data points are mean ± SD with non-linear regression. All data are analysed by two-way ANOVA. (D) Response of same vessels to 125mM KPSS displayed as force in millinewtons (mN). Data points are mean ± 95%C.I. Data are analysed by t-test.

Table 5.1 - EC_{50} and maximal responses of vessels to vasoactive pharmacological agents. EC_{50} expressed as – log [concentration in M] and maximal response of intact and denuded aortas from C57BL6 mice to phenylephrine (PE; $1.0E^{-6}$M), acetylcholine (Ach; $1.0E^{-5}$M), BzATP (50μM) and 125mM KCl. PE and BzATP responses are expressed as %KCl response, Ach responses are expressed as 100 – % relaxation, KCl responses are expressed in millinewtons (mN). Data are mean±S.E.M.

Group	- log EC_{50} PE [M]	Maximal response to $1.0E^{-6}$M PE (%KPSS)	Maximal response to $1.0E^{-5}$M Ach (%relaxation)	Maximal response to 50μm BzATP (%KPSS)	Maximal response to 125mM KCl (mN)
Intact	6.82	92.04±15.7	49.95±10.5	31.85±7.1	3.47±0.7
Denuded	7.26	102.82±5.1	25.15±5.6	50.42±10.1	2.90±0.5

5.3.2 P2X7 antagonism has no effect on renal function in either Sham or ANGII DOCA salt animals

In order to observe the effect of P2X7 antagonism on mean arterial blood pressure (MABP), renal blood flow (RBF) and glomerular filtration rate (GFR) (Figure 5.3), amongst other renal function parameters (Figure 5.3, Table 5.) in a model of renal vascular injury, P2X7 specific antagonist AZ1165712 was administered to sham and ANGII DOCA salt mice at a dose of 12mg/kg under anaesthetic during a renal clearance experiment. Previously, differences had been observed between Sham and ANGII DOCA salt animals, before vehicle or AZ11657312 administration (Chapter 3). In this study, focus was on changes in renal function within each group upon vehicle or AZ11657312 administration. However, no significant differences in renal function were observed between vehicle treated and AZ11657312 treated animals in either the Sham or ANGII DOCA salt group, with the exception of fractional excretion of potassium, which was significantly downregulated upon administration of AZ11657312 in the Sham group, compared to vehicle treated (Figure 5.3D).

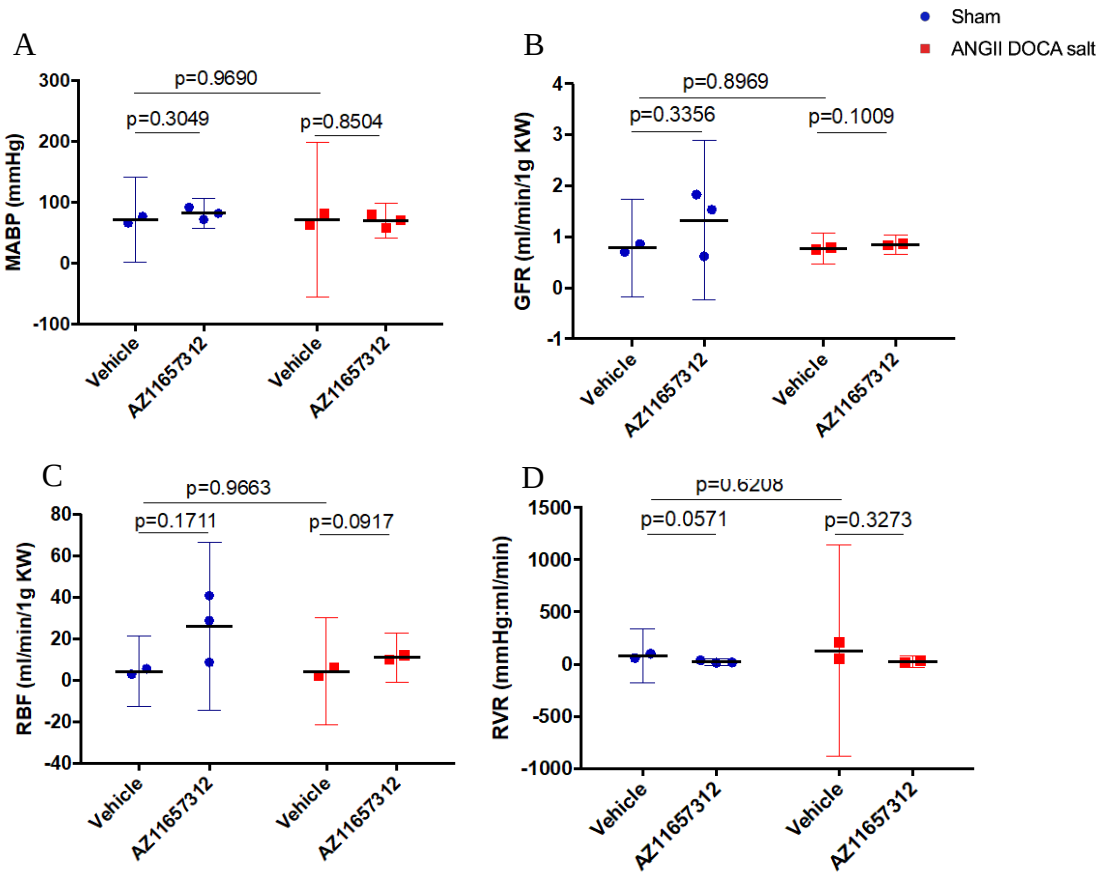

Figure 5.3 - Blood pressure, glomerular filtration rate, renal blood flow and renal vascular resistance in Sham and ANGII DOCA salt mice, treated with either vehicle or P2X7 antagonist AZ11657312. (A) Systolic blood pressure (SBP), (B) glomerular filtration rate (GFR), (C) renal blood flow (RBF) and (D) renal vascular resistance (RVR) in vehicle treated Sham mice (n=2), AZ11657312 (12mg/kg) treated Sham mice (n=3), vehicle treated ANGII DOCA salt mice (n=2) and AZ11657312 (12mg/kg) treated ANGII DOCA salt mice (n=2). Data are mean ± 95% CI, analysed by t-test.

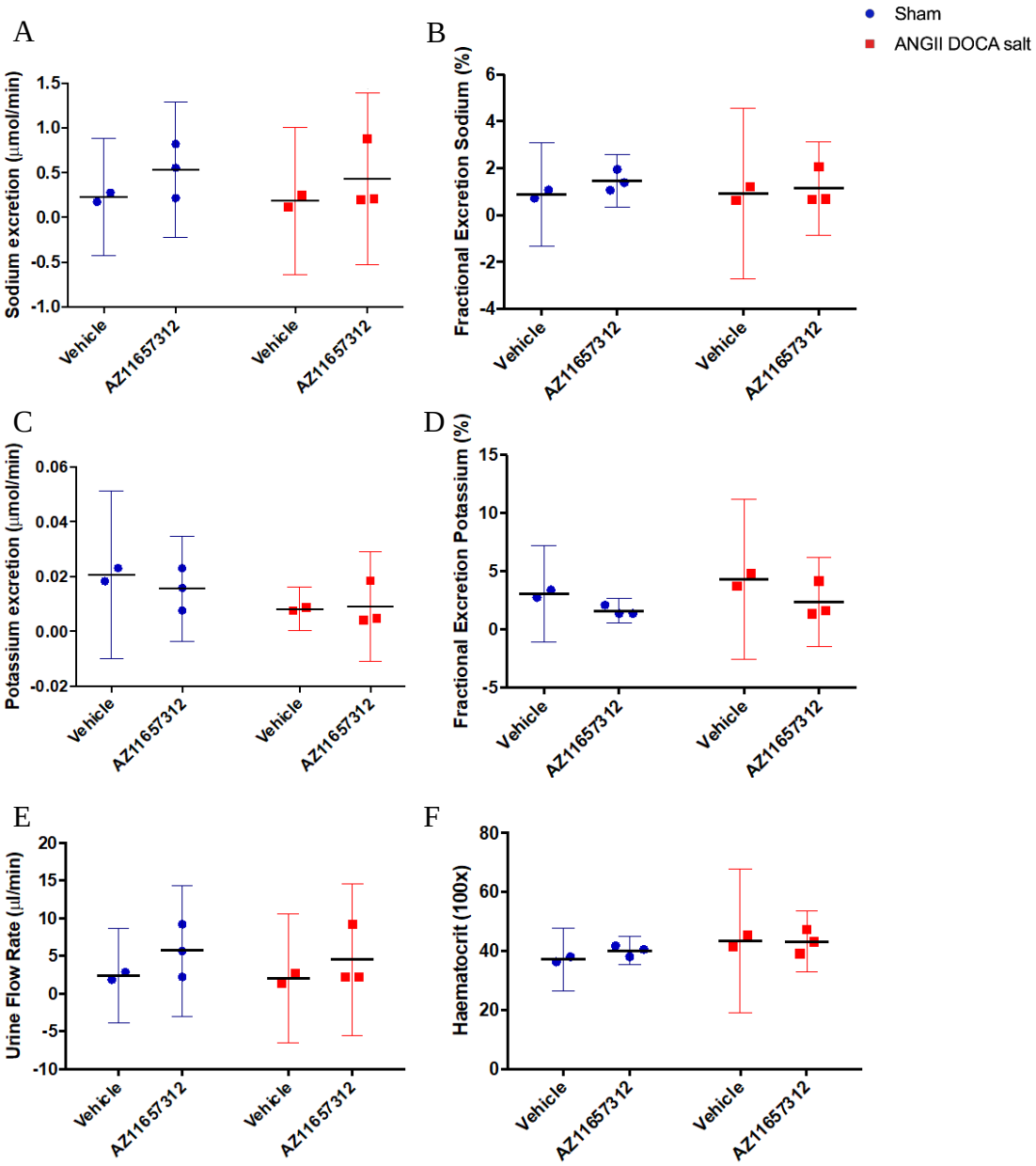

Figure 5.4 - Sodium and potassium handling in Sham and ANGII DOCA salt mice, treated with either vehicle or P2X7 antagonist AZ11657312. (A) Sodium excretion, (B) potassium excretion, (C) fractional sodium excretion, (D) fractional potassium excretion, (E) urine flow rate and (F) haematocrit in vehicle treated Sham mice (n=2), AZ11657312 (12mg/kg) treated Sham mice (n=3), vehicle treated ANGII DOCA salt mice (n=2) and AZ11657312 (12mg/kg) treated ANGII DOCA salt mice (n=3). Data are not subject to statistical analysis, because the group size is too small.

Table 5.2 - Blood pressure and plasma concentrations of sodium and potassium in Sham and ANGII DOCA salt mice treated with either vehicle or AZ11657312. Data are mean ± S.E.M. Data analysis by t-test. No significant changes were observed between vehicle or P2X7 antagonist treated mice in either Sham or ANGIIDOCA salt groups.

Measurement	**Sham mice Vehicle**	**Sham mice AZ11657312**	**ANGII DOCA salt mice Vehicle**	**ANGII DOCA salt mice AZ11657312**
Blood Pressure (under anaesthesia; mmHg)	71.5±5.5	82.0±5.7	72.0±10.0	69.7±6.6
Sodium plasma concentration (mmol)	145.0±0.0	144.3±1.2	153.5±0.5	149.3±3.2
Potassium plasma concentration (mmol)	4.0±0.0	4.0±0.0	1.5*	1.5*

* All plasma potassium measurements made in ANGII DOCA salt mice were below the lower limit of detection of equipment used. For the purpose of further calculations, the values for this group were set at the lower limit of detection of 1.5mmol/L.

5.3.3 Testing the efficacy of AZ11657312 in BMDMs shows that AZ11657312 inhibits P2X7 by ~15%

AZ11657312 was originally used due to previously successful results carried out in rats within my laboratory group. However, AZ11657312 did not have the hypothesised effect on BP and RBF in a small group of animals. Before increasing the study size, I opted to assess whether the compound was an effective antagonist of mouse P2X7. An experiment was performed to test AZ11657312 alongside the well-documented, commercially available compound A438079 (Tocris). Murine bone marrow derived macrophages (BMDMs) were treated with lipopolysaccharide (LPS) and adenosine triphosphate (ATP) to elicit production of IL-1B, which has previously been shown to be a downstream effect of P2X7 activation. Other groups of cells were then treated for either 1 hour or 2 hours with AZ11657312 (10μM) or A438079 (10μM).

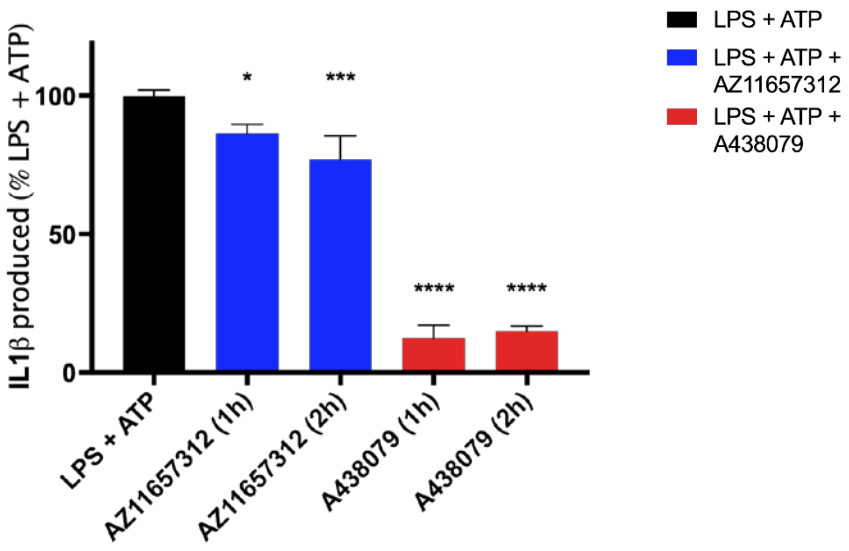

Figure 5.5 - IL1β production by murine bone marrow derived macrophages (BMDMs) in response to LPS and ATP activation when pre-incubated with P2X7 antagonists. IL-1B production in murine BMDMs in response to lipopolysaccharide (LPS) and ATP after pre-incubation for 1 hour (1h) or 2 hours (2h) with P2X7 antagonist AZ11657312 (10μM; blue bars) or P2X7 antagonist A438079 (10μM; red bars). All IL1β data shown as a percentage of IL1β concentration in control LPS and ATP treated cells. Data are mean ± S.D, n=3 for all groups, data analysed by one-way ANOVA, *p<0.05, ***p,0.005, ****p<0.0001. Data collected by Alicja Copek, QMRI, Edinburgh.

The resultant IL-1B production was then measured and compared to control LPS + ATP treated cells with no antagonism. Results showed that treatment of BMDMs with AZ11657312 only slightly inhibited IL1B production by ~15% whereas treatment with A438079 resulted in a ~85% decrease in IL1B production, suggesting that the latter is a more effective P2X7 antagonist in murine BMDMs.

5.3.4 P2X7 antagonism results in an increase in vasoconstriction in ANGII DOCA salt mouse aortas, but not in Sham aortas

Returning to wire-myography, the role of P2X7 in control of vascular tone was assessed in isolate mouse aorta, incubating vessels with either a P2X7 antagonist A438079 (10μM) or vehicle (matched volume ddH_2O), prior to stimulation with the P2X7 agonist BzATP (50μM). Vessels were also subject to a dose response of PE, Ach and SNP to check vessel health independently of P2X7 agonism/antagonism. This study was performed in Sham and ANGII DOCA salt mice over two separate experimental runs, initially with n= 4 and 5 per group and then with n= 7 and 8.). The results obtained from these two rounds of experiments were quantitatively distinct and therefore the data are presented as two separate cohorts.

Results showed that, over both experiments, response to PE and Ach was increased in ANGII DOCA salt aortas compared to Sham and there was no change in SNP response as previously discussed (Chapter 3). Similarly, KPSS responses did not differ between groups or experimental repeats.

However, response to BzATP differed between groups and this effect changed upon repetition of the experiment. In the first experiment, BzATP response was not significantly different between Sham and ANGII DOCA salt mouse aortas. Upon treatment with A438079, vasoconstriction was significantly decreased in Sham aortas, but significantly increased in ANGII DOCA salt aortas, when compared to vehicle treated controls.

In the repeated experiment, with increased group sizes, the constrictive response to BzATP was higher in ANGII DOCA salt aortas compared to Sham. Upon treatment with A438079, vasoconstriction was unchanged in Sham aortas and, again,

significantly increased in ANGII DOCA salt aortas, when compared to vehicle treated controls and the variation in this group was larger than that of the others.

The consistent finding taken from these results is that P2X7 antagonism leads to an increase in vasoconstriction in ANGII DOCA salt, but not Sham aortas.

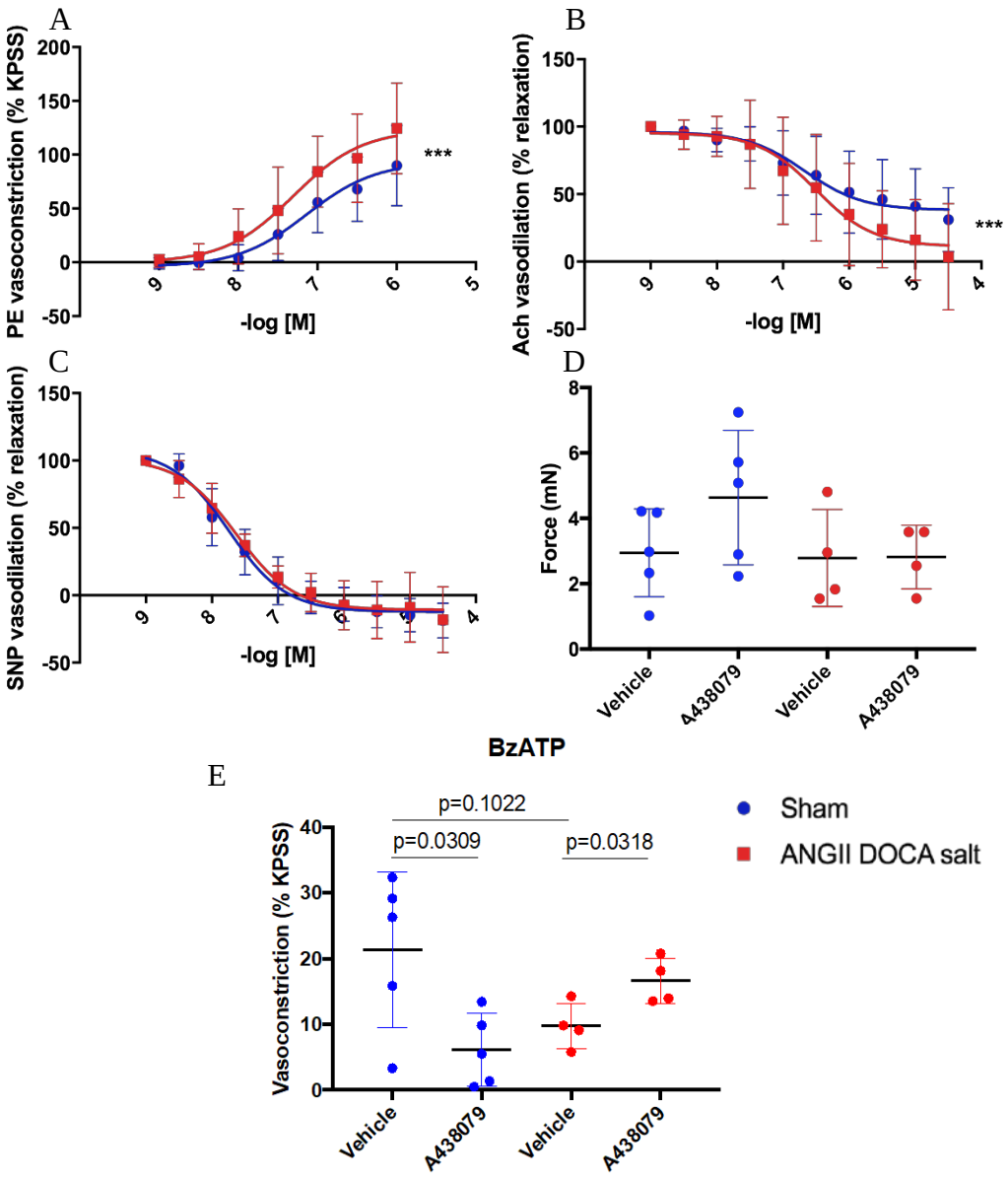

Figure 5.6 – caption on next page

Figure 5.6 - First Experiment: Response of intact aortas from Sham and ANGII DOCA salt mice to phenylephrine, acetylcholine, sodium nitroprusside, BzATP and KPSS in the presence of a vehicle or A438079 P2X7 antagonist. Response of aortas from ANGII DOCA salt mice (red, n=10) and Sham mice (blue, n=8) to (A) vasoconstrictor phenylephrine (PE), displayed as percentage force (mN) of maximum force (mN) as determined by (125mM) KCl response, (B) vasodilator acetylcholine (Ach), displayed as percentage force (mN) of force (mN) at EC50 PE, (C) vasodilator sodium nitroprusside (SNP), displayed as percentage force (mN) of force (mN) at EC50 PE, (D) 125mM KPSS displayed as force in millinewtons (mN) and (E) BzATP (50μM) displayed as percentage force (mN) of maximum force (mN) as determined by (125mM) KCl response. For KPSS and BzATP response, Sham and ANGII DOCA salt mice were further split into 2 separate groups; vehicle treated (ddH_2O; n=4 - 5) or P2X7 antagonist A438079 treated (10μM; n=4 - 5). For PE, Ach and SNP response, data points are mean ± SD with non-linear regression, analysed by two-way ANOVA, *p<0.05, **p<0.01, ***p<0.0005, ***p<0.0001. For KPSS and BzATP response, data points are mean ± 95%C.I, analysed by t-test. For KPSS response, there were no significant differences.

Table 5.3 - First Experiment: EC_{50} and maximal responses of vessels to vasoactive pharmacological agents. EC_{50} expressed as – log [concentration in M] and maximal response of aortas from Sham and ANGII DOCA salt mice in the presence of vehicle (ddH_2O) or P2X7 antagonist A438079 (10μM) to phenylephrine (PE; $1.0E^{-6}$M), acetylcholine (Ach; $1.0E^{-5}$M), sodium nitroprusside (SNP; $1.0E^{-5}$M), BzATP (50μM) and 125mM KCl. PE and BzATP responses are expressed as %KCl response, Ach and SNP responses are expressed as 100 – % relaxation, KCl responses are expressed in millinewtons (mN). Data are mean±S.E.M.

Group	- log EC_{50} PE [M]	Maximal response to $1.0E^{-6}$M PE (% KPSS)	Maximal response to $1.0E^{-5}$M Ach (% relaxation)	Maximal response to $1.0E^{-5}$M SNP (% relaxation)	Maximal response to 50μm BzATP (% KPSS)	Maximal response to 125mM KCl (mN)
Sham Vehicle (n=5)	6.90	89.96±11.8	68.96±7.5	118.83±4.1	21.41±5.3	2.95±0.60
Sham A438079 (n=5)					6.14±2.5	4.63±0.92
ANGII DOCA salt Vehicle (n=4)	6.63	124.51±14.9	96.46±13.9	118.03±8.6	9.77±16.6	2.79±0.74
ANGII DOCA salt A438079 (n=4)					16.62±1.7	2.82±0.49

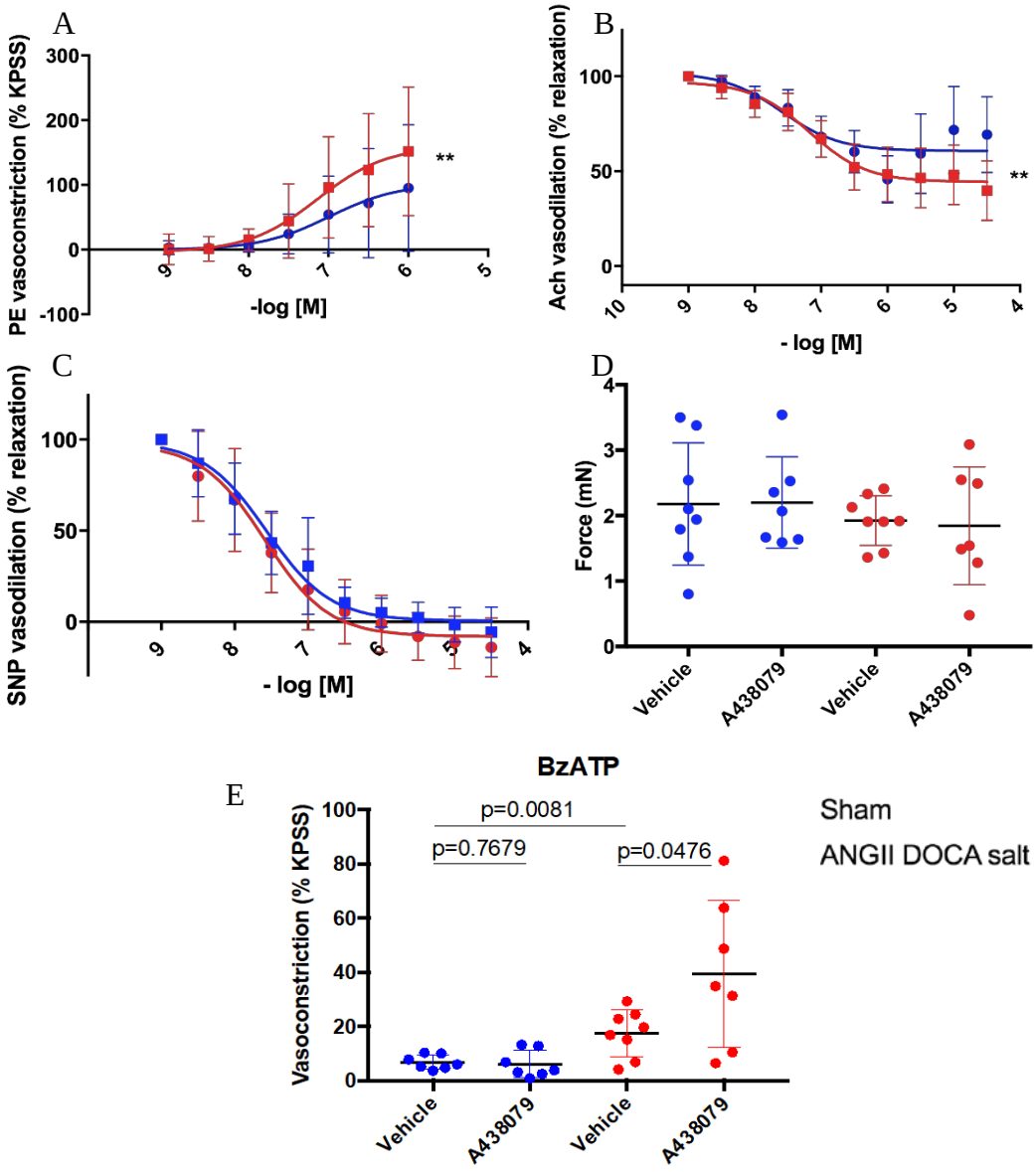

Figure 5.7 – caption on next page

Figure 5.7 - Repeated Experiment: Response of intact aortas from Sham and ANGII DOCA salt mice to phenylephrine, acetylcholine, sodium nitroprusside, BzATP and KPSS in the presence of a vehicle or A438079 P2X7 antagonist. Response of aortas from ANGII DOCA salt mice (red, n=15) and Shame mice (blue, n=15) to (A) vasoconstrictor phenylephrine (PE), displayed as percentage force (mN) of maximum force (mN) as determined by (125mM) KCl response, (B) vasodilator acetylcholine (Ach), displayed as percentage force (mN) of force (mN) at EC50 PE, (C) vasodilator sodium nitroprusside (SNP), displayed as percentage force (mN) of force (mN) at EC50 PE, (D) 125mM KPSS displayed as force in millinewtons (mN) and (E) BzATP (50μM) displayed as percentage force (mN) of maximum force (mN) as determined by (125mM) KCl response. For KPSS and BzATP response, Sham and ANGII DOCA salt mice were further split into 2 separate groups; vehicle treated (ddH_2O; n= 7 - 8) or P2X7 antagonist A438079 treated (10μM; n=7 - 8). For PE, Ach and SNP response, data points are mean ± SD with non-linear regression, analysed by two-way ANOVA, *p<0.05, **p<0.01, ***p<0.0005, ***p<0.0001. For KPSS and BzATP response, data points are mean ± 95%C.I, analysed by t-test. For KPSS response, there were no significant differences.

Table 5.4 - Repeated Experiment: EC_{50} and maximal responses of vessels to vasoactive pharmacological agents. EC_{50} expressed as – log [concentration in M] and maximal response of aortas from Sham and ANGII DOCA salt mice in the presence of vehicle (ddH_2O) or P2X7 antagonist A438079 (10μM) to phenylephrine (PE; $1.0E^{-6}$M), acetylcholine (Ach; $1.0E^{-5}$M), sodium nitroprusside (SNP; $1.0E^{-5}$M), BzATP (50μM) and 125mM KCl. PE and BzATP responses are expressed as %KCl response, Ach and SNP responses are expressed as 100 – % relaxation, KCl responses are expressed in millinewtons (mN). Data are mean±S.E.M.

Group	- log EC_{50} PE [M]	Maximal response to $1.0E^{-6}$M PE (% KPSS)	Maximal response to $1.0E^{-5}$M Ach (% relaxation)	Maximal response to $1.0E^{-5}$M SNP (% relaxation)	Maximal response to 50μm BzATP (% KPSS)	Maximal response to 125mM KCl (mN)
Sham Vehicle (n=8)	6.80	95.29±29.5	60.24±15.7	105.68±4.2	6.78±0.9	2.18±0.33
Sham A438079 (n=7)					6.14±1.9	2.20±0.26
ANGII DOCA salt Vehicle (n=8)	6.87	151.98±26.6	30.79±20.0	113.86±4.3	17.41±3.0	1.93±0.13
ANGII DOCA salt A438079 (n=7)					39.52±10.3	1.85±0.34

5.4 Discussion

As predicted, P2X7 specific agonism through BzATP administration has a vasoconstrictive effect on mouse aorta, an effect that appears to be independent of the presence of the endothelium. The endothelial effect is somewhat unexpected as expression data (Chapter 4) shows that P2X7 expression is largely located on the endothelium, however, this data was focussed on the renal vasculature rather than the aorta. Staining for P2X7 in the aorta was attempted, but unsuccessful, so this would need to be carried out before making any conclusions.

Additionally, the response of intact aortas to endothelium dependent acetylcholine, although greater than denuded vessels as expected, was not as great as previous reports and baseline data would indicate, with dilatory response reaching around 50%, rather than up to 100%. This could be due to damage of vessels or a defect in the drug and repetition of this experiment with a more reliable batch of acetylcholine could explain this phenomenon.

BzATP also binds P2X1, as well as P2X7 so receptor cross over and compensation adds complexity to the results. An agonist specific to P2X7 only would be needed to investigate this with more accuracy, but such a compound is not currently commercially available. Renal clearance studies show no effect of P2X7 antagonism on renal function with the use of AZ11657312 in either Sham or ANGII DOCA salt, except for resulting in a slight decrease in fractional potassium excretion in Sham mice. This was unexpected as previous renal clearance studies in rats had achieved significant, dose dependant decrease in blood pressure and increase in renal blood flow upon administration of the same compound at a lower dosage (Menzies et al. 2015).

The group sizes used in our mouse experiment were small and so the negative results could be a result of a lack of power, however, it may also be a species effect. Although canonical versions of the P2X7 receptor in mice and rats share 84% sequence homology, small changes in amino acid sequence can induce differential responses to P2X7 agonists (Young et al. 2007). Differential response to other P2X7 antagonists has also been reported between species (Michel et al. 2009) and as such, this may be the case with AZ11657312.

Another level of complexity is added when the different splice variants of P2X7 are considered, of which there are 2 protein isoforms observed in rats, 8 in mice and 10 in humans, all of which may present different responses to a single P2X7 agonist or antagonist.

Because no effect was seen in the renal clearance experiment using AZ11657312, a different compound was considered for further P2X7 antagonism studies - A438079, which is commercially available from Tocris and has been documented in previous studies (Ponnusamy et al. 2011; Wang et al. 2015; Kreft et al. 2016; Sathanoori et al. 2015; Menzies et al. 2017; Yan et al. 2015).

In order to observe the effect of AZ11657312 and A438079 on mouse P2X7 receptors, a cell study was carried out in which cells were treated with LPS and ATP, plus incubation with either antagonist. The resultant IL-1B production, a downstream effect of P2X7 activation, was then measured. Results showed that A438079 was much more effective in reduced IL-1B production than AZ11657312 and so this was the P2X7 antagonist carried forward for future studies.

Myography studies into the effect of P2X7 antagonism in Sham and ANGII DOCA salt mice were carried out in order to observe how the role of P2X7 changes under pathophysiological conditions, in this case a murine model of early renal vascular injury (outlined in Chapter 3). This study was carried out initially with group sizes of 4 - 5, upon which no change in response was seen between Sham and ANGII DOCA salt aortas. In this study, P2X7 antagonism with A438079 resulted in a significant decrease in BzATP-induced vasoconstriction in Sham aortas, but a significant increase in BzATP-induced vasoconstriction in ANGII DOCA salt aortas. This observed effect in ANGII DOCA salt aortas was unexpected, as we hypothesised that P2X7 is vasoconstrictive and its antagonism would lead to a reduced constriction in response to BzATP.

We therefore repeated this experiment with larger group sizes of 7 - 8. In both experiments, response of Sham and ANGII DOCA salt aortas to PE, Ach and SNP was measured independently from P2X7 agonism and antagonism. In both experiments, hyper-reactivity of aortas to PE and Ach was seen in ANGII DOCA salt mice compared to Sham and no difference was seen between groups on response to SNP.

However, in the repeated experiment, a different response was observed to BzATP - firstly, constriction of ANGII DOCA salt mouse aortas in response to BzATP was significantly higher than that of Sham mouse aortas, where no difference was seen in the first experiment. Also, although a decrease in constriction was seen upon P2X7 antagonism in Sham mice in the first experiment, no significant difference was observed in the repeated experiment, when group sizes were increased. However, consistently with the first set of data, the repeated experiment showed that P2X7 antagonism in ANGII DOCA salt aortas resulted in a significantly increased constriction in response to BzATP.

Power calculations were performed on data from the first experiment in order to generate group sizes large enough to unearth possible statistical significance upon repetition of the experiment, making the results from the repeated experiment more reliable. According to the repeated experiment, ANGII DOCA salt mouse aortas responded much more strongly to BzATP compared to Sham. This may be due to an upregulation of the P2X7 receptor, which, as discussed in Chapter 4, is not present in the canonical form, but may be present in other splice variants of P2X7. A change in P2X7 splice variant expression profile in ANGII DOCA salt mice compared to Sham mice may also explain why P2X7 antagonism had no effect in Sham mice but induced a stronger constriction in ANGII DOCA salt mice. To elucidate this, further investigation into the expression of P2X7 splice variants in this model would need to be undertaken (as discussed in Chapter 4). This would also give insight into potential differences in affinity of P2X7 agonists and antagonists for different splice variants isoforms, as discussed earlier.

However, it may not be cross specificity between P2X7 isoforms that mediate the effect seen but cross specificity between purinergic receptors in general. Although A438079 is a specific antagonist of P2X7, the P2X7 agonist BzATP can also bind to P2X1. P2X1 is well documented vasoconstrictor present in the smooth muscle of vessels, including renal vessels and the aorta (Lewis & Evans 2001; Inscho et al. 2011).

Upon P2X7 antagonism in ANGII DOCA salt aortas, it may be that BzATP binds more strongly with P2X1, leading to an overall increase in vasoconstriction, which masks the effect of P2X7. In order to pick apart this cross over, specific P2X1 antagonists

would need to be incorporated into this experiment, which would be of great interest in further studies.

Collectively, this data does show that P2X7 has a vasoconstrictive effect in the C57BL6 mouse aorta, which is potentially reversed under a murine model of renal vascular injury. However, elimination of contribution of other purinergic receptors in these experiments, such as P2X1, is needed to be sure of this. Additionally, the complexity of receptor cross talk and the presence of P2X7 splice isoforms, which differ between species, needs to be understood more clearly before the role of P2X7 in renal vascular tone modulation can be fully explained.

Chapter 6: General Discussion

Increased P2X7 expression has been implicated in a plethora of diseases, including inflammatory conditions, pain pathways and renal injury (Bartlett et al. 2014). In experimental models of renal injury or disease, such as inflammatory (Ji et al. 2012a; Ji et al. 2012b), pro-fibrotic (Goncalves et al. 2006) and vascular (Menzies et al. 2015), P2X7 knockout or antagonism has been beneficial. Nevertheless, clinical trials to use P2X7 antagonists as a therapeutic for inflammatory disease such as rheumatoid arthritis have been unsuccessful (Keystone et al. 2012; Stock et al. 2012), suggesting a persistent knowledge gap concerning the fundamental biology of P2X7 in health and disease. Closing this gap, particularly in the context of chronic kidney disease (CKD) will make repurposing of P2X7 antagonists into renal therapeutics ever more appealing (Menzies et al. 2017). However, the mechanistic underlying of the role of P2X7 in the kidney is still not well understood, due to historic lack of research into P2X7 in this organ and because of the difficulty of mimicking all the human pathophysiological elements of CKD in a rodent model.

The primary aim of this thesis was to investigate the role and expression of P2X7 in C57BL6 mice, using a recently described, slowly progressing model of CKD. The intention of my research was to contribute to a deeper understanding of P2X7 function, supporting investigation into P2X7 antagonists as renal therapeutic targets. I first characterised a new model for investigating CKD in C57BL6 mice by chronic treatment with combinatorial ANGII, DOCA and salt. As described first by Kirchhoff (Kirchhoff et al. 2009) this multi-induction approach produces progressive renal injury. In my hands, mice developed mild hypertension and renal injury manifesting primarily as perivascular fibrosis and vascular dysfunction. Localisation and functional studies into this model and in control mice have provided a comprehensive overview of the expression of P2X7 in the mouse renal vascular and supports my hypothesis that P2X7 plays a role in modulation of vascular function. P2X7 was found in endothelial cells and in PDGFRβ positive cells. P2X7 expression was upregulated in ANGII DOCA salt mice, as was the PDGFRβ cell population. Overall, renal fibrosis was not elevated but the extent of collagen deposition around the macrovasculature- perivascular fibrosis- was much higher in the experimental group. In functional studies, aorta from ANGII DOCA salt mice were hyper-responsive to vasoconstrictor

phenylephrine, an effect which was amplified upon P2X7 antagonism. My data also demonstrates the complexity of the splice variation of *p2xr*7, highlighting the importance of variant genotype in the context of using P2X7 antagonists in clinical trials.

The findings surrounding the characterisation of the ANGII DOCA salt model are discussed in detail in chapter 3. Here, I highlight the observation that the population PDGFRβ positive cells in ANGII DOCA salt kidneys was much higher than that in Sham mice, and that perivascular fibrosis, though not interstitial fibrosis, was significantly higher in the kidneys of ANGII DOCA mice. Not only this, but the vascular function of aortas from ANGII DOCA salt mice was significantly difference to those taken from Sham mice.

These outcomes from my PhD research have been discussed in early chapters. Here I highlight aspects that I consider important and briefly discuss the perspectives of my research.

6.1 Localisation and expression of P2X7 in the mouse kidney

Investigation of P2X7 in mouse kidneys showed that P2X7 can be localised to CD31 positive endothelial cells, although not the αSMA expressing smooth muscle layer of renal vessels. The presence of P2X7 in endothelial cells is well documented (Yamamoto et al. 2000; Lewis & Norman 2004; Menzies et al. 2013). Some studies suggest that P2X7 is present in the smooth muscle of renal vessels, particularly under injury models (Lewis & Norman 2004; Menzies et al. 2013), but my data does not support this. This discrepancy could potentially reflect the variability of target binding sites epitopes with different P2X7 antibodies, which may 'hit or miss' different splice variant products of the *p2xr7* gene. This complication of P2X7 was evident upon measuring P2X7 expression levels in ANGII DOCA salt mice. P2X7 was increased in ANGII DOCA salt kidneys (determined by western blot, capturing 4 splice variants protein products, including the canonical form), increased in ANGII DOCA salt aorta (determined by qPCR, capturing 3 splice variants including the canonical form) and increased in the kidneys of UUO mice (determined by RNAseq, capturing 3 splice

variants of *p2x7* including the canonical form) compared to Sham. The complexity of this splice variation is discussed in more detail later in this chapter.

Perhaps most interestingly, my localisation data shows that P2X7 co-localises to PDGFRβ positive cells in C57BL6 mouse kidneys. PDGFRβ is a marker that covers many types of cells, one of which is perivascular cells such as pericytes, which have roles in the kidney as modulators of vascular tone and differentiation into mesenchymal myofibroblasts which play roles in collagen deposition in the process of renal fibrosis (Lebleu et al. 2014). The literature on P2X7 and its role within pericytes is not extensive, however some studies have observed some links. P2X7 has been implicated in vascular control of the rat retina, via pericytes (Sugiyama 2014; Kawamura et al. 2003) and has even been identified within human pericyte cultures . It is of particular interest that the ANGII DOCA salt model exhibits vascular dysfunction, increased pericyte populations and perivascular fibrosis in conjunction with P2X7 expression, as this feeds into research theories of the progression of tubulointerstitial fibrosis.

6.2 Pericytes and perivascular fibrosis

Pericytes are found throughout the body, wrapped around capillaries, mediating vital functions such as angiogenesis and vasoconstriction. They are of particular interest in the kidney, where they can be found in a specialized form of mesangial cells within the glomerulus, and renin expressing pericytes at the afferent arteriole, thus contributing to systemic blood pressure. In these locations, they can also differentiate into pro-fibrotic mesenchymal cells, potentially initiating the process of organ fibrosis (Shaw et al. 2018).

Evidence does exist to support the theory of perivascular fibrosis as the first step towards tubulointerstitial fibrosis and organ scarring. In an ANGII rat model of renal injury, Faulkner et al. suggested that the initiation of fibrosis observed lay in perivascular myofibroblasts, rather than in tubular epithelial cells (Faulkner et al. 2005). In a UUO + IRI mouse model of fibrosis, lineage tracing techniques could not

ascribe the myofibroblasts mediating the injury to tubular epithelial origin (Humphreys et al. 2010). These studies highlight the potential significance of perivascular cells such as pericytes in the context of renal injury, but this concept is still not well understood and further exploration of this process is required. Establishing the role of P2X7 in this process may not only provide better understanding of how P2X7 contributes to renal disease, but may also shed further light on the importance of pericytes and perivascular fibrosis as the initiating step in renal fibrosis.

My data shows co-localisation of P2X7 and PDGFRβ in C57BL6, but I was not able to achieve successful co-staining in my ANGII DOCA salt model, due to antibody batch variations and hence the requirement to re-optimise my immunostaining method for each batch, which I did not have sufficient time to complete. What my data from the ANGII DOCA salt model does show is that both whole kidney P2X7 expression and presence of PDGFRβ positive renal populations were increased. My ANGII DOCA salt model shows increased perivascular fibrosis, through staining of collagen in a pattern mimicking P2X7 staining in ANGII DOCA salt kidneys. However, again due to protocol and time limitations, I was unable to optimise a method for co-staining of P2X7 and collagen. These data show potential for a locational, if not functional, overlap between P2X7 and pericyte mediated perivascular fibrosis – however the data do not provide evidence for this. Successful co-staining for P2X7 and collagen, and P2X7 and PDGFRβ (if not extra, more specific markers for pericytes, as PDGFRβ alone targets multiple cell types) would be required to provide evidence to support this direction of research.

6.3 p2xr7 splice variation

My investigation into the role of murine P2X7 in CKD highlights the complexity of splice variation within *p2xr7*, which hasn't previously gone unnoticed in the field. The canonical form of P2X7 is preferentially expressed in macrophages (Surprenant et al. 1996), whereas the P2X7k isoform variant is preferentially expressed on T-cells,

exhibiting an 8-fold higher sensitivity to P2X7 agonists (Nicke et al. 2009). P2X7k is implicated in pore formation, whereas the P2X713C, the mRNA of which has an alternative exon 13, demonstrates no pore formation at all and is expressed most notably in the brain, salivary glands and lung (Masin et al. 2012). Another P2X7 isoform with an alternative exon 13 transcript is P2X713B, which also doesn't demonstrate pore formation, and is found in brain and salivary glands, as well as the spleen (Masin et al. 2012). Perhaps most interestingly, *p2xr7*$^{-/-}$ mice produced by GlaxoSmithKline (GSK) and Pfizer show incomplete knock out of all P2X7 isoforms. Although both lines knock out the canonical form of P2X7, the GSK line still exhibits the P2X7k variant and the Pfizer line still exhibits P2X713B and P2X713B (Bartlett et al. 2014). The complexity of splice isoforms observed in rodents has also been identified to a lesser degree in human cells and tissue (Cheewatrakoolpong et al. 2005). These observations highlight the variability in P2X7 isoforms expression and function, as well as the importance of considering these isoform profiles in a research setting.

The data shown in this thesis supports the literature in that different expression profiles of *p2xr7* were observed depending on detection antibodies used, the renal injury induced and the tissue in which *p2xr7* levels were measured. Immunofluorescent experiments using sham and ANGII DOCA salt mouse kidneys resulted in differential staining depending on the P2X7 antibody used, likely because they target a different subset of P2X7 splice variant products within the same tissue. I have shown data which portrays *p2xr7* splice variant dependant expression in a model of UUO, where some variants are upregulated, and others not. I have observed an upregulation of *p2xr7* in whole kidney RNA from ANGII DOCA salt mice compared to Sham, but a downregulation in aorta RNA using the same *p2xr7* specific primers, protocol and cohort tissue.

P2X7 isoforms have been described to self-regulate expression (Masin et al. 2012). This is interesting, as RNAseq analysis of UUO kidney mRNA shows an upregulation of 4 splice variants, one of which represents a non-coding protein variant. Further

investigation of this splice variant would be interesting, as self-regulation of splice variation is often mediated through non-coding RNA (Tazi et al. 2009).

The observations made here, alongside the available literature are not only important for awareness of off target effects in research, but may also represent the initial switch that contributes to disease states. Splice variation is vital in regulating expression of protein coding genes, however it is also linked to disease states (Tazi et al. 2009). It is possible that the difference in splice variant isoforms of P2X7 seen in the ANGII DOCA salt model are a result of their intrinsic link to the disease state and P2X7 isoform profiles are completely different in injury than in healthy kidneys, although much more research is needed to explore this theory.

The key concept that is gained from these data is that *p2xr7* has a complex transcriptional regulation and profile that is likely dependant on the specific cell population (Bartlett et al. 2014). Thus, bulk transcriptomics are unlikely to be very informative and instead the potential to do RNAseq on populations, or even on individual cells, is likely to lead to an improved understanding of how this regulation is controlled in health and disease. This is of particular importance when using P2X7 agonists and antagonists in functional studies, where escape of splice variant activation or de-activation may occur. This was considered as I moved forward into vascular functional studies in ANGII DOCA salt mice.

6.4 The role of P2X7 in macrovascular function

Previous studies performed by our lab group showed that use of an AstraZeneca compound AZ11657312 as a P2X7 antagonist in rats with ANGII induced hypertension led to reduced renal injury (Menzies et al. 2017). However, we were unable to reproduce the *in vivo* effects of AZ11657312 compound seen in our previous study in ANGII rats. However, this is not a robust data set: the combination of DOCA-salt and ANGII made animals unstable under anaesthetic and this resulted in ~50% failure rate for this experimental series. Before developing *in vivo* studies further, I

decided to test the effect of AZ11657312 on a murine bone marrow derived macrophage (BMDM) population, using the well described P2X7 inhibitor, A438079 and measuring IL1β as an output of P2X7 activity. This bioassay showed that AZ showed an approximate 4-fold drop in P2X7 inhibition compared to A438079. The reasons for this are currently unexplored but it is possible that this is yet another outcome of the complexity of splice variant isoforms of P2X7. Due to this finding, A438079 was carried through to functional studies via myography.

Aortas from Sham and ANGII DOCA salt mice were subject to BzATP vasoconstriction in the presence and absence of P2X7 inhibitor A438079; this experiment was approached with the hypothesis that ANGII DOCA salt vessels would have an increased vasoconstrictor response to P2X7 agonist BzATP, which would be dampened by the addition of P2X7 inhibitor A438079. However, there was no significant difference in BzATP response between Sham and ANGII DOCA salt mouse aortas. This response was unchanged in Sham aortas upon antagonising P2X7 but was significantly amplified in ANGII DOCA salt aortas. This study was at first underpowered, so was repeated with a larger cohort with the same results.

Although P2X7 was upregulated in ANGII DOCA salt mouse kidneys compared to sham mouse kidneys, qPCR analysis of *p2xr7* showed a decreased expression in ANGII DOCA salt aortas, compared to those from Sham animals. This did not translate to a difference in BzATP response between these two groups and does not account for the increase of vascular constriction of ANGII DOCA salt aortas upon treatment with P2X7 inhibitor A438079. However, if different isoforms of P2X7 are playing different roles in different tissues, under different pathophysiological conditions, it's possible that the P2X7 isoform profile for ANGII DOCA salt mice is different to that in Sham mice. The isoforms within these profiles may well have different vasoactive properties. More P2X7 isoform-specific investigation would be needed to go any way into exploring this avenue, if this suggestion is to carry any potential.

A more likely explanation for the observations made is the close interplay between P2X receptors P2X7 and P2X1. P2X1 is well described as a dominant mediator of vasoconstriction in smooth muscle cells, playing a large role in autoregulation in the kidney (Inscho et al. 2004). I did measure P2X1 expression through IF studies and WB and saw no increase in P2X1 in the ANGII DOCA salt model. Interestingly, at high enough concentrations, BzATP can activate P2X1 as well as P2X7, whereas A438079 is highly specific to P2X7 only. This may explain why no difference was seen in BzATP response between sham and ANGII DOCA salt vessels – because BzATP was also targeting P2X1, which overrode any differences that might have been seen in P2X7. This may well also explain why ANGII DOCA salt aortas responded more strongly to BzATP in the presence of a P2X7 inhibitor in ANGII DOCA salt mice – blocking P2X7 may result in the overload of P2X1 receptors with BzATP, leading to an increased vasoconstrictive response. This effect was, however, only observed an ANGII DOCA salt animals, not sham, suggesting that P2X1 is affected by the administration of ANGII and/or DOCA salt. In support of my concept; it has previously been shown that ANGII administration in rats leads to altered signal transduction in P2X1 positive cells, which contributes to the dysfunctional renal autoregulation observed in these animals (Zhao et al. 2005). The only way to clearly interpret the role of P2X7 in this study would be to incorporate the use of a P2X1 antagonist, such as NF449, to be able to attribute the changes observed (if any) to P2X7 alone.

6.5 Conclusion

The primary aim of this body of work was to contribute to the growing investigation into P2X7 antagonists as renal therapeutic targets. Preclinical models are very supportive of this potential (Taylor et al. 2009; Arulkumaram et al. 2011; Menzies et al. 2015; Menzies et al. 2017).

My data highlights the complexity and challenge of targeting P2X7 as a renal therapeutic. The role of P2X7 in the renal vasculature in still not entirely clear,

particularly within models of CKD, and the mechanistic biology of this is not well understood. The kidney is a complex organ, composed of many different cell types, it could be that P2X7 is playing very contrasting roles in a very tissue specific manner. Not only this, but it is evident that P2X7 splice variation cannot be overlooked, with splice variants exhibiting different expressions in different tissues and different disease models, to the extent that P2X7 antagonists are affected. Without a stronger understanding of this splice variation effect, we cannot be sure of the efficacy of P2X7 antagonists in preclinical and clinical trials. Much discovery biology required to provide a mechanistic understanding of this and of the role of P2X7 in specific cell types – from immune cells, to pericytes, to endothelial.

6.6 Summary of further work

- *Build on the expression profile of p2x7r splice variants in the mouse kidney* – an extensive PCR study is required in order to fully understand what *p2x7r* splice variants are present in different renal cells in the murine kidney under both physiological and pathophysiological model. This would allow us to start unpicking the potential different roles of P2X7 isoforms.
- *Co-localise P2X7 in the mouse kidney to specific cell markers, particularly PDGFRβ and collagen.* This would elucidate the potential for a role of P2X7 in pericytes or other PDGFRβ expressing cells and the role of P2X7 in perivascular fibrosis. This could be done through building on the immunofluorescence studies outlined in this thesis.
- *Further investigation of the role of P2X7 in the microvasculature.* This could be done by using P2X1 antagonists alongside P2X7 antagonists to eliminate potential of P2X1 agonism whilst activating P2X7 by BzATP. These studies should also be carried out in the renal vasculature or other resistance vessels such as mesenteric arteries.

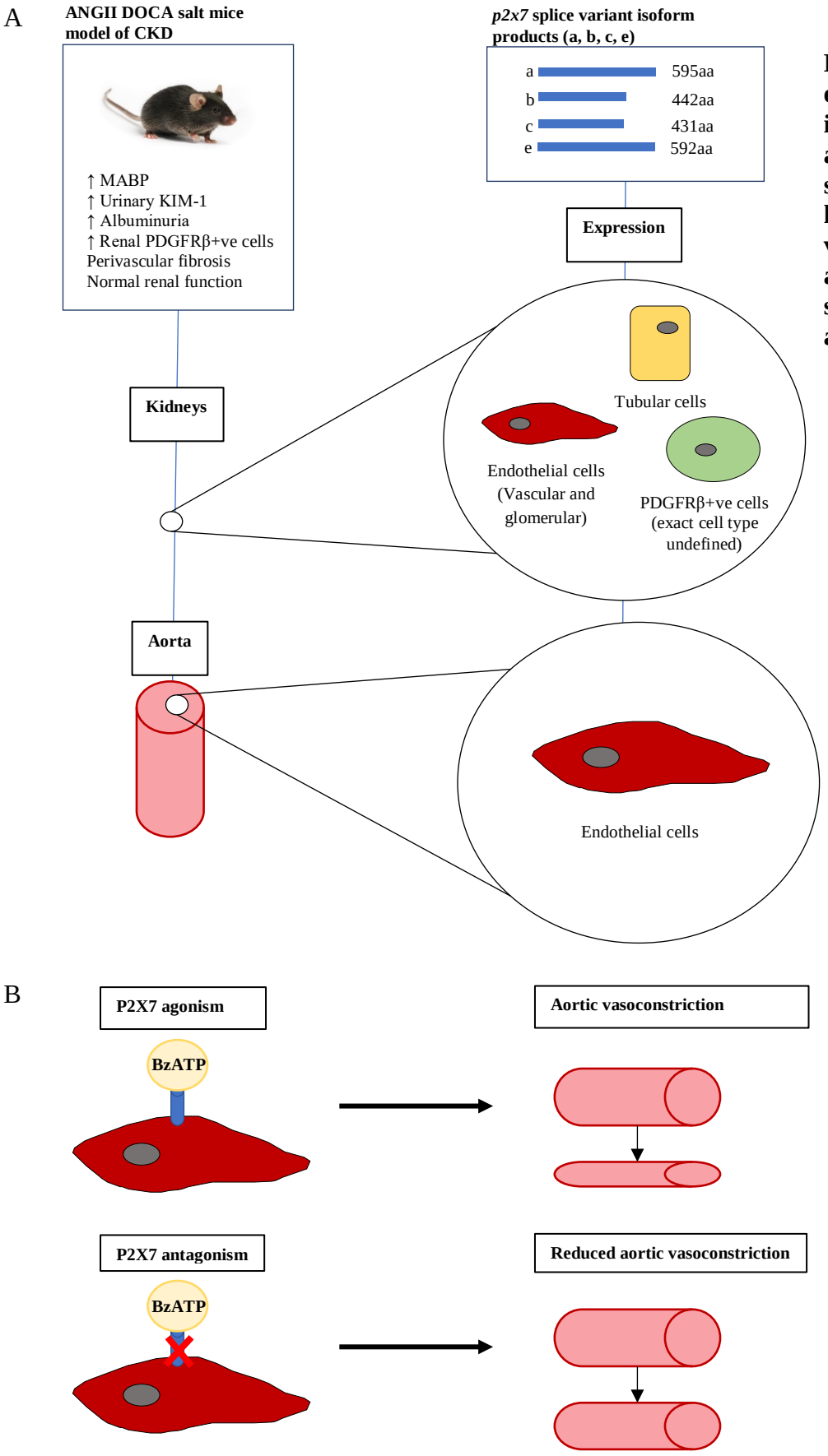

Figure 6.1 Overview of (A) expression of P2X7 isoforms in renal cells and aorta of ANGII DOCA salt model of chronic kidney disease and (B) vasoconstriction in the aorta of ANGII DOCA salt mice upon P2X7 agonism and antagonism

References

Abdulla, M.H. et al., 2011. Effect of renal sympathetic nerve on adrenergically and angiotensin II-induced renal vasoconstriction in normal Wistar-Kyoto rats. *Upsala Journal of Medical Sciences*, 116(1), pp.18–25.

Abraham, D.J. et al., 2007. New developments in fibroblast and myofibroblast biology: Implications for fibrosis and scleroderma. *Current Rheumatology Reports*, 9(2), pp.136–143.

Am, S., Péault, P. & Jj, M., 2013. Renal pericytes: Multifunctional cells of the kidneys. *Pflugers Archiv European Journal of Physiology*, 465(6), pp.767–773.

Antonio, L.S. et al., 2011. P2X4 receptors interact with both P2X2 and P2X7 receptors in the form of homotrimers. *British Journal of Pharmacology*, 163(5), pp.1069–77.

Arulkumaran, N., Unwin, R.J. & Tam, F.W.K., 2011. A potential therapeutic role for P2X7 receptor (P2X7R) antagonists in the treatment of inflammatory diseases. *Expert Opinions in Investigative Drugs*, 20(7), pp.897–915.

Bartlett, C.S. et al., 2012. EP1 Disruption Attenuates End-Organ Damage in a Mouse Model of Hypertension. *Hypertension*, 60(5), pp.1184–1191.

Bartlett, R., Stokes, L. & Sluyter, R., 2014. The P2X7 Receptor Channel: Recent Developments and the Use of P2X7 Antagonists in Models of Disease. *Pharmacological Reviews*, 66 pp.638–675.

Bidani, A.K. et al., 2013. Renal microvascular dysfunction, hypertension and CKD progression. *Current Opinion in Nephrology and Hypertension*, 22(1), pp.1–9.

Boor, P. et al., 2007. Treatment targets in renal fibrosis. *Nephrology Dialysis Transplantation*, 22(12), pp.3391–3407.

Booth, J.W.R., Tam, F.W.K. & Unwin, R.J., 2012. P2 purinoceptors: Renal pathophysiology and therapeutic potential. *Clinical Nephrology*, 78(08), pp.154–163. N107325&L=0 [Accessed July 13, 2014].

Bratton, A.C. & Marshall, E.K., 1939. A New Coupling Component for sulfanilamide determination. *Journal of Biological Chemistry*, 128, pp.537–550.

Burnstock, G., Evans, L.C. & Bailey, M. a, 2014. Purinergic signalling in the kidney in health and disease. *Purinergic signalling*, 10(1), pp.71–101.

Burnstock, G. & Ralevic, V., 2014. Purinergic Signaling and Blood Vessels in Health and Disease. *Pharmacological Reviews*, 66, pp.102–192.

Cheewatrakoolpong, B. et al., 2005. Identification and characterization of splice variants of the human P2X7 ATP channel. *Biochemical and Biophysical Research Communications*, 332(1), pp.17–27.

Chen, K. et al., 2013. ATP-P2X4 signaling mediates NLRP3 inflammasome activation: a novel pathway of diabetic nephropathy. *The International Journal of Biochemistry & Cell Biology*, 45(5), pp.932–43.

Chiao, C.-W. et al., 2013. P2X7 receptor activation contributes to an initial upstream mechanism of lipopolysaccharide-induced vascular dysfunction. *Clinical Science*, 125(3), pp.131–41.

Chiao, C.-W., Tostes, R.C. & Clinton Webb, R., 2008. P2X7 receptor activation amplifies lipopolysaccharide-induced vascular hyporeactivity via IL1B release. *Journal of Pharmacology & Experimental Therapeutics*, 326(3), pp.864–870.

Cowley, A.W. et al., 1992. Effect of renal medullary circulation on arterial pressure. *Journal of Hypertension*, 10(7), pp.S187-93.

Craigie, E. et al., 2013. The relationship between P2X4 and P2X7: a physiologically important interaction? *Frontiers in Physiology*, 4(August), p.216: 1-6.

Crawford, C. et al., 2013. Sympathetic nerve-derived ATP regulates renal medullary vasa recta diameter via pericyte cells: a role for regulating medullary blood flow? *Frontiers in Physiology*, 4(October), p.307.

Crowley, S.D. et al., 2010. Lymphocyte responses exacerbate angiotensin II-dependent hypertension. *American Journal of Physiology*, 298(4), pp.R1089-97.

Danquah, W. et al., 2016. Nanobodies that block gating of the P2X7 ion channel

ameliorate inflammation. *Science Translational Medicine*. 2 23;8(366)

Eckardt, K.-U. et al., 2013. Evolving importance of kidney disease: from subspecialty to global health burden. *Lancet*, 382(9887), pp.158–69.

Fadok, V. a et al., 1998. Macrophages that have ingested apoptotic cells in vitro inhibit proinflammatory cytokine production through autocrine/paracrine mechanisms involving TGF-beta, PGE2, and PAF. *The Journal of Clinical Investigation*, 101(4), pp.890–8.

Faulkner, J.L. et al., 2005. Origin of Interstitial Fibroblasts in an Accelerated Model of Angiotensin II-Induced Renal Fibrosis. *The American Journal of Pathology*, 167(5), pp.1193–1205.

Le Feuvre, R. a et al., 2002. Priming of macrophages with lipopolysaccharide potentiates P2X7-mediated cell death via a caspase-1-dependent mechanism, independently of cytokine production. *The Journal of Biological Chemistry*, 277(5), pp.3210–8.

Fine, L.G., Orphanides, C. & Norman, J.T., 1998. Progressive renal disease: the chronic hypoxia hypothesis. *Kidney International*. 65, pp.S74-8.

Fine, L.G., Orphanides, C. & Norman, J.T., 1998. Progressive Renal Disease - The Chronic Hypoxia Hypothesis. *Kidney & Blood Pressure Research*, 53, pp.74–78.

Förstermann, U. & Münzel, T., 2006. Endothelial Nitric Oxide Synthase in Vascular Disease. *Circulation*, 113(13).

Franco, M. et al., 2013. Impaired pressure natriuresis resulting in salt-sensitive hypertension is caused by tubulointerstitial immune cell infiltration in the kidney. *American Journal of Physiology. Renal Physiology*, 304(7), pp.F982-90.

Gansevoort, R.T. et al., 2013. Chronic kidney disease and cardiovascular risk: epidemiology, mechanisms, and prevention. *Lancet*, 382(9889), pp.339–52.

Gentile, D. et al., 2015. The role of P2X7 receptors in tissue fibrosis: a brief review. *Purinergic Signalling*, 11(4), pp.435–440.

Gonçalves, R.G. et al., 2006. The role of purinergic P2X7 receptors in the

inflammation and fibrosis of unilateral ureteral obstruction in mice. *Kidney International*, 70(9), pp.1599–606.

Greenhalgh, S.N., Iredale, J.P. & Henderson, N.C., 2013. Origins of fibrosis: pericytes take centre stage. *F1000prime reports*, 5, p.37.

Guo, C. et al., 2007. Evidence for Functional P2X 4 / P2X 7 Heteromeric Receptors. *Molecular Pharmacology*, 72, pp.1447–1456.

Guzzi, F., Cirillo, L., Roperto, R. M., Romagnani, P. &Lazzeri, E., 2019. Molecular Mechanisms of the Acute Kidney Injury to Chronic Kidney Disease Transition: An Updated View. *International Journal of Molecular Science*, 20, pp. 4941

Hatakeyama, H. Miyamori, I., Fujita, T. & Takeda, Y., 1994. Vascular aldosterone. Biosynthesis and a link to angiotensin II-induced hypertrophy of vascular smooth muscle cells. *The Journal of Biological Chemistry*, 269, pp.24316–24320.

Hansen, R.R. et al., 2011. P2X7 receptor-deficient mice are susceptible to bone cancer pain. *Pain*, 152(8), pp.1766–76.

Harhun, M.I. et al., 2014. ATP-Evoked Sustained Vasoconstrictions Mediated by Heteromeric P2X1/4 Receptors in Cerebral Arteries. *Stroke*, 45, pp.2444–2450.

Harhun, M.I., Povstyan, O. V. & Gordienko, D. V., 2010. Purinoreceptor-mediated current in myocytes from renal resistance arteries. *British Journal of Pharmacology*, 160, pp.987–997.

Howarth, A.R., Conway, B.R. & Bailey, M. a., 2015. Vascular and inflammatory actions of P2X receptors in renal injury. *Autonomic Neuroscience*, 191, pp.135–140.

Hu, Z.W. et al., 1995. Angiotensin II induces transcription and expression of alpha 1-adrenergic receptors in vascular smooth muscle cells. *The American Journal of Physiology*, 268(3 Pt 2), pp.H1006-14.

Humphreys, B.D. et al., 2010. Fate Tracing Reveals the Pericyte and Not Epithelial Origin of Myofibroblasts in Kidney Fibrosis. *The American Journal of Pathology*, 176(1), pp.85–97.

Hung, S.-C. et al., 2013. P2X4 assembles with P2X7 and pannexin-1 in gingival epithelial cells and modulates ATP-induced reactive oxygen species production and inflammasome activation. *PloS one*, 8(7), p.e70210.

Inscho, E.W., 2009. ATP, P2 receptors and the renal microcirculation. *Purinergic Signalling*, 5(4), pp.447–60.

Inscho, E.W. et al., 2011. P2X1 receptor-mediated vasoconstriction of afferent arterioles in angiotensin II-infused hypertensive rats fed a high-salt diet. *Hypertension*, 57(4), pp.780–7.

Inscho, E.W. et al., 2003. Physiological role for P2X 1 receptors in renal microvascular autoregulatory behavior. *Journal of Clinical Investigation*, 112(12), pp.1895–1905.

Inscho, E.W. et al., 2004. Renal autoregulation in P2X1 knockout mice. *Acta physiologica Scandinavica*, 181(4), pp.445–53.

Ivy, J.R. & Bailey, M. a, 2014. Pressure natriuresis and the renal control of arterial blood pressure. *The Journal of Physiology*, 18, pp.3955–3967.

Ji, X., Naito, Y., Hirokawa, G., et al., 2012. P2X(7) receptor antagonism attenuates the hypertension and renal injury in Dahl salt-sensitive rats. *Hypertension Research : Official Journal of the Japanese Society of Hypertension*, 35(2), pp.173–9.

Ji, X., Naito, Y., Weng, H., et al., 2012. P2X7 deficiency attenuates hypertension and renal injury in deoxycorticosterone acetate-salt hypertension. *American Journal of Physiology. Renal Physiology*, 303(8), pp.F1207-15.

Johnson, R.J. et al., 2005. A unifying pathway for essential hypertension. *American Journal of Hypertension*, 18(3), pp.431–40.

Kawamura, H. et al., 2003. ATP: a vasoactive signal in the pericyte-containing microvasculature of the rat retina. *The Journal of Physiology*, 551(3), pp.787–799.

Keystone, E.C. et al., 2012. Clinical evaluation of the efficacy of the P2X7 purinergic receptor antagonist AZD9056 on the signs and symptoms of rheumatoid arthritis

in patients with active disease despite treatment with methotrexate or sulphasalazine. *Annals of the Rheumatic Diseases*, 71(10), pp.1630–5.

Kim, M.J. et al., 2014. Exaggerated renal fibrosis in P2X4 receptor-deficient mice following unilateral ureteric obstruction. *Nephrology, Dialysis, Transplantation*, 29(7), pp.1350–61.

Kirchhoff, F. et al., 2008. Rapid development of severe end-organ damage in C57BL/6 mice by combining DOCA salt and angiotensin II. *Kidney International*, 73(5), pp.643–50.

Kreft, E. et al., 2015. Renal vasculature reactivity to agonist of P2X7 receptor is increased in streptozotocin-induced diabetes. *Pharmacological Reports*, pp.4–7.

Kreft, E. et al., 2016. Renal vasculature reactivity to agonist of P2X7 receptor is increased in streptozotocin-induced diabetes. *Pharmacological Reports*, 68(1), pp.71–74.

Labasi, J.M. et al., 2002. Absence of the P2X7 Receptor Alters Leukocyte Function and Attenuates an Inflammatory Response. *The Journal of Immunology*, 168(12), pp.6436–6445.

Lajdova, I. et al., 2017. Expression of purinergic P2X7 receptors in subpopulations of peripheral blood mononuclear cells in early-stage of chronic kidney disease. *Journal of Physiology and Pharmacology*, 68(5), pp.779–785.

Lajdova, I. et al., 2012. Purinergic P2X7 receptors participate in disturbed intracellular calcium homeostasis in peripheral blood mononuclear cells of patients with chronic kidney disease. *Kidney & Blood Pressure Research*, 35(1), pp.48–57.

Lebleu, V.S. et al., 2014. Origin and Function of Myofibroblasts in Kidney Fibrosis. *Nature Medicine*, 19(8), pp.1047–1053.

Lewis, C.J. & Evans, R.J., 2001. P2X receptor immunoreactivity in different arteries from the femoral, pulmonary, cerebral, coronary and renal circulations. *Journal of Vascular Research*, 38(4), pp.332–40.

Li, F. et al., 2014. Inhibition of P2X4 suppresses joint inflammation and damage in

collagen-induced arthritis. *Inflammation*, 37(1), pp.146–53.

Lin, S.L. et al., 2011. Targeting endothelium-pericyte cross talk by inhibiting VEGF receptor signaling attenuates kidney microvascular rarefaction and fibrosis. *American Journal of Pathology*, 178(2), pp.911–923.

Lister, M.F. et al., 2007. The role of the purinergic P2X7 receptor in inflammation. *Journal of Inflammation*, 4, p.5.

Long, D. a, Norman, J.T. & Fine, L.G., 2012. Restoring the renal microvasculature to treat chronic kidney disease. *Nature reviews. Nephrology*, 8(4), pp.244–50.

Lopez-Giacoman, S. & Madero, M., 2015. Biomarkers in chronic kidney disease, from kidney function to kidney damage. *World Journal of Nephrology*, 4(1), pp.57–73..

Lorenz, J.N. & Gruenstein, E., 1999. A simple, nonradioactive method for evaluating single-nephron filtration rate using FITC-inulin. *The American Journal of Physiology*, 276(1 Pt 2), pp.F172-7.

Martha Franco, X. et al., 2017. Physiopathological implications of P2X 1 and P2X 7 receptors in regulation of glomerular hemodynamics in angiotensin II-induced hypertension. The *American Journal of Physiology: Renal Physiology*, 313, pp.9–19.

Masin, M., Young, C., Lim, K., Barnes, S.J., et al., 2012. Expression, assembly and function of novel C-terminal truncated variants of the mouse P2X7 receptor: re-evaluation of P2X7 knockouts. *British Journal of Pharmacology*, 165(4), pp.978–93.

Masin, M., Young, C., Lim, K., Barnes, S.J., et al., 2012. Expression, assembly and function of novel C-terminal truncated variants of the mouse P2X7 receptor: Re-evaluation of P2X7 knockouts. *British Journal of Pharmacology*, 165(4), pp.978–993.

Mattson, D.L., Roman, R.J. & Cowley, a. W., 1992. Role of nitric oxide in renal papillary blood flow and sodium excretion. *Hypertension*, 19(6_Pt_2), pp.766–769.

Menzies, R.I. et al., 2013. Effect of P2X4 and P2X7 receptor antagonism on the pressure diuresis relationship in rats. *Frontiers in Physiology*, 4, p.305.

Menzies, R.I. et al., 2017. Hyperglycemia-induced Renal P2X7 Receptor Activation Enhances Diabetes-related Injury. *EBioMedicine*. 19, pp 73 - 83

Menzies, R.I. et al., 2015. Inhibition of the purinergic P2X7 receptor improves renal perfusion in angiotensin-II-infused rats. *Kidney International*, pp.1–9.

Menzies, R.I. et al., 2017. Purinergic signaling in kidney disease. *Kidney International*, 91(2), pp.315–323.

Menzies, R.I., Unwin, R.J. & Bailey, M. a., 2015. Renal P2 receptors and hypertension. *Acta Physiologica*, 213, pp.232–241.

Michel, A.D. et al., 2009. Mechanism of action of species-selective P2X 7 receptor antagonists. *British Journal of Pharmacology*, 156(8), pp.1312–1325.

Mohammed-Ali, Z. et al., 2017. Endoplasmic reticulum stress inhibition attenuates hypertensive chronic kidney disease through reduction in proteinuria. *Scientific Reports*, 7, p.41572.

Monassier, L., Combe, R. & Fertak, L. El, 2006. Mouse models of hypertension. *Drug Discovery Today: Disease Models*, 3(3), pp.273–281.

Montezano, A.C. et al., 2014. Angiotensin II and Vascular Injury. *Current Hypertension Reports*, 16(6), p.431.

Mullins, L.J. et al., 2016. Renal disease pathophysiology and treatment: contributions from the rat. *Disease Models & Mechanisms*, 9(12), pp.1419–1433.

Nakayama, M. et al., 2011. Increased risk of cardiovascular events and mortality among non-diabetic chronic kidney disease patients with hypertensive nephropathy: the Gonryo study. *Hypertension Research : Official Journal of the Japanese Society of Hypertension*, 34(10), pp.1106–10.

Nicke, A. et al., 2009. A functional P2X7 splice variant with an alternative transmembrane domain 1 escapes gene inactivation in P2X7 knock-out mice. *The Journal of Biological Chemistry*, 284(38), pp.25813–22.

Nishiyama, a. et al., 2000. Relation Between Renal Interstitial ATP Concentrations and Autoregulation-Mediated Changes in Renal Vascular Resistance. *Circulation Research*, 86(6), pp.656–662.

Norman, J.T. & Fine, L.G., 2006. Intrarenal oxygenation in chronic renal failure. *Clinical and Experimental Pharmacology & Physiology*, 33(10), pp.989–96.

North, R.A., 2002. Molecular physiology of P2X receptors. *Physiological reviews*, 82(4), pp.1013–67.

O'Conner, P.M. & Cowley Jr., A.W., 2010. Modulation of pressure-natriuresis by renal medullary reactive oxygen species and nitric oxide. *Current Hypertension Reports*, 12(2), pp.86–92.

Palomino-Doza, J. et al., 2008. Ambulatory blood pressure is associated with polymorphic variation in P2X receptor genes. *Hypertension*, 52(5), pp.980–5.

Pelegrin, P. & Surprenant, A., 2006. Pannexin-1 mediates large pore formation and interleukin-1beta release by the ATP-gated P2X7 receptor. *The EMBO journal*, 25(21), pp.5071–82.

Ponnusamy, M. et al., 2011. P2X 7 receptors mediate deleterious renal epithelial-fibroblast cross talk. *American Journal of Physiology. Renal Physiology*, 300, pp.62–70.

Remuzzi, G. et al., 2013. Kidney failure: aims for the next 10 years and barriers to success. *Lancet*, 382(9889), pp.353–62.

Rockey, D.C., Bell, P.D. & Hill, J.A., 2015. Fibrosis — A Common Pathway to Organ Injury and Failure D. L. Longo, ed. *New England Journal of Medicine*, 372(12), pp.1138–1149.

Rodríguez-Iturbe, B. et al., 2014. Autoimmunity in the pathogenesis of hypertension. *Nature Reviews. Nephrology*, 10(1), pp.56–62.

Romagnani, P., Remuzzi, G., Glassock, R., Levin, A., Jager, K. J., Tonelli, M., Massy, Z., Wanner, C. & Anders, H., 2019 Chronic kidney disease. *Nature Reviews; Disease Primers* 3, pp17088

Sathanoori, R. et al., 2015. The ATP Receptors P2X7 and P2X4 Modulate High Glucose and Palmitate-Induced Inflammatory Responses in Endothelial Cells J. Arreola, ed. *PLoS ONE*, 10(5), p.e0125111.

Schindelin, J. et al., 2012. Fiji: an open-source platform for biological-image analysis. *Nature Methods*, 9(7), pp.676–82.

Shaw, I. et al., 2018. Pericytes in the renal vasculature: roles in health and disease. *Nature Reviews Nephrology*, 14(8), pp.521–534.

Shirley, D.G. et al., 2013. Extracellular Nucleotides and Renal Function. In R. J. Alpern, M. J. Caplan, & O. W. Moe, eds. *Seldin and Giebisch's The Kidney: Physiology and Pathophysiology*. Academic Press, pp. 511–537.

Smith, H.W. et al., 1945. The Renal learances of Substituted Hipppuric Acid Derivatives and Other Aromatic Acids in Dog and Man. *The Journal of Clinical Investigation*, 24(3), pp.388–404.

Solini, A. et al., 2005. Purinergic modulation of mesangial extracellular matrix production: Role in diabetic and other glomerular diseases. *Kidney International*, 67(3), pp.875–885.

Solini, A. et al., 2013. The purinergic 2X7 receptor participates in renal inflammation and injury induced by high-fat diet: possible role of NLRP3 inflammasome activation. *The Journal of Pathology*, 231(3), pp.342–53.

Stachon, P. et al., 2017. P2X7 Deficiency Blocks Lesional Inflammasome Activity and Ameliorates Atherosclerosis in Mice. *Circulation*, 135(25), pp.2524–2533.

Stock, T.C. et al., 2012. Efficacy and safety of CE-224,535, an antagonist of P2X7 receptor, in treatment of patients with rheumatoid arthritis inadequately controlled by methotrexate. *The Journal of Rheumatology*, 39(4), pp.720–7.

Sugiyama, T., 2014. Role of P2X7 receptors in the development of diabetic retinopathy. *World Journal of Diabetes*, 5(2), pp.141–5.

Surprenant, a et al., 1996. The cytolytic P2Z receptor for extracellular ATP identified as a P2X receptor (P2X7). *Science (New York, N.Y.)*, 272(5262), pp.735–8.

Surprenant, A. et al., 1996. The Cytolytic P2Z Receptor for Extracellular ATP Identified as a P2X Receptor (P2X7). *Science (New York, N.Y.)*, 272(5262), pp.1–9.

Tampe, D. & Zeisberg, M., 2014. Potential approaches to reverse or repair renal fibrosis. *Nature Reviews. Nephrology*, 10(4), pp.226–37.

Taylor, S.R.J. et al., 2009. P2X7 deficiency attenuates renal injury in experimental glomerulonephritis. *Journal of the American Society of Nephrology : JASN*, 20(6), pp.1275–81.

Tazi, J., Bakkour, N. & Stamm, S., 2009. Alternative splicing and disease. *Biochimica et Biophysica Acta (BBA) - Molecular Basis of Disease*, 1792(1), pp.14–26.

Turner, C.M. et al., 2007. Increased expression of the pro-apoptotic ATP-sensitive P2X7 receptor in experimental and human glomerulonephritis. *Nephrology, Dialysis, Transplantation :* 22(2), pp.386–95.

Turner, C.M. et al., 2003. The Pattern of Distribution of Selected ATP-Sensitive P2 Receptor Subtypes in Normal Rat Kidney: An Immunohistological Study. *Cells Tissues Organs*, 175(2), pp.105–117.

Vonend, O. et al., 2004a. Glomerular expression of the ATP-sensitive P2X receptor in diabetic and hypertensive rat models. *Kidney International*, 66(1), pp.157–66.

Vonend, O. et al., 2004b. Glomerular expression of the ATP-sensitive P2X receptor in diabetic and hypertensive rat models. *Kidney International*, 66(1), pp.157–66.

Walker, A. et al., 2005. Regulation of Neutrophil Apoptosis and Removal of Apoptotic Cells. *Current Drug Target -Inflammation & Allergy*, 4(4), pp.447–454.

Wang, H. et al., 2015. P2RX7 sensitizes Mac-1/ICAM-1-dependent leukocyte-endothelial adhesion and promotes neurovascular injury during septic encephalopathy. *Cell Research*, pp.1–17.

Wang, Q. et al., 2004. P2X7 receptor-mediated apoptosis of human cervical epithelial cells. *American Journal of Physiology. Cell Physiology*, 287(5), pp.C1349-58.

Xu, X.J. et al., 2012. Splice variants of the P2X7 receptor reveal differential agonist

dependence and functional coupling with pannexin-1. *Journal of Cell Science*, 125(Pt 16), pp.3776–89.

Yamamoto, K. et al., 2000. Fluid Shear Stress Activates Ca2+ Influx Into Human Endothelial Cells via P2X4 Purinoceptors. *Circulation Research*, 87(5), pp.385–391.

Yamamoto, K. et al., 2006. Impaired flow-dependent control of vascular tone and remodeling in P2X4-deficient mice. *Nature Medicine*, 12(1), pp.133–7.

Yan, Y. et al., 2015. P2X7 receptor inhibition protects against ischemic acute kidney injury in mice. *American Journal of Physiology. Cell Physiology*, p.ajpcell.00245.2014.

Yang, H.-C., Zuo, Y. & Fogo, A.B., 2010. Models of chronic kidney disease. *Drug Discovery Today: Disease Models*, 7(1–2), pp.13–19.

Young, M.T., Pelegrin, P. & Surprenant, A., 2007. Amino acid residues in the P2X7 receptor that mediate differential sensitivity to ATP and BzATP. *Molecular Pharmacology*, 71(1), pp.92–100.

Zeisberg, M. et al., 2003. BMP-7 counteracts TGF-beta1-induced epithelial-to-mesenchymal transition and reverses chronic renal injury. *Nature Medicine*, 9(7), pp.964–968.

Zeisberg, M. & Zeisberg, E.M., 2015. Precision renal medicine: a roadmap towards targeted kidney fibrosis therapies. *Fibrogenesis & Tissue Repair*, 8(1), p.16.

Zhang, Y. et al., 2014. P2X7 receptor blockade protects against cisplatin-induced nephrotoxicity in mice by decreasing the activities of inflammasome components, oxidative stress and caspase-3. *Toxicology and Applied Pharmacology*, 281(1), pp.1–10.

Zhao, D. & Navar, L.G., 2008. Acute angiotensin II infusions elicit pressure natriuresis in mice and reduce distal fractional sodium reabsorption. *Hypertension*, 52(1), pp.137–42.

Zhao, X. et al., 2005. Impaired Ca $^{2+}$ Signaling Attenuates P2X Receptor–Mediated

Vasoconstriction of Afferent Arterioles in Angiotensin II Hypertension. *Hypertension*, 46(3), pp.562–568.